UNIVERSIDADE DE SÃO PAULO
INSTITUTO DE QUÍMICA

Programa de Pós-Graduação em Química

TAYANA MAZIN TSUBONE

Especificidade e biodisponibilidade de fotossensibilizadores: Em busca de um fotossensibilizador otimizado para Terapia Fotodinâmica

Versão corrigida da Tese conforme Resolução CoPGr 5890
O original se encontra disponível na Secretaria de Pós-Graduação do IQ-USP

São Paulo

Data do Depósito na SPG:
23/02/2017

TAYANA MAZIN TSUBONE

Specificity and bioavailability of photosensitizers: In the search of an optimized photosensitizer for Photodynamic Therapy

Thesis presented to the Graduate Program in Chemistry at the Institute of Chemistry, University of Sao Paulo to obtain the degree of Doctor in Science.

Advisor: Prof. Dr. Maurício da Silva Baptista

São Paulo
2017

DEDICATED

to

My parents, Elza e Mário, for making me be who I am and always encouraging me to reach my dreams and goals.

My sister, Luana, for the all the care, love and friendship since childhood.

My husband, Tiago, for being my partner and my best friend. His support during all the way with patience, love and encouragement gave me strength in this step of my life.

ACKNOWLEDGEMENTS

I deeply acknowledge my advisor Prof. Dr. Maurício S. Baptista for all opportunities and learning provided to me. I also would like to express my gratitude for the patience and comprehension during the whole process of my training, professional growth and development of this thesis. For sure, Professor Maurício is an example of leadership and professionalism to inspire.

I acknowledge Dr. Waleska K. Martins for the collaboration always with new ideas. Thanks to be friendly, always willing to help me and show me that strategy and persuasion is so important as working hard.

I acknowledge Dr. Christiane Pavani for the friendship, collaboration and support on experiments with culture cell. Thank you to encourage me to extend from the boundaries of fundamental chemistry to a slightly more biological world.

I acknowledge Dr. Rosangela Itri and Dr. Helena Junqueira for the collaboration and for receiving and supporting me in your laboratory during experiments with GUVs at Institute of Physics.

I thank the laboratory staff: Alessandra and Helena for maintain the organization and performance of laboratory. Also, my gratitude for providing optimized work conditions which are essential to the development of our scientific job.

I thank technical assistance: Cleidiane, Laryssa, Rebeca, Luana and Ingrid to prepare and organize all solutions and materials necessary to work at the cell culture room. Your job is so important and facilitate a lot our work in the lab.

I thank everybody from my laboratory who have contributed direct or indirectly during my graduate: Nayra, Orlando, Mariana, Isabel, Tatiana, Laryssa, Paulo, Juliana, Marina, Aline, Carolina, Felipe, Thiago Tasso, Tiago dos Santos Rodrigues, Divino, Adjaci, Waleska, Christiane, Helena.

I acknowledge Adjaci to help me with the synthesis of porphyrin.

I thank Cleidiane Sousa for the friendship and by the teachings on my initial phase on cell culture room.

I thank Laryssa Santos for your friendship and by helping me with some experiments.

I would like to thank to Mariana Reis for the friendship and funny moments in the lab.

I thank Adriana Matsukuma and Wilton Rocha Lima for technical assistance with confocal microscopy and flow cytometer.

I acknowledge the staff from Secretary Office of Graduate Program (Milton, Marcelo and Emiliano) for the help and cooperation with required documentation to important steps in the Graduate Program.

I deeply acknowledge Dr. Joachim Kohn for receiving me during three months in your laboratory (*New Jersey Center for Biomaterials – Rutgers University*) by the *International Summer Exchange Program – 2014* to develop part of my PhD thesis (Chapter 4).

I acknowledge Dr. Zheng Zhang for collaboration, patience and for helping me even after I left the *New Jersey Center for Biomaterials*. My gratitude for be always willing to support and encourage me with Tyrospheres work.

I acknowledge Dr. Ritu Goyal for collaboration and helping me during the period I was on *New Jersey Center for Biomaterials*.

I thank Carmen for helping me with all visa process to USA and for welcome me so kindly. My gratitude for make me feel as I was in home even in another country.

I thank everybody from *New Jersey Center for Biomaterials* who helped me direct or indirectly.

My gratitude to my friends Maria, Jessica, Pryia and Carmen for making my experience abroad fun, full of adventure and unforgettable. Your friendship has made the distance from my country, my husband and my family less arduous.

I thank my friends André, Nathalia, Layara and Denize for friendship and fun weekends in the “stone city”.

I would also like to highlight the importance of my family (Tiago, Elza, Luana and Mario) in my journey as PhD student. Their patience, encouragement, love and support gave me the strength and resilience to complete this marathon.

I thank CNPq for the scholarship grant during the first semester of my graduate.

I acknowledge FAPESP for the grant fellowship during the direct PhD (2012/10049-4 and 2013/16532-1). I also would like to thank the opportunities to participate of three months internship and international conferences/congress.

“Be the change you want to see in the word.”

Mahatma Gandhi

RESUMO

Tsubone, T. M. **Especificidade e biodisponibilidade de fotossensibilizadores: Em busca de um fotossensibilizador otimizado para Terapia Fotodinâmica.** 2017. 163p. Tese de Doutorado - Programa de Pós-Graduação em Química. Instituto de Química, Universidade de São Paulo, São Paulo.

Terapia fotodinâmica (TFD) tem sido foco substancial de investigação e desenvolvimento para aplicação na área da medicina por várias décadas. Entretanto, TFD é ainda muito menos conhecido que tratamentos já bem consolidados (quimioterapia, radioterapia, cirurgia) e não tem alcançado uma posição proeminente na prática clínica. Na expectativa de levantar alguns pontos sobre estratégias a nível molecular para aumentar a eficácia da TFD tornando os protocolos de TFD mais preciso e confiável, três principais estratégias são destacadas nesta tese: (i) otimização da interação do fotossensibilizador (FS) com membranas, (ii) especificidade do fotossensibilizador em alvos intracelulares e (iii) biodisponibilidade do fotossensibilizador na forma monomérica através do uso de um nanocarreador.

Uma série de fotossensibilizadores anfifílicos (PpNetNI, CisDiMPyP, $TPPS_{2a}$, $AlPcS_{2a}$) foram avaliados em termos de propriedades fotofísica e fotoquímica, interação com membranas e fotodano em membranas. Os dados indicaram que os diferentes grupos periféricos não afetam significativamente as propriedades fotofísicas das porfirinas, entretanto isso impacta diretamente na interação FS-membrana. CisDiMPyP exibe maior ligação em membranas do que PpNetNI (ambos são porfirinas anfifílicas positivamente carregadas e com propriedades fotofísicas similares), provavelmente porque os grupos periféricos fenil fornecem impedimento estérico evitando empilhamento π-π e também aumentando as interações hidrofóbicas com a membrana. Embora $TPPS_{2a}$ contém dois grupos com cargas negativas, este tem maior interação com membranas negativamente carregadas do que PpNetNI indicando que interações hidrofóbicas e dipolares desempenham um papel importante na definição da afinidade destas moléculas em membranas. A menor incorporação da $AlPcS_{2a}$ em membranas foi atribuída à maior rigidez da molécula e maior polaridade no centro de seu cromóforo devido ao metal. Dentro desta série de quatro compostos anfifílicos estudados em membranas, foram selecionadas as duas porfirinas com maiores interações e fotodano em membrana (CisDiMPyP and $TPPS_{2a}$) para maiores investigações em células eucarióticas.

Apesar da similaridade de estrutura e propriedades fotofísicas, CisDiMPyP e TPPS2a dispõem de cargas opostas. Como consequências destas cargas opostas, cada

fotossensibilizador é direcionado para uma organela específica. No caso de porfirina carregada positivamente (CisDiMPyP), esta se localiza principalmente em mitocôndrias e desencadeia a morte apoptótica. Por outro lado, a porfirina carregada negativamente ($TPPS_{2a}$) é direcionada para os lisossomos prejudicando as funções pró-sobrevivência da autofagia e resultando em morte celular associada a autofagia. O fotodano em lisossomos e a indução da morte celular associada à autofagia causada por $TPPS_{2a}$ mostraram ser mais eficazes para inibir a proliferação celular, mesmo que a incorporação celular e a eficiência de ligação em membrana da $TPPS_{2a}$ sejam mais baixas. Isso vai contra alguns paradigmas da literatura que descrevem que a relação entre a maior fototoxicidade e maior interação com membranas e ressalta a mitocôndria como alvo intracelular chave.

Nanoesferas derivadas da tirosina foram utilizadas como nanocarreadores das porfirinas CisDiMPyP and $TPPS_{2a}$ com o objetivo de aumentar a biodisponibilidade do FS. A escolha deste copolímero foi devida sua biodegradabilidade, biocompatibilidade, boa capacidade de encapsulamento, fácil micelização e extrema estabilidade das micelas. Embora as porfirinas não alteram as propriedades das nanoesferas (ex. tamanho, carga superficial, estabilidade), as nanoesferas são capazes de melhorar as propriedades fotoquímicas e fotofísicas fornecendo melhor geração e tempo de vida do $^1O_2$. Além disso, estas nanopartículas aumentar a fototoxicidade de porfirinas sem alterar a localização intracelular e o mecanismo de morte celular.

Palavras-chave: Terapia Fotodinâmica, porfirinas, membranas, nanoesferas poliméricas, localização intracelular, mecanismo de morte celular.

ABSTRACT

Tsubone, T. M. **Specificity and bioavailability of photosensitizers: In the search of an optimized photosensitizer for Photodynamic Therapy.** 2017. 163p. PhD Thesis - Graduate Program in Chemistry. Instituto de Química, Universidade de São Paulo, São Paulo.

For several decades, Photodynamic Therapy (PDT) has been the focus of research and development to facilitate medical field application. However, PDT is still much less known than conventional treatments (e.g. chemotherapy, radiotherapy, surgery). Despite advantages of PDT for a variety of applications, it has not achieved an equally prominent position in clinical practice.

A critical aspect during PDT treatments is the PDT efficacy and the determination of accurate treatment protocols. Three main strategies are highlighted in this thesis, to elucidate mechanisms at the molecular level to enhance the PDT efficiency and furthermore facilitate more accurate and reliable PDT protocols: (i) optimization of the photosensitizer (PS) interaction with membranes, (ii) specificity of PS to intracellular targets and (iii) bioavailability of photosensitizers in a monomeric form by using a nanocarrier.

A series of amphiphilic photosensitizers (PpNetNI, CisDiMPyP, $TPPS_{2a}$, $AlPcS_{2a}$) were evaluated in terms of photophysical and photochemical properties, membrane interaction and membrane photodamage. Data indicated that the different peripheral groups do not significantly affect the photophysical properties of the porphyrins. However, these groups directly impact the membrane interaction. CisDiMPyP exhibits a higher binding to membranes than PpNetNI (both are positively-charged amphiphilic porphyrins with similar photophysical properties), probably because the phenyl peripheral hydrophobic groups provide a steric barrier, avoiding π-π stacking and also increasing the hydrophobic interaction with the membrane. Although $TPPS_{2a}$ contains two negatively charged groups, it has a larger interaction with negatively charged membranes than PpNetNI indicating that both, hydrophobic and dipolar, interactions play an important role for the affinity of these molecules to membranes. The smaller incorporation of $AlPcS_{2a}$ into membranes was attributed to the higher rigidity of this molecule and larger polarity in the center of chromophore due to the metal. Within the series of four amphiphilic photosensitizers studied in membranes, it was selected two porphyrins (CisDiMPyP and $TPPS_{2a}$) with the best membrane interaction and membrane photodamage to further investigations in eukaryotic cells.

While the structure and the photophysical properties ofCisDiMPyP and $TPPS_{2a}$ are similar, these PS have opposite charges. As a consequence of the opposite charges, each photosensitizer aims at different organelle. In case of the positively-charged porphyrin (CisDiMPyP), it localizes mainly in mitochondria and triggersapoptotic death. On the other hand, the negatively-charged porphyrin ($TPPS_{2a}$) are directed to lysosomes, impairing the autophagy pro-survival functions and resulting in autophagy-associated cell death. The lysosomal photodamage and induction of autophagy-associated cell death caused by $TPPS_{2a}$ showed to be more effective to inhibit cell proliferation, even though the cellular uptake and the membrane binding efficiency of $TPPS_{2a}$ is lower. This goes against some paradigms in literature which describe a relationship between stronger phototoxicity and larger interaction with membranes and defend mitochondria as key intracellular target.

Tyrosine-derived nanospheres were used as nanocarriers for porphyrins (CisDiMPyP and $TPPS_{2a}$) aiming at an increased bioavailability of the PS. The choice of this copolymers is due its biodegrability, biocompatibility, high loading capacity, high micellization yield and extremely stable micelles. Although porphyrins provide no changes to nanospheres properties (e.g. size, superficial charge, stability), Tyrospheres are able to improve photophysical and photochemical properties with better $^1O^2$ generation and lifetimes. Moreover, Tyrospheres enhance phototoxicity of porphyrins without alter subcellular localization and cell death mechanism

Keywords: Photodynamic Therapy, porphyrins, membranes, polymeric nanospheres, intracellular localization, cell death mechanism.

LIST OF FIGURES

LIST OF TABLES

LIST OF ABREVIATIONS

$^1O_2$	Singlet Oxygen
3-MA	3-methyladenine
AAU	Autophagy arbitrary units
ALA	5-aminolevulinic acid
$AlPcS_{2a}$	Al(III) Phthalocyanine chloride disulfonate disodium salt (adjacent isomer)
AO	Acridine Orange
ATP	Adenosine triphosphate
AV	Annexin V-FITC
BAF	Baflomicin-A1
BPD-MA	benzoporphyrin derivative monoacid ring A
BSA	Bovine serum albumin
CASP3	Caspase-3
CisDiMPyP	Cis-di(4-N-methyl-pyridyl)diphenylporphyrin
CL	Cardiolipin
CQ	Chloroquine
CTSB	Cathepsin B
CV	Crystal violet
DAPI	4',6-diamidino-2-phenylindole
DLS	Dynamic light scattering
DMEM	Dubelcco´s Modified Eagle medium
DMF	Dimethyl formamide
DMSO	Dimethyl sulfoxide
DOPC	Dioleoyl phosphatidylcholine
DPPC	Dipalmitoyl phosphatidylcholine

DPPG	Dipalmitoyl phosphatidylglycerol
DSPC	Distearoyl phosphatidylcholine
ER	Endoplasmic Reticulum
FACS	Flow cytometer
FBS	Fetal bovine serum
FLIM	Fluorescence lifetime imaging
GUV	Giant unillamelar vesicles
HeLa	Human adenocarcinoma cell line
K_b	Binding constant
LC3	Microtubule-associated protein light chain 3
LC3-I	Cytosolic form of LC3
LC3-II	LC3-phosphatidylethanolamine conjugate
LC_{50}	Lethal concentration to kill 50% of cells
LED	Light emission diode
LMP	Lysosome membrane permeablization
LTR	LysoTracker Red
MAL	Methyl-aminolevulinate
MB	Methylene Blue
m-THPC	meta-tetra(hydrohyphenyl)chlorin
MTR	MitoTracker Red
MTT	(3-(4,5-Dimethylthiazol-2-yl)-2,5-diphenyltetrazolium bromide
NPe6	N-aspartyl chlorin e6
NR	Neutral Red
P62-SQSTM1	Ubiquitin-binding protein p62
PBS	Phosphate buffered saline
PDI	polydispersity index

PDT	Photodynamic Therapy
PEG	Poly(ethylene glycol)
PI	Propidium Iodide
PI3K	Phosphatidylinositol 3-kinase
PpIX	Protoporphyrin IX
PpNetNI	Dimethyl-8,13-divinil-3,7,12,17-tetramethyl-21H, 23H-porphyrins-2,18-bis[N,N,N-trimethyl-2-(propanoilamino)etanoamonium
PS	Photosensitizer
Rh123	Rhodamine 123
RLS	Resonant light scattering
ROS	Reactive oxygen species
SD	Standard deviation
TNF	Tumor necrosis factor
$TPPS_{2a}$	Tetraphenylporphine disulphonic acid disodium salt (adjacent isomer)
$\Delta\psi_m$	Mitochondrial membrane inner potential
ϕ_f	Fluorescence quantum yield
ϕ_Δ	Singlet oxygen quantum yield

CONTENTS

PREFACE

This PhD thesis consists of three separate works that will be published in peer reviewed journals. Although they belong to related themes, each report can be read and understood independently. An introduction provides an overview of the relevant aspects of the overall topic, essential background information and a general literature review. Following the three-main works, a general conclusion briefly summarizes the major findings of this thesis and the perspectives for further research. Specifically, this PhD thesis composed of:

Chapter 1: Introduction and objectives to the general topic area,

Chapter 2: Work describing the relationship photosensitizer-membrane and its importance,

Chapter 3: Work demonstrating the relevance of charges bearing photosensitizer and their consequences in terms of intracellular localizations and cell death mechanism,

Chapter 4: Work revealing the use of a tyrosine-derived polymer as carrier of photosensitizers in Photodynamic Therapy,

Chapter 5: General conclusion and implications for further research.

CHAPTER 1

INTRODUCTION AND OBJECTIVES

The essential background information to the overall topic, general literature review and the aim of this work is provided in this chapter.

1. INTRODUCTION

Photosensitization reactions play a fundamental role in our world for the interaction between light and matter. It is still a matter of conjecture as to whether life evolved by the use of sun energy reacting photochemically, generating simple gaseous molecules such as methane, ammonia, and carbon dioxide - providing early organic molecules, which eventually formed nucleic acids and proteins (Rohatgi-Mukherjee 1978; Suppan 1994). Through the ages, nature has improved the use of sunlight for various beneficial and essential photobiological processes such as photosynthesis, biosynthesis of vitamin D, vision and phototaxis (considered a very early form of "vision"). Although the beneficial roles of light on living systems have been well established, it is important to mention that photochemical reactions also result in damage or even in lethal consequences to living organisms (Suppan 1994). For example, the photosensitization process can modify or destroy nucleic acids, which carry the genetic code in a sequence of nucleotides. This results in profound consequences, such as mutagenic effects, photoaging, and death of organisms (*e.g*. microbes) (Suppan 1994). Over time, humans have observed spontaneous photoinduced phenomena and gathered knowledge, eventually transformed into technology. The special interest of this thesis is the application of photoinduced processes as a strategy for the treatment of diseases, also known as Photodynamic Therapy (PDT).

1.1. **Historic development of Photodynamic Therapy (PDT)**

Since ancient times, the Egyptians used the photosensitization reactions to treat diseases such as vitiligo through ingestion of plants containing psoralens, followed by the exposure to sunlight (Sternberg, Dolphin, and Brickner 1998). In 1900, Raab demonstrated that unicellular organisms (e.g. *Paramecia*) could be effectively killed by the combination of acridine dye and light (Raab 1900). At the end of the 19th century, Niels Finsen found that red-light exposure

could treat *lupus vulgaris*, which was a very common skin disease at that time (Finsen 1901). The awarding of the *Nobel Prize* to Finsen in 1903, for the development of phototherapy (Dolmans, Fukumura, and Jain 2003), is considered the beginning of the modern light therapy Later, Tappeiner and Jesionek treated skin tumors with eosin and white light and described this phenomenon as "Photodynamic action" (Von Tappeiner and Jesionek 1903). These early developments were followed by a large burst of experiments to test combinations of reagents and light which led to the identification of many photosensitizing compounds, such as anthracenes, tetrapyrroles, thiazines and xanthenes (see timeline in Figure 1.1).

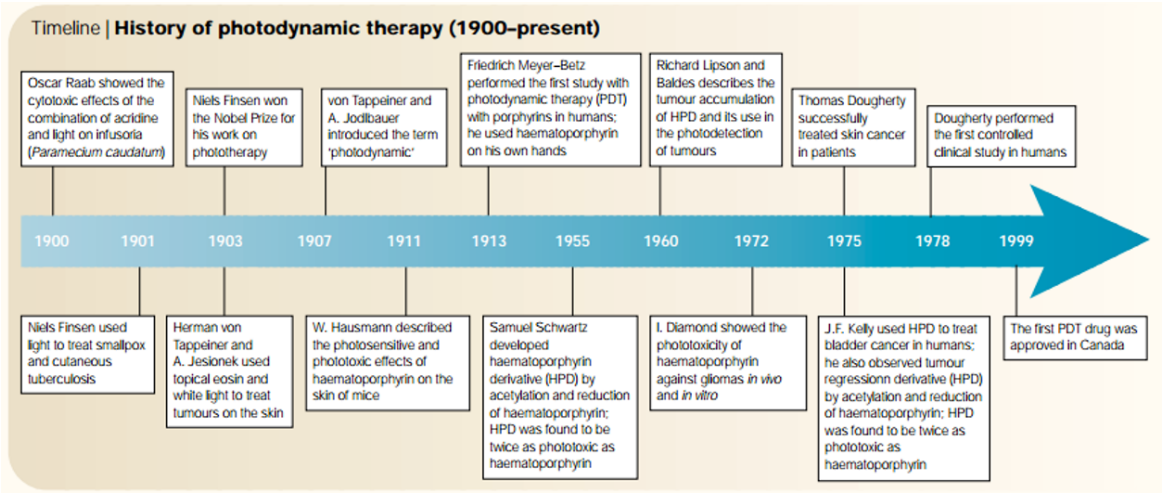

Figure 1.1. Summary of the relevant dates and discovery related to Photodynamic Therapy. Reprinted by permission from Macmillan Publishers Ltd (Dolmans, Fukumura, and Jain 2003).

The application of photosensitization reactions to clinical medicine (currently known as Photodynamic Therapy) has been used in the treatment of several illness, starting in the 1940´s (Auler and Banzer 1942). First successful applications of skin cancer were reported in the 1970´s (T J Dougherty et al. 1975). Finally, the first PDT drug was approved in the late 1990´s in Canada. Nowadays, PDT is commonly used to treat a variety of malignant tumors and furthermore for many non-oncological diseases such as for the treatment of age-related macular degeneration (Bressler and Bressler 2000), psoriasis (C. a Morton et al. 2002), arthritis (K B

Trauner et al. 1998; Kenneth B Trauner and Hasan 1996) and photoinactivation of virus and bacteria (Jori and Brown 2004).

1.2. **Photophysics and photochemistry process on PDT**

The basic concept of PDT involves two individually non-toxic components that are combined to induce cellular and tissue effects in an oxygen-dependent manner (Henderson and Dougherty 1992; Dolmans, Fukumura, and Jain 2003). The components consist of a photosensitizer (PS) and light (on suitable wavelength), which together and in the presence of oxygen generate reactive oxygen species (ROS), cytotoxic agents that can inactivate tumor cells.

The photophysical action behind PDT starts when the PS absorbs light energy. After absorption of a photon, the PS molecule gets excited from its singlet ground state (PS) to an electronically excited higher singlet state (^{1}PS*) – Figure 1.2., process A. Almost instantaneous on the time scale of singlet oxygen kinetics the higher excited singlet state of the PS undergoes internal conversion into its first excited singlet state (Kasha's rule, process E). From this state, inter-system crossing can occur (Figure 1.2, process C), allowing a multiplicity change of the PS, converting the photosensitizer to an excited triplet state (^{3}PS*). Species on the excited triplet state (^{3}PS*) are more easily reduced or oxidized than the molecules in the ground state (PS) and have a longer lifetime than singlet excited state (^{1}PS*) (Itri et al. 2014). Therefore, subsequent of the generation of the excited triplet state (^{3}PS*) two types of reactions may occur: Type I and Type II (Foote 1987; Foote 1991; Vidòczy 1992; Baptista et al. 2017).

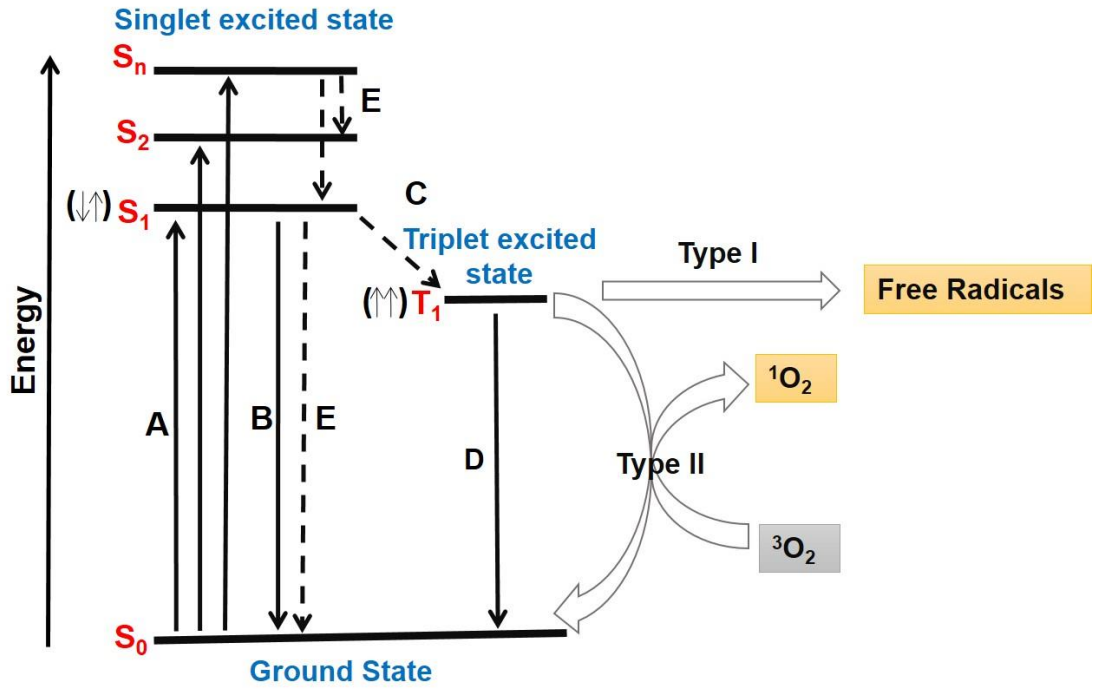

A: Absorption, **B**: Fluorescence, **C**: Intersystem crossing, **D**: Phosphorescence,
E: Internal conversion,
Type I: Hydrogen/electron transfer, **Type II:** Energy transfer

Figure 1.2. Jablonski diagram depicting the possible photophysical processes.

Table 1.1. Reaction occurring during photodynamic action. Reprinted by permission from (Ormond & Freeman 2013).

Excitation	$PS + h\upsilon \rightarrow {}^1PS^* \rightarrow {}^3PS^*$		
Photoprocess	**Reaction**		**Product**
Type I	$^3PS^* + PS$	→	$PS^{-\bullet} + PS^{+\bullet}$
	$^3PS^* + D$	→	$PS^{-\bullet} + D^+$
	$PS^{-\bullet} + O_2$	→	$PS + O_2^{-\bullet}$
	$^3PS^* + O_2$	→	$PS^{+\bullet} + O_2^{-\bullet}$
	$2O_2^{-\bullet} + 2H^+$	→	$O_2 + H_2O_2$
	$Fe^{2+} + O_2^{-\bullet}$	→	$Fe^{2+} + O_2$
	$Fe^{2+} + H_2O_2$	→	$O_2 + OH^- + OH^\bullet$
Tipo II	$^3FS^* + O_2$	→	$FS + {}^1O_2$

D is an electron donor molecule.

Type I processes involve an electron (or hydrogen) transfer process, where the triplet state of the photosensitizer interacts with the biological substrate resulting in the formation of radicals and radical ions - which on subsequent interaction with molecular oxygen give rise to reactive oxygen species (ROS) (see Table 1.1) such as hydroxyl radical ($OH^{\bullet}$), superoxide ion ($O_2^{-\bullet}$) and hydrogen peroxide (H_2O_2) - (Foote 1987; Ormond and Freeman 2013; Baptista et al. 2017).

Type II processes involve a direct energy transfer between the excited triplet state of the photosensitizer ($^3PS^*$) and molecular oxygen ($^3O_2$) producing singlet oxygen ($^1O_2$) - (Foote 1968b; Foote 1987). Singlet oxygen ($^1O_2$) is a highly reactive species because of its diamagnetic spin configuration (Figure 1.3), which favors the electrophilic attack of electrons donor molecules (Frankel 1984). The empty orbital present in $^1O_2$ (Figure 1.3) enables its addition to double bonds of lipids, proteins and nucleic acids, consequently oxidizing such biomolecules (Politzer, Griffin, and Laseter 1971; Davies 2003; Girotti 2001).

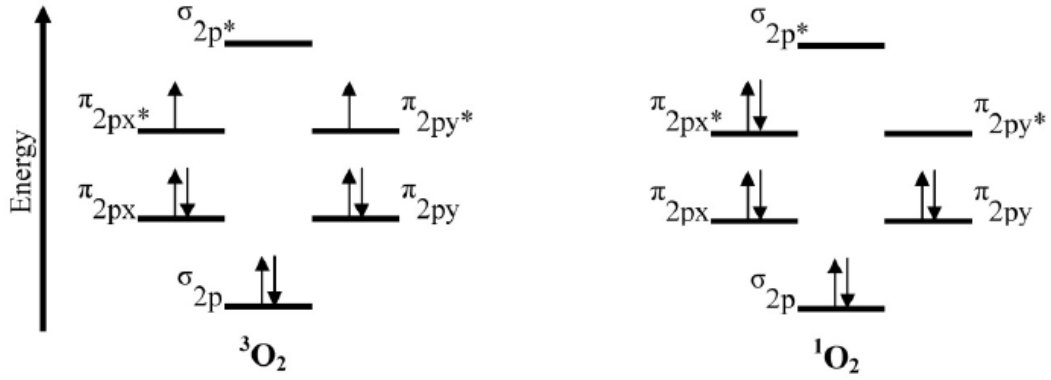

Figure 1.3. Orbital representation of triplet ($^3O_2$) and singlet ($^1O_2$) states of oxygen. Reprinted by permission from (Ormond & Freeman 2013).

In general, both mechanisms (Type I and Type II) may occur simultaneously. The relative importance of one mechanism with respect to the other will depend, among other factors, on the substrate, the distance between the photosensitizer and the substrate as well as the oxygen concentration. The main targets of excited PS or $^1O_2$ are electron donor molecules, i.e., carbon-carbon unsaturated bonds, amines, sulfides, anions and neutral nucleophiles (Frankel 1984;

Foote 1968a; Cadet and Mascio 2006; Itri et al. 2014; Baptista et al. 2017). It means that these photosensitization reactions can induce the photooxidation of relevant biomolecules (such as membranes, proteins and DNA), impairing their biological functions and promoting cell death (Thomas J. Dougherty et al. 1998; Henderson and Dougherty 1992).

1.3. **Specificity rather than total power**

Reactive oxygen species (ROS) are responsible by photooxidation of biomolecules and the cell death. However, ROS are very reactive towards biomolecules and thus have short lifetimes in biological environments, which implies that these species have a limited diffusion distance within cells. The relationship between the lifetime, reactivity and the diffusion distance for these species is illustrated in Figure 1.4 (Robert W Redmond and Kochevar 2006).

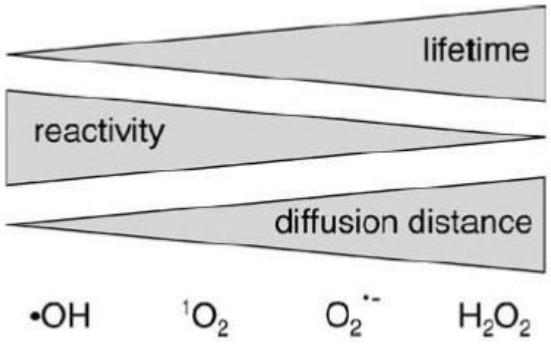

Figure 1.4. Trends in lifetime, reactivity with biomolecules and diffusion distance of common ROS in cells. Reprinted by permission from John Wiley and Sons (Robert W Redmond and Kochevar 2006).

To give just two examples: The $OH^{\bullet}$ lifetime in cells was estimated to be around 9 ns, which results in an average diffusion distance of 93 Å (Roots and Okada 1975). The lifetime of $^1O_2$ in living cells already reported vary between 0.4 µs – 1.7 µs, which means that $^1O_2$ diffusion distance is limited to less than 0.3 µm (Schlothauer, Hackbarth, and Röder 2009; Steffen Hackbarth et al. 2010; S. Hackbarth et al. 2012; Robert W Redmond and Kochevar 2006). This is a very small distance on the scale of cell dimensions. Typical cells in tissue have diameters of 10 – 30 µm; organelles such as mitochondria, lysosomes and endoplasmic reticulum exhibit

a diameter of around 500 nm, the size of a globular protein and the thickness of typical membranes are approximately 10 nm (Robert W Redmond and Kochevar 2006).

Therefore, the high reactivity and, respectively, the short lifetime are limiting factors for the distribution of ROS within cells. It is fundamentally important that the photosensitizer localizes close to the target which is intended to be damaged. In fact, Oliveira and co-workers demonstrated that producing ROS in specific intracellular targets is the best strategy to maximize the PDT efficacy instead of generating large amounts of ROS in a non-specific way (Oliveira et al. 2011). They compared two photosensitizers: methylene blue (MB) and crystal violet (CV), which have a different ability of generating ROS. Even though MB produces ROS with a higher quantum yield compared to CV (Figure 1.5), CV showed same efficiency in killing cells as MB (Figure 1.5). It was attributed to the highly specific localization of CV in mitochondria (99%), supporting the idea that generating big amounts of ROS does not means that the PS will be more effective. A high degree of intracellular specificity may provide a greater magnitude of photoinduced cell death (Oliveira et al. 2011).

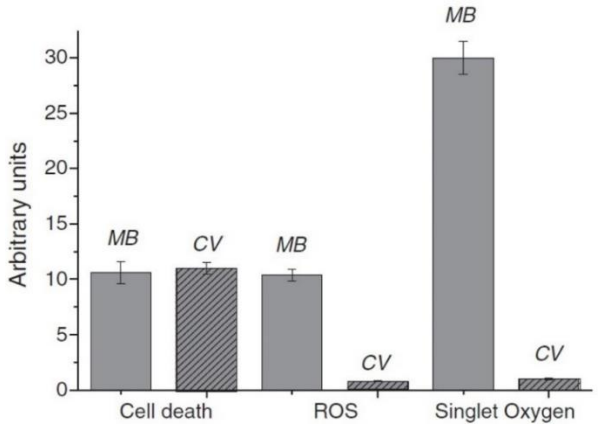

Figure 1.5. Comparison of cell death, ROS and singlet oxygen generation between two photosensitizers: methylene blue (MB) and crystal violet (CV). Reprinted with permission from Elsevier (Oliveira et al. 2011).

Taking into account that localization and the possible diffusion of ROS are very imporantant features, the development of better new-photosensitizers that are more efficient in

cell killing should focus on intracellular specificity rather than high ability of ROS generation nonspecific.

1.4. **Intracellular targets and cell death mechanisms in PDT**

Improving intracellular specificity triggers to different biological consequences in terms of mechanisms of cell death. The cell death mechanisms are generically classified into three types of cell death: apoptosis or type I programmed cell death, autophagy or type II programmed death and necrosis or non-regulated cell death (Figure 1.6).

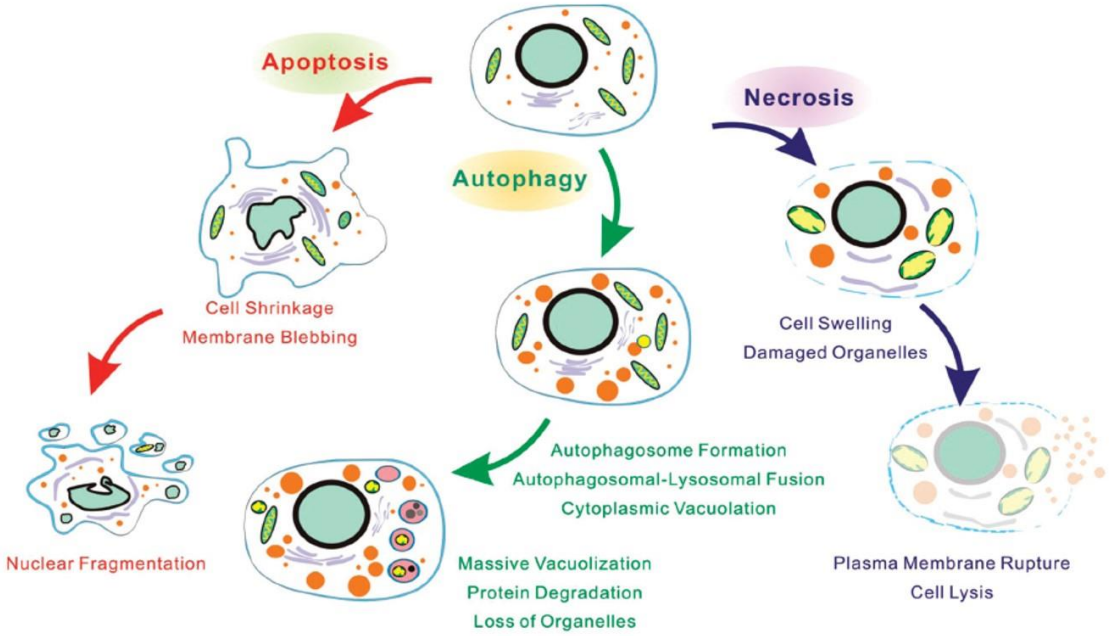

Figure 1.6. Morphological features of major types of cell death: apoptosis, autophagy and necrosis. Reprinted from open access Metallomics Journal (Tan et al. 2014).

Necrosis occurs as a result of extreme physical conditions or severe cellular damage induced by e.g. an external injury. It is characterized by cell swelling, morphological changes, hampered organelle integrity, loss of cell membrane integrity and eventual breakdown of the cell with a leakage of its contents into the surrounding area (Yoo and Ha 2012) - see Figure 1.6. The uncontrolled release of cell fragments due to necrotic death into the extracellular space initiate an inflammatory response, which hampers the elimination of dead cells by phagocytosis

(Yoo and Ha 2012; Ana P. Castano, Demidova, and Hamblin 2004). Depending on the level of inflammation it can be necessary to remove necrotic tissue surgically.

Apoptosis is a programmed and regulated cell death mechanism. Unlike necrosis, apoptosis prevents uncontrolled leakage of intracellular material into the neighboring environment and thereby avoids uncontrolled tissue inflammation (Yoo and Ha 2012; Ana P. Castano, Demidova, and Hamblin 2004; Buytaert, Dewaele, and Agostinis 2007). Apoptotic cells are morphologically characterized by cell shrinkage, chromatin condensation, chromosomal DNA fragmentation and membrane blebbing while maintenaning the integrity of the organelles and plasma membrane (Plaetzer et al. 2005; Agostinis et al. 2004) – Figure 1.6. Besides characteristic morphological changes, apoptosis also is accompanied by characteristic intracellular biochemical changes which can be used to identify cells in the process of apoptosis. Apoptosis is mediated by the activation of a protease family that has a cysteine in its active site: caspases, which act as death effector molecules. There are two signaling systems that can induce the activation of caspases: the extrinsic death receptor pathway and the intrinsic mitochondrial pathway, which are represented in Figure 1.7.

The extrinsic pathway of apoptosis is activated when proteins of extracellular signaling bind to death receptors on the cell surface. Death receptors belong to the receptor superfamily of tumor necrosis factor receptors (TNFR), which includes the TNF-related apoptosis inducing ligand (TRAIL) receptor and Fas (Beesoo et al. 2014). After activation, death receptors promote the recruitment of initiator procaspases (procaspase-8, procaspase-10 or both). The activation of caspase 8 can trigger the activation of downstream effector caspases such as caspase 3 which cleaves target proteins leading to apoptosis as illustrated in Figure 1.7 (Hirsch et al. 1998; Ashkenazi and Dixit 1998).

The intrinsic signaling pathway involves a stimulus (e.g. mitochondrial photodamage) that produces intracellular signals, acting directly on targets within cells and are mitochondrial-

initiated events. The stimulus activates the mitochondrial pathway, resulting in the release of cytochrome c and the formation of apoptosome complex (see Figure 1.7). Then, caspase-9 is activated by the apoptosome and in turn activates caspase-3 (Beesoo et al. 2014). Intrinsic and extrinsic pathways are not isolated processes but, instead, there can be much crosstalk between them. For example, the pro-apoptotic protein Bid can serve as a crosstalker between both (intrinsic and extrinsic pathway), inducing a mitochondrial amplification loop upon its caspase-mediated proteolytic processing (Beesoo et al. 2014).

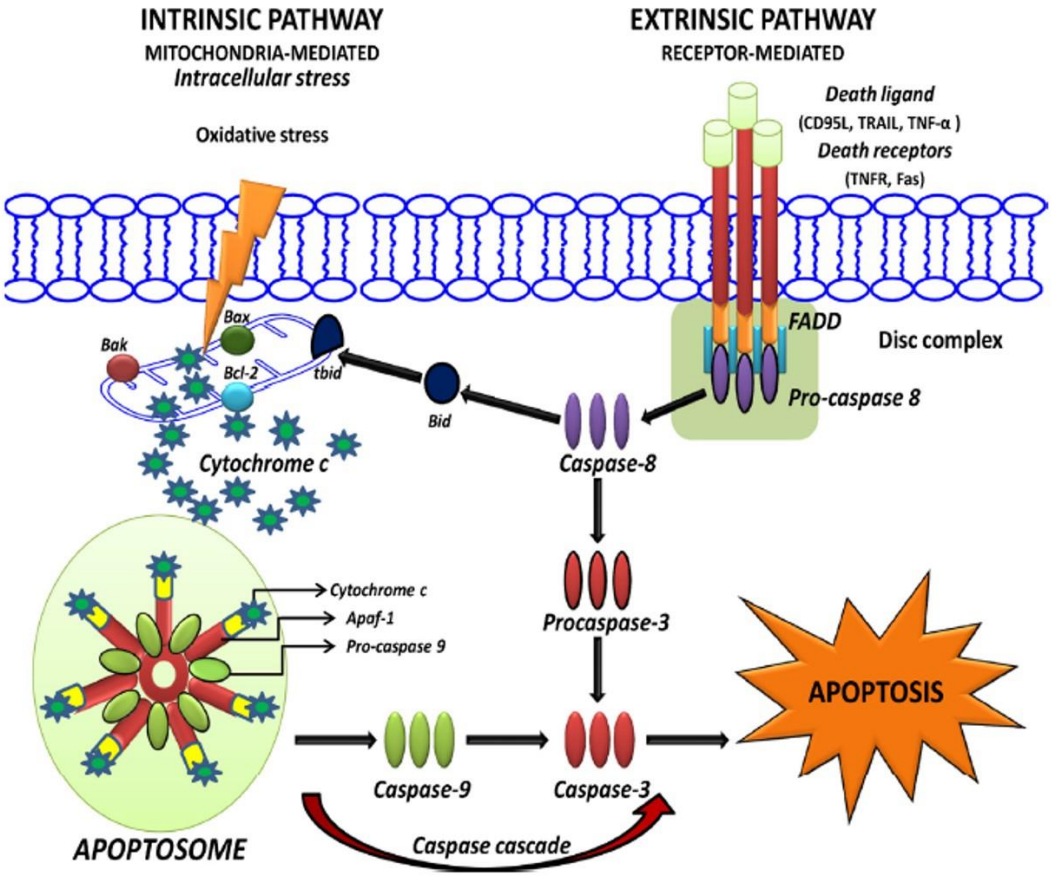

Figure 1.7. Extrinsic and intrinsic pathways involved in apoptosis. Adapted with permission from Elsevier (Beesoo et al. 2014).

Apoptosis has been shown to be a dominant form of cell death by following PDT in multiple experimental settings (Oleinick, Morris, and Belichenko 2002; Luo, Chang, and Kessel 1996; Plaetzer et al. 2005), however, it is known that cancer cells can be resistant to apoptosis as cell death mechanism (Mohammad et al. 2015).

In addition to necrosis and apoptosis, PDT protocols can also induce autophagy-associated cell death. Autophagy is a catabolic pathway, fundamental for cell homeostasis, removing misfolded proteins, clearing damaged organelles as well as eliminating intracellular pathogens (Glick, Barth, and Macleod 2010). The first step of the autophagy process is an isolation of membranes, also known as a phagophore, which are derived from lipid bilayers of the endoplasmic reticulum (ER) and/or the Golgi. The nucleation and assembly of the initial phagophore membrane requires the class III phosphatidylinositol 3-kinase (PI3K) complex, which is composed of the vacuolar protein sorting 34 (VPS34) PI3K, along with its regulatory subunits ATG14L, VPS15 and beclin 1. The phagophore membrane elongation and autophagosome formation requires two ubiquitin-like conjugation pathways. The first produces the ATG5–ATG12 conjugate, which forms a multimeric complex with ATG16L, whereas the second involves the cleavage of LC3 to LC3-I and its subsequent conjugation to phosphatidylethanolamine (PE) to form LC3-II in the autophagosomal membrane. Then, LC3-II binds to the adaptor proteins (e.g. p62-SQSTM 1) and their associated protein or organellar cargo (Abounit, Scarabelli, and Mccauley 2012). This loaded autophagosome matures through fusion with the lysosome, forming a structure called autolysosomes (Figure 1.8), which contains lysosomal proteases and enzymes (e.g. cathepsins) able to degrade the cargo (Mizushima 2007; Glick, Barth, and Macleod 2010). The steady-state formation and degradation of these structures is named autophagic flux (Figure 1.8).

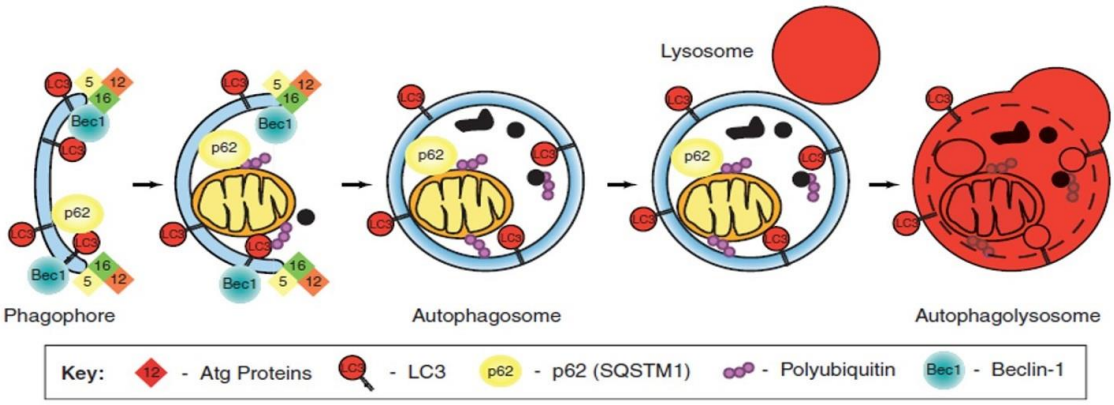

Figure 1.8. Main steps of the autophagic flux. Adapted with permission from Elsevier (Gump and Thorburn 2011).

Although autophagy is primary developed as a survival strategy of cells, an unbalance of autophagic flux (intense induction or inhibition of the autophagy process) can lead to cell death related with autophagy. In 2006, Kessel and Agostinis groups were the first to report that PDT can induce cell death associated with autophagy under conditions in which apoptosis was inhibited (David Kessel, Vicente, and Reiners 2006; Buytaert et al. 2006). After that, Oleinick´s group showed that autophagy occurs during cell death following PDT in human cancer cells, competent or not, for normal apoptosis (Xue et al. 2007). Three years later, Dini and collaborators described that the use of the pan-caspase inhibitor (z-VAD) and necrosis inhibitor Necrostatin-1 (Nec-1) was unable to completely prevent cell death, suggesting that autophagy plays a crucial role in the death process (Dini et al. 2010). Note that in both cases the authors indicate that the autophagy-associated cell death is independent of whether the cells are apoptosis-deficient (Xue et al. 2007; Dini et al. 2010). The implication of apoptosis in autophagy-associated cell death is still unclear: some works suggests that autophagy can occur independent of the presence of apoptotic pathways, while other reports demonstrating that when apoptosis is substantially delayed, autophagy has a cytoprotective role (Dewaele et al. 2011; Andrzejak, Price, and Kessel 2011; Du et al. 2014; Lihuan et al. 2014). Also, it is still not

completely understood whether the main role of autophagy in PDT protocols is rather pro-survival or pro-death (Garg et al. 2015).

After this overview of the main cell death mechanisms reported in PDT, it is important to keep in mind that these cell death pathways are defined by the intracellular target and the amount of photooxidative damage (Mroz et al. 2011; Ana Paula Castano, Demidova, and Hamblin 2005; Agostinis et al. 2004; Bacellar et al. 2015; T. M. Tsubone et al. 2017). Photosensitizers that localize mainly in the plasma membrane can produce irreparable damage, resulting in necrotic cell death, probably due to loss of plasma membrane integrity and rapid depletion of intracellular ATP (Yoo and Ha 2012; Ana P. Castano, Demidova, and Hamblin 2004). Once it has already been established that the plasma membrane is not a good target due to tendency of generating necrotic cells (Yoo and Ha 2012; Fabris et al. 2001), three other intracellular sites for PS accumulation will be analyzed: (i) mitochondria, (ii) Gogi/Endoplasmic reticulum (ER) and (iii) lysosomes.

(i) It is well known that damage to mitochondria is the key to induce apoptotic cell death (David Kessel and Luo 1998; Mroz et al. 2011). The localization of photosensitizers in mitochondria can photodamage the anti-apoptotic proteins (e.g. Bcl-2 and Bcl-xL) and/or the mitochondrial membrane with subsequent alteration in the mitochondrial membrane potential, a release of cytochrome c to the cytoplasm and the activation of caspase cascades (similar consequences of photodamaging Bcl-2) triggering the apoptotic response (D Kessel and Castelli 2001; David Kessel and Reiners 2002). Mitochondrial photodamage can also trigger necrosis or cell death related to autophagy, depending on the PDT - dose (PS concentration and light dose). When high PDT doses are applied, drastic mitochondrial permeability and ATP level depletion can take place in an uncontrolled manner, resulting in necrosis. Low PDT doses promote limited mitochondrial permeability, which activates autophagy as repair mechanism to protect

cells, this process can end up with autophagy-associated cell death (Andrzejak, Price, and Kessel 2011; David Kessel and Jr 2007; Garg et al. 2015).

(ii) Golgi/ER apparatus has been less considered than the damage in mitochondria, but can also trigger programmed cell death if the PDT dose is not too high. The main consequence of the ER photodamage is the loss of SERCA2 (sarco/endoplasmic reticulum Ca^{2+}-ATPase) protein levels causing breakage of calcium homeostasis and triggering of apoptosis (Agostinis et al. 2004; Buytaert et al. 2006). Also, it has been reported that ER photodamage can trigger autophagy-associated cell death, when the cells are protected from apoptosis (e.g. by Bax/Bak knockout)- (Buytaert et al. 2006).

(iii) Lysosomal photodamage leads to membrane rupture and the release of lysosomal proteolytic enzymes into the cytoplasm. These enzymes can cleave the proapoptotic protein Bid to a truncated form inducing an indirect apoptotic response (Reiners et al. 2002). It has also been proposed that lysosomal photodamage should prevent lysosome fusion with autophagosomes impairing autophagic processes by negating autophagic pro-survival functions (D. H. Kessel, Price, and Reiners 2012).

Although it is well established, which could be the consequences of photosensitization in each organelle, it is still not clear which is the most effective intracellular targetto provide a better cell-killing efficiency of PDT. Chapter 3 of this thesis adresses the question, whether mitochondria or lysosomes are the better intracellular target of photo-oxidation.

1.5. **Structure-activity relationship of targeting cell organelles**

The photosensitizers' structure is an important parameter to determine the subcellular localization and consequently the efficiency and mode of cell death. There are three fundamental properties governing the sites of photosensitizer uptake and distribution within cells: the degree of hydrophobicity, the type and number of charges and the degree of

asymmetry present in molecule (Bacellar et al. 2015; Ana P. Castano, Demidova, and Hamblin 2004; Ezzeddine et al. 2013).

- *Polarity, asymmetry and hydrophobicity*: The degree of hydrophobicity is generally measured by Log P, defined as the logarithm of the partition coefficient of the molecule between organic solvent (e.g. octanol) and water or by simple pharmacokinetic models based on alternating aqueous and lipid compartments (Gerola, Tsubone, et al. 2011; Fábio M. Engelmann et al. 2007). As example, Pavani and co-workers demonstrated that an increase in the size of the alkyl chains around the chromophore is directly associated to a photosensitizer accumulation and enhanced photodynamic efficiency (Pavani et al. 2009). Usually, a higher asymmetry can also provide a better interaction with plasma membrane and/or organelles membranes (Fabio M. Engelmann et al. 2007; Ezzeddine et al. 2013). Engelmann and co-authors showed that binding and photodynamic efficiency is inversely proportional to the number of positively charges groups of porphyrins, except for *cis*-molecules due the amphiphilic nature of this asymmetric compound (Fabio M. Engelmann et al. 2007). The effect of side chains attached in different positions (*ortho*, *meta* and *para*) may also affect the cellular uptake and photodynamic efficiency. Ezzedine *et al*. demonstrated that cellular uptake and photodynamic efficiency of cationic hexyl isomers increase in the followed order: *para* > *meta* > *ortho* (Ezzeddine et al. 2013). This is because the variation of the position of substituents directly affects the polarity, asymmetry and hydrophobicity of compound (Ezzeddine et al. 2013).
- *Charge*: The total net charge and charge position within the molecule strongly influences the uptake and intracellular localization of photosensitizers. For example, photosensitizers with cationic side chains usually localize in mitochondria, because it has a negative electrochemical transmembrane potential (six times higher than the plasma membrane) which promotes initial electrostatic attraction to positive compounds (Jensen

et al. 2010; Pavani et al. 2009; Hoye et al. 2008; Kandela, Bartlett, and Indig 2002; Oseroff et al. 1986). On the other hand, negatively charged compounds tends to localize in lysosomes (Woodburn et al. 1991; Reiners et al. 2002; D. H. Kessel, Price, and Reiners 2012) due to actively concentrated H^+ ions (protons) that lysosomes must maintain, which results in positive electrochemical potentials. Additionally, photosensitizers that bear weakly basic amines can enter in lysosomes in their uncharged form, get protonated due to the low pH inside this organelle and become trapped in lysosomes (Zong et al. 2014; Boya and Kroemer 2008).

1.6. **Historical perspective of the development of photosensitizers (PS)**

In the 1990s, Photofrin® (Table 1.2) was the first photosensitizer approved by the Food and Drug Administration (FDA) in Canada (1993), for the treatment of bladder cancer. After that, it was approved for early stage lung cancer in Japan in 1994, for esophageal cancer in 1995, to treat early non-small cell lung cancer in 1998 and for Barrett´s esophagus in 2003 (Pushpan et al. 2002). After several PDT treatments performed with Photofrin®, scientists realized that it was far from being the ideal compound for PDT applications. The main disadvantages of using Photofrin® as PS are: (a) the long-lasting skin photosensitivity in such a way that patients may have to avoid sunlight for up to around eight weeks, (b) the low absorption in the wavelength range between 600-800nm (known as "therapeutic window"), (c) a low tumor selectivity, and (d) Photofrin® is a complex mixture of several unidentified structures (D Kessel 1986; David Kessel et al. 1987; Ana P. Castano, Demidova, and Hamblin 2004).

Because of the prolonged skin photosensitization and difficulties with topical application of Photofrin® (poor skin penetration), 5-aminolevulinic acid (Levulan®) was introduced to circumvent these problems. It was a milestone in the development of PDT; it is a porphyrin precursor and the small molecules show a better penetration into the epidermis (Kennedy,

Pottier, and Pross 1990; Szeimies and Abels 2001). The 5-aminolevulinic acid (ALA)-based drugs are not photoactive by themselves, but they are metabolized in the heme biosynthesis cycles to photosensitizing porphyrins compounds, such as Protoporphyrin IX (PpIX) (Babilas et al. 2010).

Although ALA presents some advantages compared to Photofrin®, when using ALA as precursor of Protoporphyrin (PpIX) the tumor thickness should not exceed 2 – 3 nm to induce sufficient damage on the tumor tissues portions. An alternative is the methyl ester of ALA (methyl-aminolevulinate, MAL), whose maximum intracellular concentration of protoporphyrin IX is reached after a shorter incubation time (MAL: 3h vs ALA: 4–6h) (Juzeniene et al. 2002).

The reduction of one or two of the macrocyclic peripheral conjugated double bonds in porphyrins ring give rise to chlorin and bacteriochlorin. The main advantage of this this change is a shift of the wavelength of maximum absorption to the red, facilitating light absorption in deeper sites. Because of the high absorption of melanin and hemoglobin at wavelengths < 600 nm and the high absorption of water molecules at wavelengths > 1200 nm, the wavelength range between 600 and 800 nm has been determined as "therapeutic window" for clinical PDT, considering that in wavelengths > 850-900 nm the photons may not have sufficient energy to participate in a photochemical reaction. Then, several photosensitizers of chlorin and bacteriochlorin families have been evaluated for PDT, mainly because they show a high absorption in the "therapeutic window". The approved photosensitizers based on these families include: benzoporphyrin derivative monoacid ring A (BPD-MA, Visudyne®), *meta*-tetra(hydroxyphenyl)chlorin (*m*-THPC, Foscan®), tin ethyl etiopurpurin (SnET2, Purlytin™), *N*-aspartyl chlorin e6 (NPe6, Talaporfin, Ls11) and palladium bacteriopheophorbide (WST09, Tookad®) (Ormond and Freeman 2013) - Table 1.2.

The Phthalocyanines (Pc) dyes family is suitable for photodynamic applications also mainly because of the high absorption in the "therapeutic window" (Ali and van Lier 1999). Aluminum phthalocyanine tetrasulphonate ($AlPcS_4$, Photosen®) has been approved in Russia to treat stomach, skin, lip, oral, and breast cancer. Silicon phthalocyanine (Pc4) is another photosensitizer in clinical trials for treatment of actinic keratosis, Bowen's disease, skin cancer (Ormond and Freeman 2013) - Table 1.2.

Table 1.2. Properties of some photosensitizer dyes approved for PDT treatment and used in PDT-related clinical trials.

Compound	**Trademark**	**Application**
Porfimer sodium 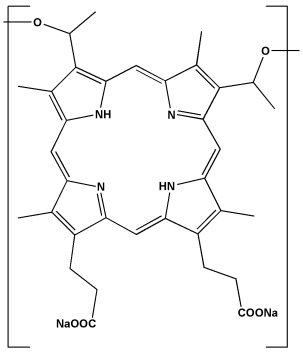	Photofrin®	Bladder cancer, esophageal cancer, lung cancer, Barrett´s esophagus
5-Aminolevulinic acid (ALA) 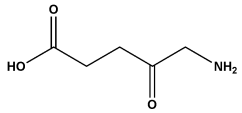	Levulan®	Actinic keratosis
Methyl-aminolevulinate (MAL) 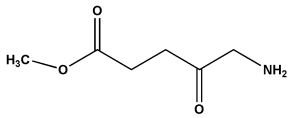	Metvix®	Actinic keratosis
Benzoporphyrin derivate monoacid ring A (BPD-MA)	Visudine®	Age-related macular degeneration

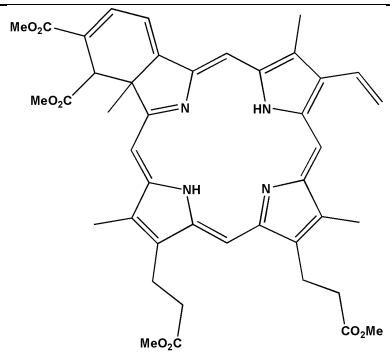		
Meta-tetra(hydroxyphexyl)chlorin (*m*-THPC) 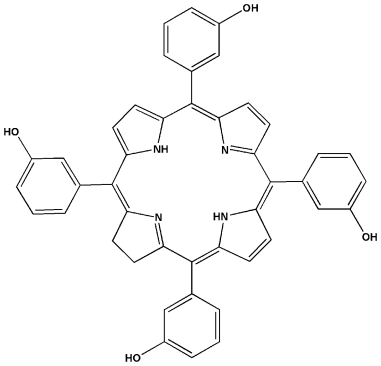	Foscan®	Neck and head cancer
Tin ethyl etiopurpurin (SnET2) 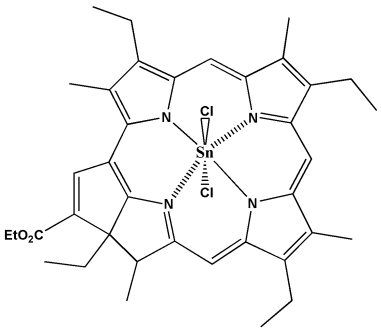	Purlytin®	Breast adenocarcinoma, basal cell carcinoma, Kaposi´s sarcoma, age-related macular degeneration
N-aspartyl chlorin e6 (NPe6) 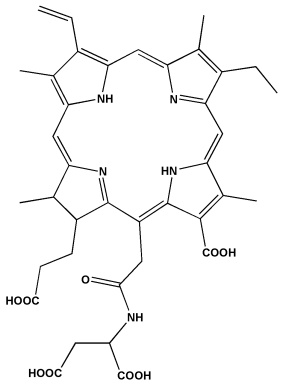	Laserphyrin®, Litx®	Lung cancer
Palladium bacteriopheophorbide (WST09)	Tookad®	Prostate cancer

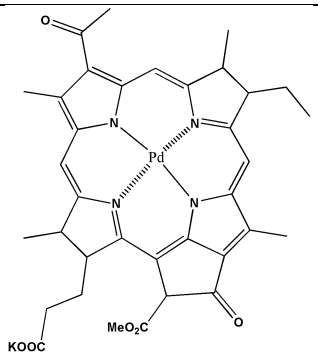		
WST11 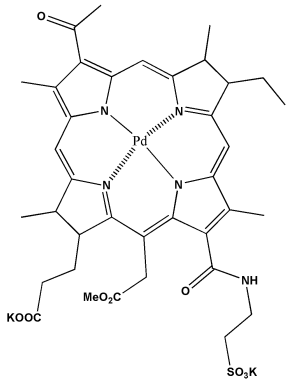	Stakel®	Prostate cancer
Aluminum phthalocyanine tetrasulphonate ($AlPcS_4$) 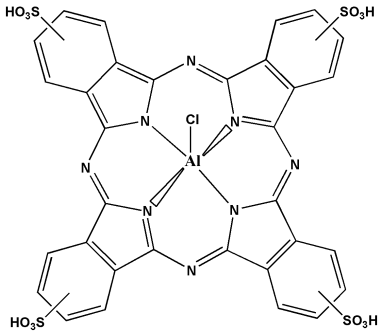	Photosens®	Stomach, skin, lips, oral cavity, tongue, breast cancer
Silicon phthalocyanine (Pc_4) 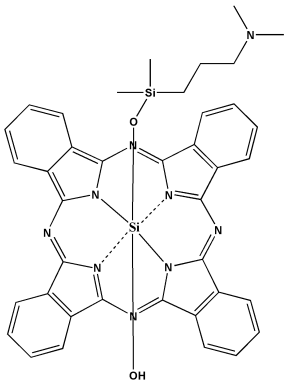	Clinical trial	Actinic keratosis, Bowen´s disease, skin cancer, mycosis fungoides

Basically, photosensitizers can be classified according to their chemical structure and generation. First generation of photosensitizers are porphyrin-based PS and included hematopophyrin and its derivatives, named hematoporphyrin derivative (HpD). Second generation photosensitizers were developed to circumvent some deficiencies of the first-generation compounds and include expanded porphyrins, chlorins, bacteriochlorins, pheophorbides and phthalocyanines. Third generation photosensitizers contain first and second generation PS conjugated to, or packaged within carrier molecules such as antibodies, liposomes and polymers in order to improve selectivity and bioavailability (Moser 1998).

Significant process has already been made in terms of developing new photosensitizers, providing some advances in clinical PDT protocols, as described in the examples above. However, some features of photosensitizer, such as low solubility, low bioavailability and low specificity still need to be overcome. Most photosensitizers are aromatic compounds with large delocalized π electron systems (e.g. porphyrins, chlorins, phthalocyanines), favoring strong π-π interactions between two molecules. This means that photosensitizers can form dimers and/or larger aggregates in aqueous media, which reduces their photoactivity due to self-quenching of the excited state (Nishiyama et al. 2009). Therefore, considerable efforts have been directed at the design of delivery systems that can incorporate photosensitizers in monomeric form without decreasing their activity and without toxic effects (see further discussion on section 1.7).

1.7. **Nanoparticles as tool for increase bioavailability of PS**

The use of several nanoparticles, including liposomes, dendrimers, polymeric nanoparticles, polymeric micelles, and hydrogel nanoparticles (Figure 1.9) has been a strategy for overcoming some of the afore-mentioned problems. The main advantages that these types of systems offer are: (i) protection of PS from premature degradation, (ii) increased PS solubility and circulation time in the bloodstream, (iii) improved intracellular penetration, (iv)

good biodegradability and biocompatibility, (v) improvement of intrinsic efficiency and (vi) controlled delivery of PS (Garapati et al. 2015; Jia and Jia 2012).

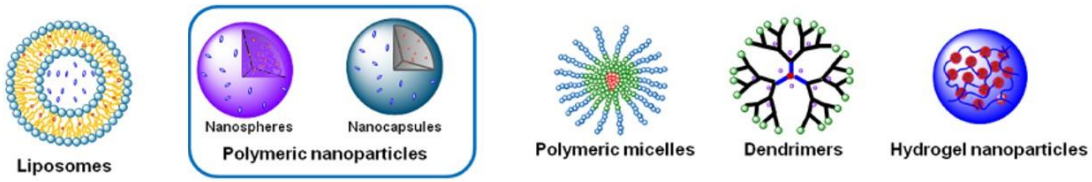

Figure 1.9. Examples of nanocarriers. Adapted from open access of Frontiers in Chemistry (Conniot et al. 2014).

One example of a nanoformulation already commercially available is the liposomal formulation of Foscan (Foslip®) which consist in 5,10,15,20-tetra(*m*-5,10,15,20-tetra(*m*hydroxyphenyl) chlorin (*m*THPC or Foscan) loaded into dipalmitoyl phosphatidylcholine/dipalmitoyl phosphatidylglycerol (DPPC/DPPG) liposomes, in a ratio of 9:1 (Buchholz et al. 2005). This liposomal formulation (Foslip®) presents a higher efficacy, reduced damage of healthy tissue and lower toxicity in the absence of light compared to the non-formulated Foscan® (Kiesslich et al. 2007; Lassalle et al. 2009). Another example of a liposomal formulation of a photosensitizer used in PDT is verteporfin (Visudyne®), the first photodynamic drug approved for the treatment of age related macular degeneration (Paszko et al. 2011). The liposomes of Visudyne® are composed of unsaturated egg phosphatidyl glycerol (EPG) and dimyristoyl phosphatidyl choline (DMPC) in a 3:5 molar ratio and are clinically used to reduce the risk of vision loss (Chang and Yeh 2012).

Our group also has previous examples for nanoparticles produced with phenothiazines or porphyrins (Tada et al. 2014; Tada and Baptista 2015; Tada et al. 2007; Rossi et al. 2008; Tada et al. 2010). For instance, in 2008 Rossi et al. proposed a nanoparticle-carrier based on silica for the photosensitizer Protoporphyrin (PpIX), aiming at an application in PDT (Rossi et al. 2008). As a result, PpIX loaded silica particles have been shown to have an efficiency of singlet oxygen generation, much higher than free PpIX. This was attributed to changes of the

monomer-dimer equilibrium due to photosensitizer immobilization in the silica nanoparticles (Rossi et al. 2008). In 2010, Tada and co-workers demonstrated that nanoparticles can be used as a tool to modulate the generation of singlet oxygen and to protect the PS from medium interferences (Tada et al. 2010). This type of modulation was based on the thionin and methylene blue at different ratios of dimer to monomer into silica nanoparticles. As a consequence, nanoparticles with an excess of dimer have a lower singlet oxygen generation efficiency than those without dimer formation (Tada et al. 2010). Both examples denote the importance of dimer/monomer ratio as a parameter that must be considered in the controlled rational design of nanoparticles to photosensitizers.

Also physicochemical properties of nanoparticles such as size, surface charge, shape, hydrophobicity, surface chemistry can influence the interaction and uptake by cells (Frohlich 2012). The nanoparticles size strongly influences the cellular uptake mechanism, dictating their ultimate intracellular fate and thus overall biological effect. Usually, nanoparticles with larger diameters (> 0.5μm) tend to be taken up via macropinocytosis and/or phagocytosis by specific cells, such as macrophages, while smaller nanoparticles (< 150nm) usually enter the cell through endocytosis via classic receptor-mediated endocytosis (clathrin-dependent) or caveolae-mediated endocytosis (Conniot et al. 2014). The nanoparticles surface charge also seems to play an important role in their particle internalization. In general, positively charged molecules/systems will show a high affinity to the cell membrane due to its negative charge. On the other hand, after cellular uptake, it has been observed that negatively charged or neutral nanoparticles tend to localize within lysosomes, whilst positively charged nanoparticles showed the ability to escape from these (Murugan et al. 2015). These physicochemical properties modulated by the molecular structures can govern the characteristics of nanoparticles (e.g. hydrophobic and charge) in such a way that manipulating these pertinent nanoparticles

characteristics may facilitate PDT applications of nanoparticles at specific target sites (Murugan et al. 2015; Conniot et al. 2014).

Recently, polymeric micelles have been especially recognized as a promising system for a photosensitizer carrier (Avci, Sibel Erdem, and Hamblin 2014). Block copolymers with amphiphilic character generally are defined as macromolecules with a large solubility difference between the hydrophilic and hydrophobic segments (see Figure 1.10). This immiscibility results in their self-assembled structure, spontaneously forming polymeric micelles (Karayianni and Pispas 2016). Then, polymeric micelles have a core-shell structure in which the inner core accommodates hydrophobic drugs, improving solubility and stability in the biological system, while hydrophilic segment provide the compatibility of the micelles in the aqueous environment (Figure 1.10) and protect the loaded drugs from interaction with blood components (Biswas et al. 2016).

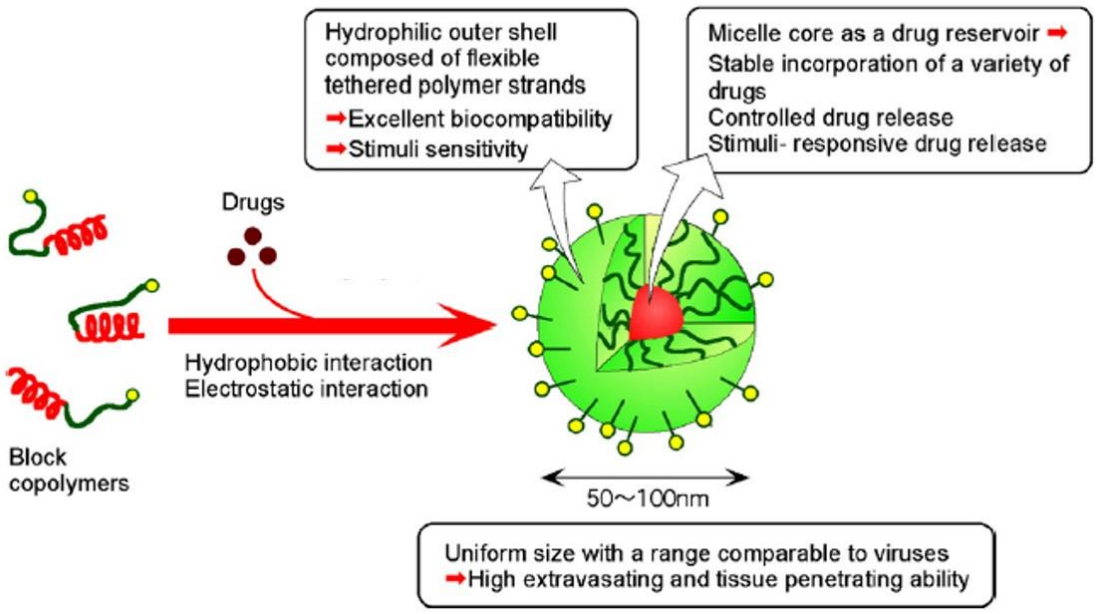

Figure 1.10. Polymeric micelles as intelligent nanocarriers. Reprinted with permission from Elsevier (Nishiyama and Kataoka 2006).

Several amphiphilic copolymers including di-block (A–B) or triblock (A–B–A) have been used to form micelles. The most common hydrophilic block in the copolymeric structure

is poly(ethylene glycol) (PEG). The PEG end blocks are well characterized and known to be non-toxic, electrically neutral, biodegradable and a flexible polymer that has commonly been used to coat nanoparticles. PEG also provides low interaction of the nanocarrier-surface with serum components (e.g. proteins) prolonging their circulation time and making it attractive for in vivo applications (Biswas et al. 2016; Nardin, Bolikal, and Kohn 2004). There are various polymer blocks used to form the inner cores of micelles such as polyethers (e.g. poly(propylene oxide) (PPO)), polyesters (e.g. poly(L-lactide) (PLA)) and polyamino acids (e.g. poly(L-histidine) (pHis)). As example, Li and coworkers described a formulation of protoporphyrin XI (PpIX) with $MePEG_{500}$-b-PCL_{4100} (methoxy poly (ethylene glycol)-b-poly-caprolactone) diblock copolymer, able to keep the subcellular localization (in or around the plasma membrane) and increase the cellular uptake (around two-fold magnitude) and the phototoxicity (one order of magnitude using 18 J/cm^2) in RIF-cells when compared to free PpIX (Li et al. 2007). Another example of better results in PDT by using polymeric micelles was reported by Knop *et al*. who showed that the pheophorbide-a incorporated in poly(ethyleneoxide-b-ε-caprolactone) micelles was able to efficiently generate singlet oxygen in the medium and also showing an enhanced photocytotoxicity (*ca* 2-fold) and cellular uptake compared to free pheophorbide-a. They explain this by to the incorporation of unaggregated monomeric molecules of the PS in the polymeric micelles, i.e. 200 molecules of polymer and 4 molecules of monomeric pheophorbide-a per nanostructure (Knop et al. 2009). These examples suggest that formulation of photosensitizers with polymeric micelles may allow a higher PDT efficiency that can be achieved at a reduced dose of photosensitizer and light.

Using amino acids as hydrophobic core has the advantage of biocompatibility and biodegradability, due to the use of naturally occurring amino acids (Biswas et al. 2016). Kohn´s group has demonstrated the applicability of an amphiphilic triblock copolymer (ABA-type) made of poly(ethylene glycol) and oligomers of desaminotyrosyl-tyrosine esters in the

treatment of skin diseases such as psoriasis (Zhang et al. 2013a). This type of triblock copolymer forms a nanoparticle family that is fully-degradable and nontoxic *in vitro* and *in vivo* (Larisa Sheihet et al. 2012; Nardin, Bolikal, and Kohn 2004). These tyrosine-derived nanospheres (Tyrospheres) provide a hydrophobic core, a naturally compatible environment for loading hydrophobic compounds together with hydrophilic shells (PEG) that stabilizes the nanospheres. Further details about Tyrospheres are provided in the introduction of Chapter 4.

1.8. OBJECTIVES

The overall goal of this thesis is to uncover mechanisms to improve the PDT efficiency by causing specific damage and controlled cell death. The specific objectives cited bellow will be discussed in three different chapters:

- *Chapter 2 – Membrane interaction of amphiphilic photosensitizers*: Investigate the interaction and photoactivity of several amphiphilic photosensitizers with membranes model in order to figure out which molecular features can improve PS uptake;
- *Chapter 3 – Modulating PDT efficiency by the charge of the photosensitizer*: Study the effect of two photosensitizers with similar structure but opposite charges in the intracellular localization, mode of cell death and phototoxicity aiming understand which subcellular target can provide enhanced phototoxicity with minimum PDT-dose;
- *Chapter 4 – Enhanced PDT efficiency provided by tyrosine-derived nanospheres*: Evaluate if tyrosine-derived nanospheres can improve solubility and bioavailability of PS as well the PDT efficiency in cells.

CHAPTER 2

MEMBRANE INTERACTION OF AMPHIPHILIC PHOTOSENSITIZERS

The level of interaction between photosensitizers and membranes was evaluated by binding and photoactivity assays using different membrane mimic systems, which were small unilamellar liposomes and giant unilamellar vesicles and erythrocytes from human blood. Our results give insights about the structure-photoactivity relationship allowing the choice of two PS with better interaction and stronger photoactivity in terms of membrane damage to continue studies in eukaryotic cells.*

* Part of the work presented in this chapter is derived from submitted paper to *Scientific Reports*. "Enhanced efficiency of cell death by lysosome-specific photodamage." Tayana M. Tsubone, Waleska K. Martins, Christiane Pavani, Helena C. Junqueira, Rosangela Itri and Maurício S. Baptista.
This work was presented as poster on *37ª Reunião Anual da Sociedade Brasileira de Química* in May 2014 at Natal – Brazil and in *16th International Congress on Photobiology* in September 2014 at Cordoba - Argentina.

2. MEMBRANE INTERACTION OF AMPHIPHILIC PHOTOSENSITIZERS

2.1. INTRODUCTION

Membranes exhibit an important role in organisms, mainly organizing tissues, cells and organelles. In the case of cell membranes, the role of the cytoplasmic membrane is maintaining the physical integrity of the cell and controlling the movement of molecules and/or ions into and out of cells. Consequently, recognition, binding, and permeation of molecules are a fundamental research topic in terms of new drugs design. In PDT, the role of membrane binding of photosensitizers (PS) is crucial to the extension of photo-induced damage and consequently to the efficiency of cell death (Pavani, Iamamoto, and Baptista 2012; Bacellar et al. 2014; Oliveira et al. 2011). Because the lifetime of $^1O_2$ is short and its diffusion distance is limited, a PS localization strategically close to the target is always desirable (Robert W Redmond and Kochevar 2006).

In this regard, new photosensitizers have been developed in the search of more efficient compounds for photodynamic therapy (PDT). Many structural changes have been made in the chromophore and the peripheral groups, trying to improve the efficiency of reactive species generation by light and improving the proximity to targets such as cellular membranes and/or organelle membrane (Uchoa, Oliveira, and Baptista 2010; Uchoa et al. 2011; Gerola, Tsubone, et al. 2011; F. Ricchelli 1995). Many studies on the interaction of photosensitizers with cells or organisms indicate that the degree of hydrophobicity, the type and number of charges and the degree of structural asymmetry in a molecule, plays an important role in the PS-membrane interaction, intracellular localization and cell-killing efficiency (Mojzisova et al. 2009; Ana P. Castano, Demidova, and Hamblin 2004).

Engelmann and collaborators reported a detailed study comparing the efficiency of a series of porphyrins in photodamaging erythrocyte membranes and demonstrated that

amphiphilic molecules are able to penetrate deeply in membranes and increase the photodynamic efficiency (Figure 2.1) (Fabio M. Engelmann et al. 2007). In fact, Cordeiro *et al.* confirmed this hypothesis by molecular dynamic simulations (Cordeiro, Miotto, and Baptista 2012). They showed that the accessibility of the photosensitizer to the membrane interior rich in oxygen was correlated with membrane interaction and photodynamic efficiency (Cordeiro, Miotto, and Baptista 2012).

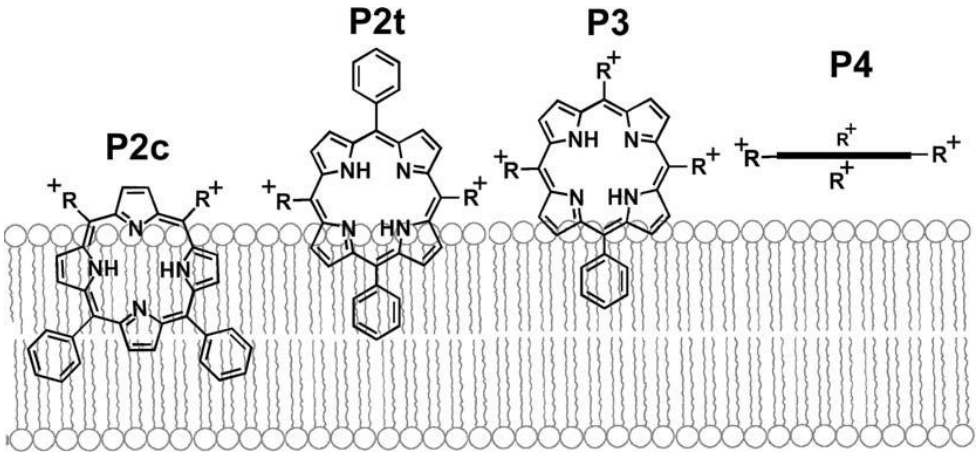

Figure 2.1. Scheme showing the probable disposition in biological membranes of porphyrins with the different number of charges and symmetry. P2c: meso-di-cis(4-N-methyl-pyridyl)diphenylporphyrin, P2t: meso-trans-cis(4-N-methyl-pyridyl)diphenylporphyrin, P3: meso-tri(4-N-methyl-pyridyl)monophenylporphyrin, P4: meso-tetra(4-N-methyl-pyridyl)porphyrin. Reprinted by permission from Springer (Fabio M. Engelmann et al. 2007).

Based on this premise, herein we worked with four amphiphilic compounds (Figure 2.2) with different charges and peripheral groups in order to understand their influence on the membrane interaction and the consequences on photo-induced damage. In this study the effect of opposite charges and different substituent groups is investigated. Firstly, we synthesized a porphyrin derivative from Protoporphyrin IX (PpIX) whose carboxylic groups from positions 13^3 and 17^3 were modified to a quaternary ammonium compound (PpNetNI), generating an amphiphilic structure with positive charges to facilitate the interaction with the membrane (Uchoa, Oliveira, and Baptista 2010). In addition to the synthesized porphyrin (PpNetNI), three other commercial amphiphilic photosensitizers were included in the study (CisDiMPyP, $TPPS_{2a}$

and $AlClPcS_{2a}$) in such way that we compare the different peripherical groups from two positive amphiphilic porphyrins and two negative amphiphilic compounds (Figure 2.2).

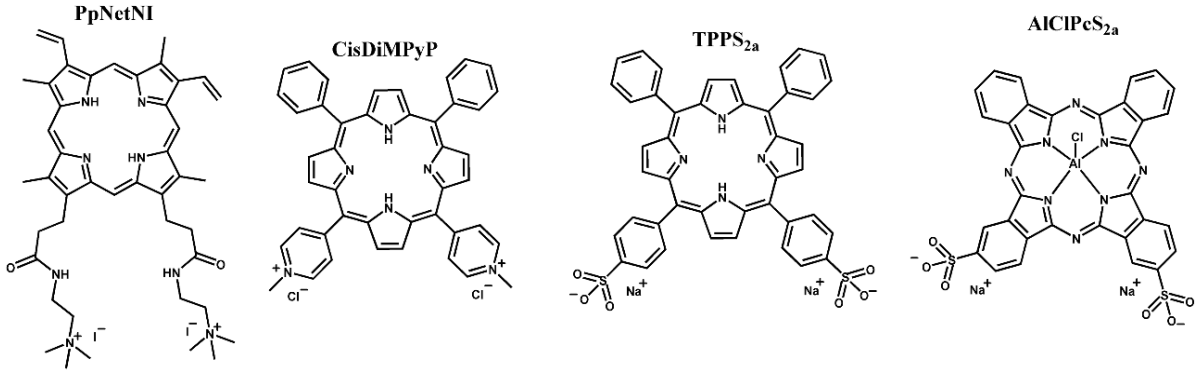

Figure 2.2. Molecular structure of the amphiphilic photosensitizers studied in this work (PpNetNI, CisDiMPyP, $TPPS_{2a}$ e $AlPcS_{2a}$).

2.2.METHODOLOGY

2.2.1. Synthesis of PpNetNI

The functionalization of PpIX was performed in three steps. Firstly, 200mg PpIX were refluxed under a dry argon atmosphere with an excess of freshly-distilled thionyl chloride (2 mL). The system was refluxed during 1 hour, the solvent and the excess of thionyl chloride were removed by suction at reduced pressure. Second, the purple residue formed was cooled to 0ºC under an argon atmosphere and stirred with an excess of nucleophilic compound (N,N-dimethylethylamine). The system was stirred for 12 hours and the solvent was removed by suction at reduced pressure. Then, the product was purified by column chromatography using silica as stationary phase and dichloromethane/methanol = 20:1 (v/v) as mobile phase. In a third step, the quaternization of PpNetNA was carried out in dichloromethane using methyl iodide. Purification was accomplished by crystallization in dichloromethane/methanol (Uchoa, Oliveira, and Baptista 2010).

2.2.2. Photophysical properties

Absorption spectra were registered using a Shimadzu UV-2400-PC spectrophotometer. Molar absorptivity values (ε) were determined in methanol by plotting the absorption in the maximum wavelength (λ_{max}) as a function of PS concentration and applying Lambert-Beer's law. Fluorescence spectra were recorded with a Varian Cary Eclipse spectrofluorimeter (excitation at 515 nm, slits: 5 nm on excitation and 10 nm on emission). The fluorescence quantum yields (ϕ_f) of the photosensitizers in methanol were calculated by measuring the area under emission spectrum, using $TPPS_4$ in methanol (ϕ_f = 0.16) as standard for the porphyrins and Methylene blue in methanol (ϕ_f = 0.03) as standard for phthalocyanine (Basu 1991; Olmsted 1979). Absorbance values of samples and reference solutions were kept below 0.1 at the excitation wavelength, in order to avoid inner filter effects. The singlet oxygen production quantum yield (ϕ_Δ) of the photosensitizers in methanol was determined using an Edinburgh Analytical Instruments time resolved NIR fluorimeter equipped with a Hamamatsu R55009 photomultiplier cooled by liquid nitrogen (-80ºC), using the F900 6.8.12 acquisition software (Edinburg Instruments). A Continuum Surelite III Nd:YAG laser (wavelength: 532 nm; pulse duration: 5 ns; pulse frequency: 10 Hz, Q-switch 240 ns) was used to excite a dye laser with (2-{2-[4-(dimethylamino)phenyl]ethenyl}-6-methyl-4H-pyran-4-yl-idene)propanedinitrile in ethanol emitting at 640 nm (Continuum Jaguar). $TPPS_4$ in methanol (ϕ_Δ = 0.69) was used as standard for the porphyrins and Methylene blue (ϕ_Δ = 0.50) was used as standard for the phthalocyanines (R W Redmond and Gamlin 1999). All samples had an absorbance of ~0.3 at 640 nm, in order to equalize the number of absorbed photons. ϕ_Δ values were calculated using the equation 2.1.

$$\phi_\Delta^{PS} = \frac{I_{PS}}{I_{Std}} . \phi_\Delta^{Std} \qquad \text{Equation 2.1}$$

I is the maximum phosphorescence intensity of the singlet oxygen decay curve and ϕ_Δ is the singlet oxygen quantum yield. Symbols as subscript refer to the standard (Std) and photosensitizer (PS).

2.2.3. PS binding to membranes

2.2.3.1. Binding constant (K_b)

Liposome suspensions were prepared with 20% cardiolipin (heart-disodium salt, CL) and 80% 1,2-distearoylsn-glycero-3-phosphocholine (DSPC). 6.3 mg (8 μmols) DSPC and 3 mg (2 μmols) CL were dissolved in chloroform, which was evaporated under argon flux, producing a film. Next, 2 mL of 5 mM Tris/HCl buffer solution (pH 7.4) was used for hydration and the system was vortexed for 5 minutes. Heavier liposomes were isolated by three consecutive cycles of sedimentation (centrifugation at 13500 rpm for 10 min, 25ºC). The supernatant (containing smaller vesicles) was discarded and the pellet was re-suspended with an equivalent volume of buffer solution. After repeating this procedure three times, the final lipid concentration was determined by the molybdate method (Rouser, Fleischer, and Yamamoto 1970). The phospholipid concentration in this solution was 0.1 mM. These suspensions were incubated with the photosensitizers (~7 μM) for 1 hour followed by a further centrifugation step to separate the aqueous fraction, containing free PS and the liposomal fraction containing bound PS (Fabio M. Engelmann et al. 2007). The concentrations of free and bound porphyrins were determined by measuring the absorption spectra of the supernatant solution and the liposomes resuspension. The PS binding constants (K_b) to membranes were calculated as described in Engelmann et al (Fabio M. Engelmann et al. 2007).

2.2.3.2. PS binding percentage to lecithin vesicles

30 mg of soy lecithin was dissolved in chloroform, dried in argon flux and the film was hydrated with 5 mM Tris/HCl buffer (pH 7.4). The cycles of sedimentation already described

above were performed to obtain the liposome resuspension. Liposomes were incubated in the presence of photosensitizers (~7 µM) for 15 minutes followed by centrifugation to separate the aqueous fraction containing free PS from the liposomal fraction containing bound PS. The absorption spectrum of the supernatant solution and the liposome resuspension were recorded and Equation 2.2. was used to calculate binding percentage.

$$\%\, Binding = 100\ \frac{Abs_t - Abs_s}{Abs_t} \qquad \text{Equation 2.2}$$

where Abs_t is the absorbance of photosensitizer in the liposome-free solution (total amount of photosensitizer) and Abs_s is absorbance of PS solution in the supernatant (free-photosensitizer).

2.2.3.3. Binding percentage of photosensitizers in erythrocytes

5 mL of human blood were aspirated in a syringe containing ~ 4 drops of sodium citrate solution (0.13 M) in phosphate buffer (pH 7.4) to prevent blood coagulation. The blood was centrifuged at 3000 rpm for 10 minutes at 25°C. Then, the supernatant was discarded and the pellet was re-suspended with the same volume of phosphate buffered saline (PBS – pH 7.4). This procedure was repeated three times to isolate erythrocytes and remove proteins, white blood cells, platelets and coagulation factors (such as Ca^{2+}) (Fabio M. Engelmann et al. 2007). Erythrocytes (~1x10^7 erythrocytes/mL) were incubated with the photosensitizers (7 µM) for 20 minutes followed by centrifugation (3000 rpm, 10 minutes at 25°C) to separate the aqueous fraction containing free photosensitizer from the erythrocytes containing bound photosensitizers (Fabio M. Engelmann et al. 2007). Since the presence of the heme group in erythrocytes presents an absorbance spectrum similar to our porphyrins, but shows no fluorescence emission, we used the fluorescence spectrum to calculate the difference between free and bound PS using Equation 2.3.

$$\% \text{ Binding} = 100 \frac{F_t - F_s}{F_t} \qquad \text{Equation 2.3}$$

where F_t is fluorescence spectrum area of photosensitizer solution pre-interaction with erythrocytes (total amount of photosensitizer) and F_s is fluorescence spectrum area of photosensitizer solution in the supernatant (free-photosensitizer).

2.2.4. Photoactivity of photosensitizers in membranes

2.2.4.1. Erythrocytes

The centrifugation process was performed three times to isolate erythrocytes as described above in *Binding percentage of photosensitizers in erythrocytes*.(Fabio M. Engelmann et al. 2007) The final erythrocyte pellet was re-suspended in phosphate buffered saline (PBS – pH 7.4), and then diluted with PBS buffer to reach a scattering intensity of ~ 1.0 in 650 nm. Erythrocytes in the absence and presence of photosensitizers (7 μM) were irradiated using a light emitting diode system (LED), with the maximum emission wavelength at 522 nm ± 20 nm (wavelength ± spectral width) to porphyrins and 633 nm ± 20 nm to phthalocyanine whose final light dose was 2.1 J/cm^2. The decrease in the suspension light scattering was monitored at 650 nm as a function of the time using an Infinite M200 plate reader.

2.2.4.2.Giant unilamelar vesicles (GUVs)

GUVs of 1,2-dioleoyl-sn-glycero-3-phosphocoline (DOPC) were prepared by using the electroformation method.(Angelova and Dimitrov 1986) For this, 10 μL of a 2.5 mM lipid solution (DOPC) in chloroform were spread onto the surfaces of two conductive slides coated with Fluor Tin Oxide. The slides were placed spaced apart in a Teflon frame with their conductive sides facing each other. The chamber was filled with 0.2 M sucrose aqueous solution and connected to a sine wave generator at 2 V and 10 Hz for 2 hours. After this period the dispersion of GUVs was collected and diluted 15-fold in a 0.2 M glucose solution according to the previous procedure (Mertins et al. 2014; Caetano et al. 2007).

GUVs were observed by phase contrast microscopy (inverted microscope Axiovert 200, Carl Zeiss) in the absence and presence of photosensitizers (0.7 μM) under constant irradiation. The observation of GUVs was performed using Ph2 63x objective and the images were registered with an Axiocam HSm digital camera (Carl Zeiss). The irradiation of the samples was performed using the Zeiss Filter Set 05 (excitation BP 395-440 nm, 460nm beam splitter mirror FT, 470nm emission long-pass filter, 135 μW/cm^2) for porphyrins and the Zeiss Filter Set 32 (excitation BP 665/45 nm, beam splitter FT 695nm, emission BP 725/50nm, 135 μW/cm^2) for phthalocyanine. The effects induced by PS photoirradiation of the GUV were fading of the optical contrast. This was quantified by taking into account the changes in the brightness intensity using the *Image J* software ((Mertins et al. 2014).

2.3. RESULTS AND DISCUSSION

2.3.1. Synthesis and characterization of PpNetNI

PpNetNI was synthesized by functionalization of carboxylic groups at positions 13^3 and 17^3 from Protoporphyrin IX (PpIX), the synthetic route is illustrated in Figure 2.3. As the first step the carbonylic groups of PpIX were transformed to acyl chloride as shown in Figure 2.3. In a second step, the reaction between chloride and N,N- dimethylethylamine generated amine groups (PpNetNA in Figure 2.3), whose the quaternization using methyl iodide resulted on the quaternary ammonium compound (PpNetNI in Figure 2.3).

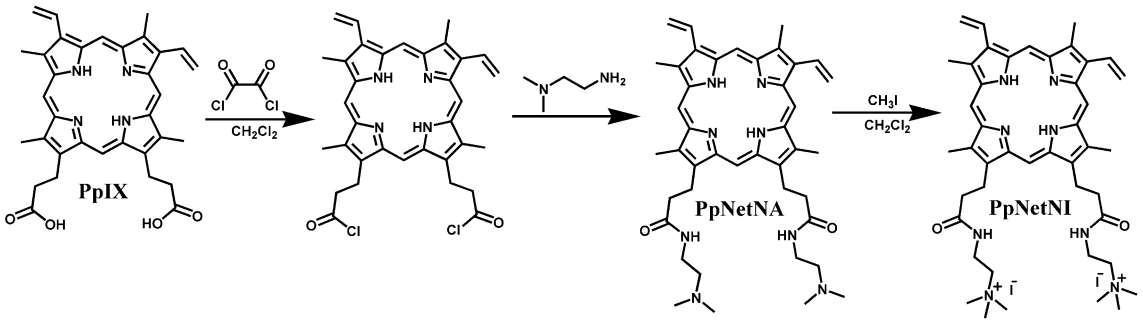

Figure 2.3. Synthetic route to the production of PpNetNI. Reprinted and adapted with permission from (Uchoa, Oliveira, and Baptista 2010).

The characterization of PpNetNI was performed by elemental analysis, mass spectrometry and ^{1}H NMR. The results of the elemental analysis confirmed PpNetNI as final product (Table 2.1). Note that the difference between the experimental values and theoretical values were less than 2% indicating a satisfactory result (Table 2.1).

Eletrospray ionization mass spectrometry (ESI-MS) showed five main peaks: a higher peak at m/z 366.24 followed by four other isotopic peaks with Δm/z 0.5 (Figure 2.4). The number of isotope peaks and the relative intensity of each peak depends on the chemical formula of the ionic fragment and the natural isotopic composition of its constituting elements. The highest peak corresponds to isotopes with the lowest mass numbers that predominate in the nature (i.e. ^{12}C, ^{1}H, ^{14}N and ^{16}O) and represent our base peak (or 100.0% of $^{12}C_{44}{}^{1}H_{60}{}^{14}N_{8}{}^{16}O_{2}$ with mass = 732.48 and charge = +2). The next intensive peak is at m/z 366.74 which represents 51.7% isotopes which can be attributed to the isotope of carbon (i.e. $^{13}\underline{C_{1}}{}^{12}C_{43}{}^{1}H_{60}{}^{14}N_{8}{}^{16}O_{2}$), hydrogen (i.e. $^{12}C_{44}{}^{2}\underline{H_{1}}{}^{1}H_{59}{}^{14}N_{8}{}^{16}O_{2}$), nitrogen (i.e. $^{12}C_{44}{}^{1}H_{60}{}^{15}\underline{N_{1}}{}^{14}N_{7}{}^{16}O_{2}$) and/or oxygen (i.e. $^{12}C_{44}{}^{1}H_{60}{}^{14}N_{8}{}^{17}\underline{O}{}^{16}O$). The peak at m/z 367.24 correspond to 12.0% of isotopes and may be contributed by oxygen (i.e. $^{12}C_{44}{}^{1}H_{60}{}^{14}N_{8}{}^{18}\underline{O}{}^{16}O$). The last two peaks have a negligibly low intensity (m/z 367.74 is 2.1% and m/z 368.24 is 1.9%) because of the extremely low probability of occurrence.

Table 2.1. Elemental analysis data of carbon, hydrogen and nitrogen.

Compound	% C Exp (calc)	% H Exp (calc)	% N Exp (calc)
PpNetNI	48.95 (50.43)	5.97 (5.83)	11.59 (10.46)

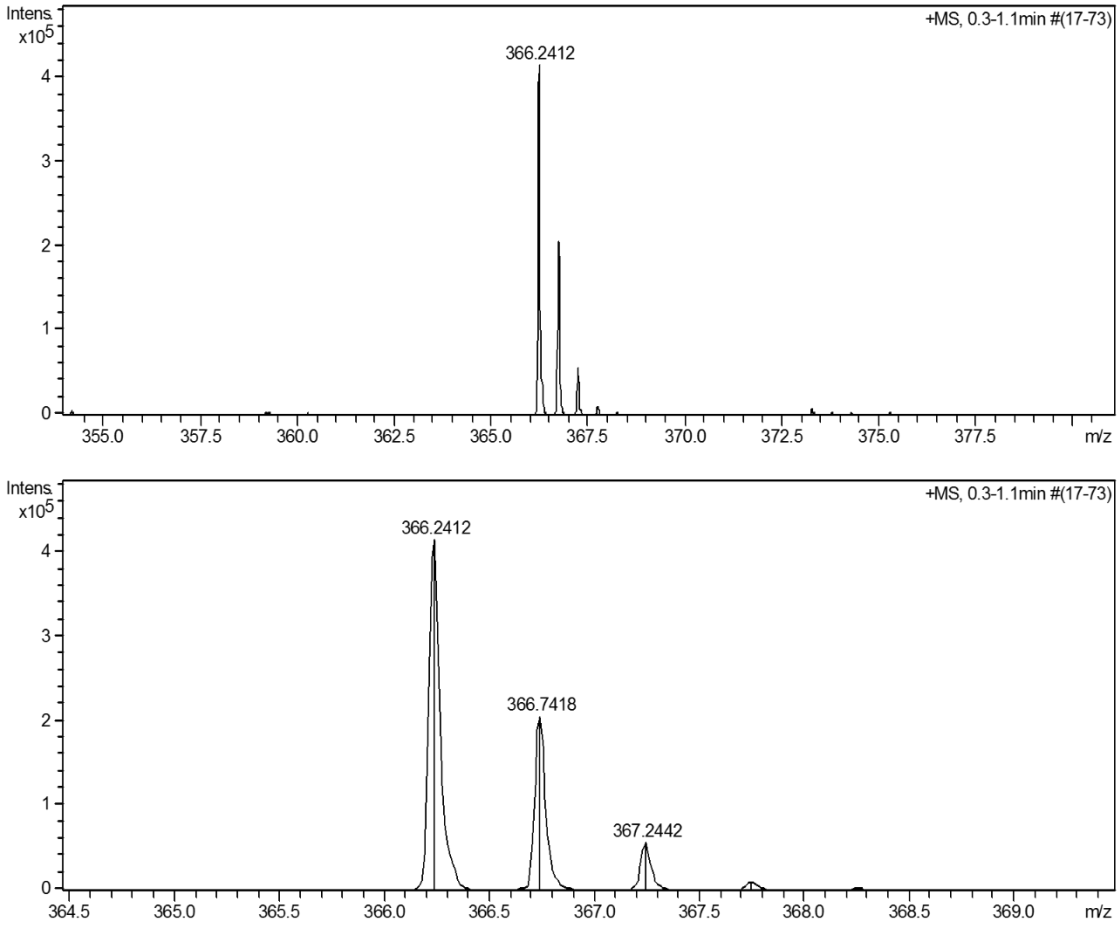

Figure 2.4. Mass spectrometry of PpNetNI.

The nuclear magnetic resonance of proton (^{1}H NMR) identified the signals of the synthesized compound, also confirming the production of PpNetNI (the ^{1}H NMR spectrum is showed in Appendix I). The two intense singlet signals at 1.68 ppm and 1.70 ppm (Figure 2.5A) were attributed to hydrogens 1, 2, 3 and 1', 2', 3' of quaternary ammonium. Also, two triplets at 1.91 ppm and 1.88 ppm of hydrogens 4 and 4' next to quaternary ammonium (Figure 2.5A) were observed. The triplet signal at 4.51 ppm represent hydrogens 5 and 5' (Figure 2.5C). The four signals from a singlet localized at 3.76 ppm, 3.74 ppm, 3.72 ppm and 3.70 ppm correspond

to hydrogens e, f, g and h of methyl next to the porphyrin chromophore (Figure 2.5D). Hydrogens i and j from the vinyl groups cause 4 signals, a dublet of dublets, at 6.40 ppm, 6.36 ppm, 6.20 ppm and 6.17 ppm (Figure 2.5E). Hydrogens of meso positions (a, b, c and d) were detected as singlet signal at 10.34 ppm, 10.28 ppm, 10.25 ppm and 10.22 ppm (Figure 2.5B).

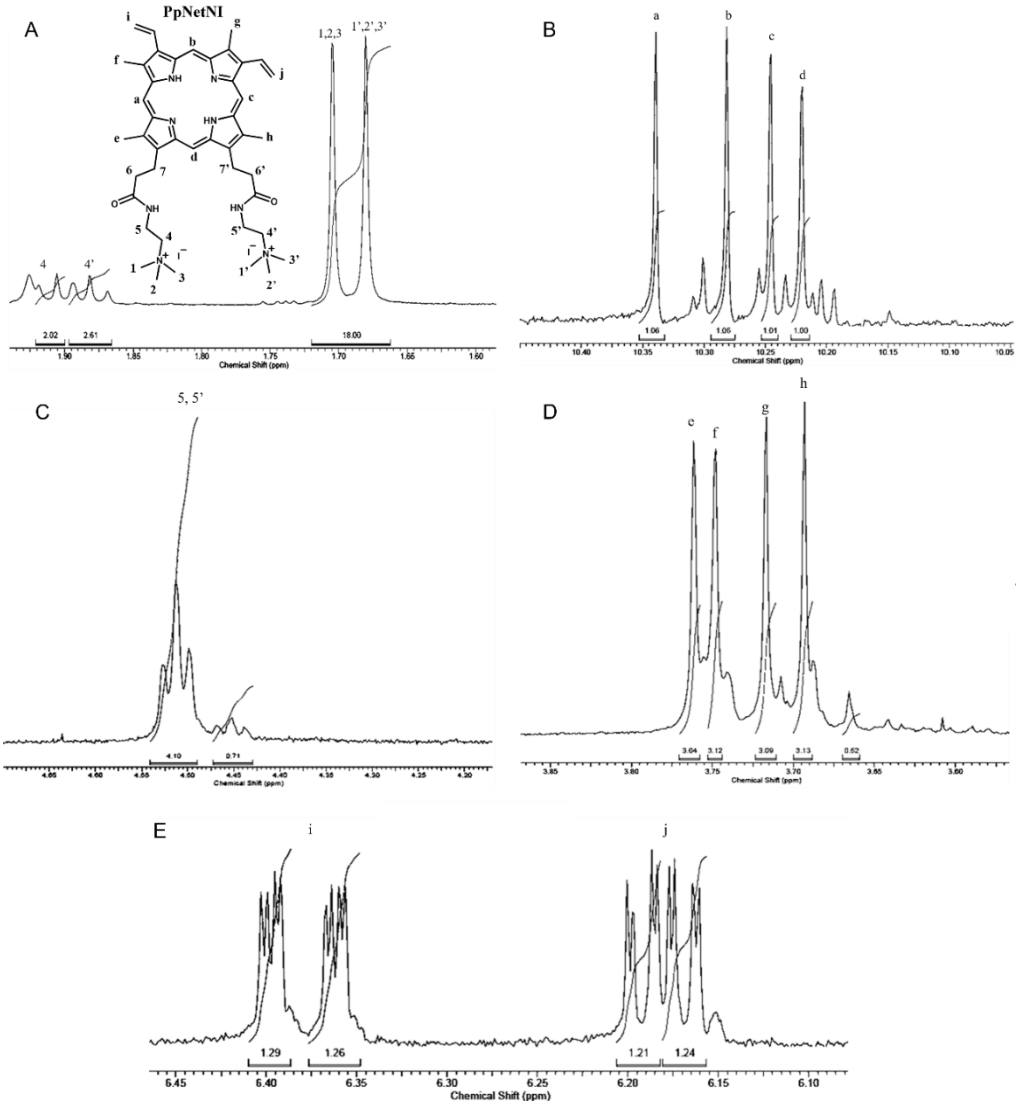

Figure 2.5. NMR ^{1}H spectrum of PpNetNI in MeOD. Chemical shift range of (A) 1.6 – 2.0 ppm, (B) 10.10 – 10.40 ppm, (C) 4.20 – 4.65 ppm, (D) 3.60 – 3.85 ppm and (E) 6.10 – 6.45 ppm.

The reaction yield was around 84% (0.21g of PpNetNI), which is similar to that found by Uchoa et al. (Uchoa, Oliveira, and Baptista 2010).

2.3.2. Spectroscopy and photophysical studies

All four PS exhibit typical photophysical properties, as expected from these class of compounds. PpNetNI, CisDiMPyP and $TPPS_{2a}$ have absorption spectra typical for free-base porphyrins (Figure 2.6.A), exhibiting a high intensity band known as Soret band, which results from transitions of the fundamental state to the second excited state ($S_0 – S_2$) and four (less intense) Q bands, which are caused by transitions from the fundamental state to the first excited state ($S_0 – S_1$) – (Bajema, Gouterman, and Meyer 1968). Unlike porphyrins, the spectrum of the phthalocyanine ($AlClPcS_{2a}$) has a higher intensity of the Q band (Figure 2.6.A) that represents a transition from the fundamental state to the first excited state ($S_0 – S_1$) - (Bajema, Gouterman, and Meyer 1968). Values of the absorption maxima and molar absorption coefficients (ε) are presented in Table 2.2.

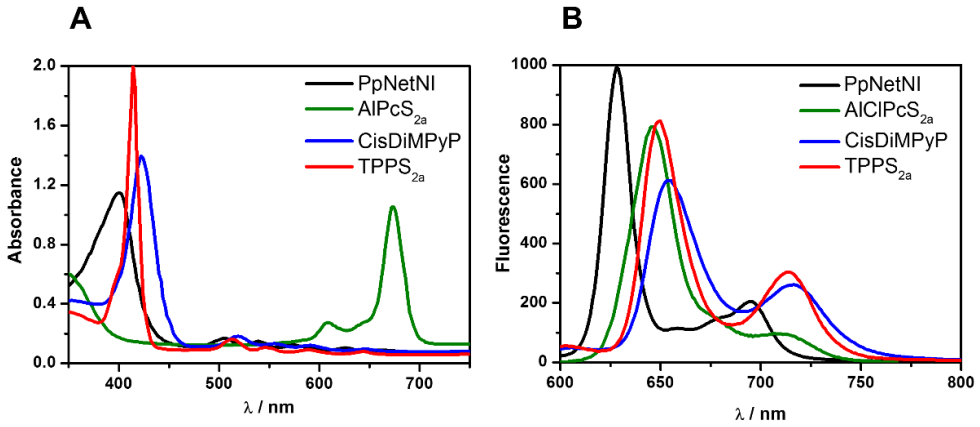

Figure 2.6. (A) Electronic absorption spectra of photosensitizers in methanol. PS concentrations: 9.5 µM PpNetNI, 5 µM $AlPcS_{2a}$, 8 µM CisDiMPyP, 5 µM $TPPS_{2a}$. (B) Fluorescence emission spectra of photosensitizers in methanol. (λ_{exc} = 502 nm for PpNetNI, λ_{exc} = 603 nm for $AlClPcS_{2a}$, λ_{exc} = 513 nm for CisDiMPyP and $TPPS_{2a}$).

The fluorescence emission spectra of the photosensitizers (Figure 2.6B) show two emission bands, which corresponds to transitions of the excited state to ground state. All porphyrins have very similar fluorescence spectra with small fluorescence quantum yields (ϕ_f < 0.15 - Table 2.2) indicating that fluorescence is not the main decay process of these molecules. On the other hand, the phthalocyanine shows values of ϕ_f, which are two times

greater than those of the porphyrins (ϕ_f < 0.24 - Table 2.2). This is due to higher rigidity of the phthalocyanine molecular structure compared with the molecular structure of porphyrins (Joseph R. Lakowicz 2006).

Table 2.2. Molar absorptivity values (ε) in the maximum absorption wavelength (λ_{max}), emission bands, fluorescence (ϕ_f) and singlet oxygen quantum yields (ϕ_Δ) of each photosensitizer.

PS	*Absorption λ_{max}/nm ($\varepsilon/10^3 M^{-1}cm^{-1}$)*					*Emission λ/nm*		ϕ_f *	ϕ_Δ **
	Soret	**Q_{IV}**	**Q_{III}**	**Q_{II}**	**Q_I**	**Q_I**	**Q_{II}**		
PpNetNI [a]	399 (120)	502 (10)	536 (7.5)	572 (4.5)	627 (3.2)	628	695	0.12 ± 0.04	0.72 ± 0.04
CisDiMPyP [a]	422 (171)	517 (14)	554 (7.3)	590 (6.0)	646 (2.5)	658	717	0.11 ± 0.03	0.74 ± 0.09
$TPPS_{2a}$ [a]	413 (450)	511 (17)	545 (7.5)	588 (4.2)	645 (3.5)	652	714	0.13 ± 0.03	0.71 ± 0.05
$AlPcS_{2a}$ [b]	350 (55)	-----	603 (30)	-----	670 (188)	645	712	0.24 ± 0.05	0.40 ± 0.02

**λ_{exc} = 640 nm e λ_{em} = 1270 nm. *Porphyrins: λ_{exc} = 513 nm; emission > 600nm, Slits: 5 nm on excitation and 10 nm on emission, methanol solutions; Phthalocyanine: λ_{exc} = 603 nm, Slits: 2.5 nm on excitation and 5 nm on emission. [a]Standard used was $TPPS_4$ ϕ_Δ = 0.69 (R W Redmond and Gamlin 1999) and $TPPS_4$ ϕ_f = 0.16 (Basu 1991). [b]Standard used was MB ϕ_Δ = 0.50 (R W Redmond and Gamlin 1999) and ϕ_f = 0.03 (Olmsted 1979).

While the fluorescence quantum yields (ϕ_f) of the porphyrins are low, the singlet oxygen quantum yields are very high. In fact, all these tested porphyrins are very efficient generators of $^1O_2$ ($\phi_\Delta \sim 0.7$), demonstrating that the different peripheral groups do not significantly affect their photophysical properties (Table 2.2). However, the $AlClPcS_{2a}$ does not generate $^1O_2$ as efficient as the porphyrins (ϕ_Δ = 0.4 - Table 2.2). Note that the consequence of the higher absorption in red region of phtalocyanines is that the radiative lifetimes of the lowest excited singlet states are shorter, which means higher fluorescence quantum yields (ϕ_F) and shorter excited singlet-lifetimes. This situation results in lower quantum yields for formation of the excited triplet state (ϕ_T) and consequently lower $^1O_2$ generation (Darwent et al. 1982).

In summary, the photophysical data indicates that porphyrins have high extinction coefficients; low fluorescence quantum yields and are efficient generators of $^1O_2$. On the other hand, phthalocyanine has a lower $^1O_2$ generation and a higher fluorescence quantum yield.

These results are in agreement with other literature reports that show that porphyrins with a high absorption intensity in the Soret band, exhibit lower fluorescence quantum yields (Seybold and Gouterman 1969) and a high efficiency of $^1O_2$ generation (R W Redmond and Gamlin 1999; Wilkinson, Helman, and Ross 1993). The phthalocyanines with a high absoprtion in the Q band have higher values of fluorescence quantum yields (Ogunsipe, Maree, and Nyokong 2003; Ambroz et al. 1991) and a lower generation of $^1O_2$ (R W Redmond and Gamlin 1999; Wilkinson, Helman, and Ross 1993).

2.3.3. Evaluation of photosensitizer affinity to membranes

The interaction of drugs with cells occurs by the initial binding of the drug to the cytoplasmic membrane as well as by their ability to enter and permeate membranes. Thus, it is important to understand the photosensitizer-membrane interaction. Moreover, the level of interaction of a photosensitizer with membranes has a fundamental role in the extension of photo-induced damage and consequently, on the cell-killing efficiency (Fernanda Ricchelli et al. 2005; Bacellar et al. 2014; Pavani, Iamamoto, and Baptista 2012; Gerola, Santana, et al. 2011). Therefore, we evaluate the interaction level of PS to membranes using three different systems: vesicles containing DSPC/CL (8:2), soy-lecithin liposomes and erythrocyte membranes (Figure 2.7).

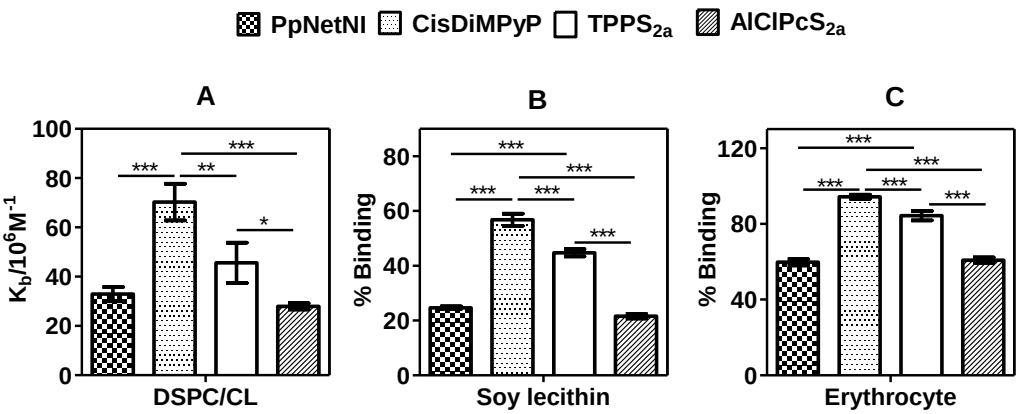

Figure 2.7. (A) Binding constant (K_b) to DSPC/CL vesicles (8 µmol of DSPC and 2 µmol CL in 2mL of 5 mM Tris buffer at pH 7.4). (B) Percentage of binding to soy lecithin vesicles (0.12 mM soy lecithin in 5 mM Tris buffer at pH 7.4), (C) Percentage of binding to erythrocytes ($1x10^7$ erythrocytes/mm^3 in PBS pH 7.4). [Photosensitizer] = 7 µM. Bars represent the mean ± SD (*p<0.05, **p<0.03 and ***p<0.001).

Although all photosensitizers exhibit amphiphilic characteristics, note that $AlPcS_{2a}$ and PpNetNI have a lower binding to membranes than $TPPS_{2a}$ and CisDiMPyP (Figure 2.7). In the case of phthalocyanine ($AlPcS_{2a}$) the smaller incorporation in the membrane is probably due the higher rigidity, molecular size and to the aluminum coordinated at the center of the molecule providing larger volume and polarity. As for $AlPcS_{2a}$, the interaction level of PpNetNI with membranes was small compared to other photosensitizers (Figure 2.7). The design of PpNetNI was made to include an amphiphilic character and positive charges on molecule. According to the literature, these factors should increase the binding to membranes (Uchoa, Oliveira, and Baptista 2010; Fabio M. Engelmann et al. 2007). However, the binding value of PpNetNI was even lower than that of $TPPS_{2a}$, a negatively charged molecule. It is noteworthy that under our experimental conditions (Tris buffer 5mM pH 7.4) the absorption spectrum indicated aggregation of PpNetNI (Figure 2.8), such as an increased baseline, band broadening, an intensity decrease and wavelength shift of the Soret band to blue region (from 399 nm to 378 nm), which is typical for type-H porphyrins aggregates (Maiti, Mazumdar, and Periasamy 1998). These aggregates probably decrease the membrane interaction level.

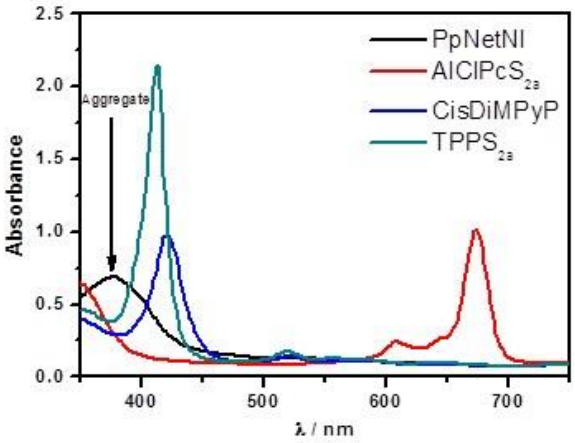

Figure 2.8. Absorption spectrum of photosensitizers (7 µM) in Tris buffer 5 mM (pH 7.4).

$TPPS_{2a}$ and CisDiMPyP are of similar molecular structure, their affinity to membranes is larger than $AlPcS_{2a}$ and PpNetNI. This is because the phenyl peripheral hydrophobic groups have a lesser rigidity than the peripheral groups of $AlPcS_{2a}$ and furthermore provide steric barriers to avoid chromophore π-π stacking (i.e. type-H aggregation) – in contrast to PpNetNI. Note also that the positively charged CisDiMPyP exhibits a stronger interaction with membranes than the negatively charged $TPPS_{2a}$ (Figure 2.7). This is because membranes have a net negative charge, favoring the electrostatic interaction with CisDiMPyP. Although $TPPS_{2a}$ contains two negatively charged groups, it also has a considerable interaction with membranes (larger than $AlPcS_{2a}$ and PpNetNI), indicating that both hydrophobic and dipolar interactions play an important role in defining the affinity of these molecules to membranes.

All data together (Figure 2.7) demonstrates that the interaction level between photosensitizer and membrane has the same tendency for three different systems, in such way that the decreasing order is: CisDiMPyP > $TPPS_{2a}$ > $AlPcS_{2a}$ ≥ PpNetNI.

2.3.4. Photoactivity of photosensitizers in membranes

In order to investigate, if the level of interaction would affect the ability to induce membrane damage and permeability by photosensitization, the photodynamic efficiency of the

photosensitizers was evaluated in terms of photodamage to the membranes using two different systems: erythrocytes and giant unilamellar vesicles (GUVs).

The erythrocyte membrane integrity was evaluated by measuring the intensity of light scattering in the cell suspension. The decrease of the scattering indicates membrane disruption and equilibration of refractive index between the inner and outer compartments of the erythrocyte cell. This allowed us to compare the relative efficiency of photosensitizers in terms of hemolysis kinetics (Fabio M. Engelmann et al. 2007). Erythrocyte suspensions were irradiated in the presence of the photosensitizers and the decrease in light scattering was monitored at 650 nm (Figure 2.9.A).

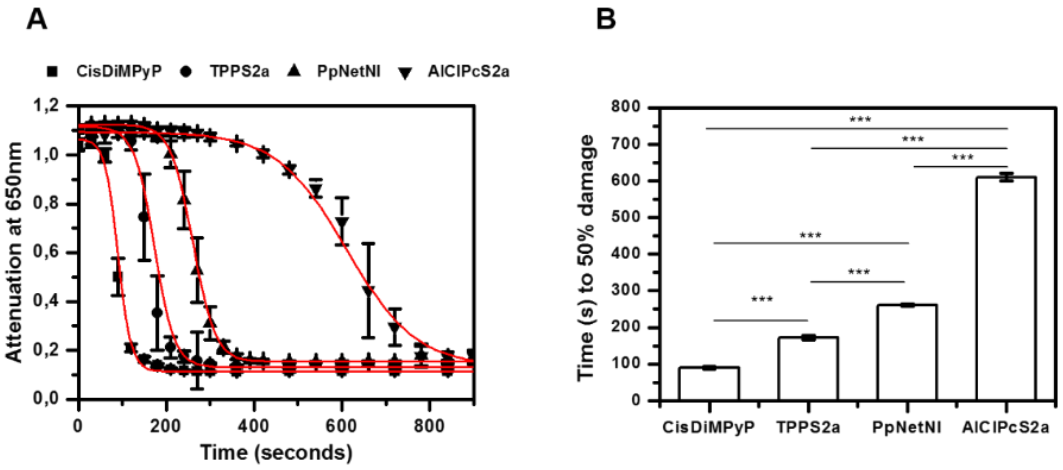

Figure 2.9 (A) Light attenuation monitored at 650 nm during photoirradiation of erythrocytes in the presence of photosensitizers. Each point corresponds to the mean of two independent experiments and error bars represent standard deviation (SD). (B) Time (in seconds) to reach 50% photodamage induced in the erythrocytes membranes by each photosensitizer. [photosensitizer] = 7 µM in PBS pH 7.4, LED 522 ± 20nm in case of porphyrins and LED 633 ± 20nm in case of phthalocyanine, 7 mW/cm^2.

It was observed that the decrease in scattering intensity was fastest for CisDiMPyP and slowest for AlClPcS$_{2a}$ (Figure 2.9.A). The elapsed time that caused 50% of photodamage was 90 ± 4 seconds for CisDiMPyP, 172 ± 6 seconds for TPPS$_{2a}$, 260 ± 3 seconds for PpNetNI and 610 ± 10 seconds for AlClPcS$_{2a}$ (Figure 2.9.B). Therefore, the decreasing order of the relative

efficiency of membrane damage of the photosensitizers is: CisDiMPyP > $TPPS_{2a}$ > PpNetNI > $AlClPcS_{2a}$ (Figure 2.9).

The observation of GUVs during the photosensitization process by optical microscopy provides information about membrane leakage and physics alterations. GUVs are made with an asymmetry in the distribution of sugars (sucrose in the internal compartment and glucose in the external medium), resulting in an optical contrast when observed by phase contrast microscope (Figure 2.10A). The loss of phase contrast indicates that the membrane allowed the transition of glucose and sucrose (Figure 2.10D), while a stable optical indicates that the membrane remains impermeable to sugars (Mertins et al. 2014). In this regard, the intensity values of phase contrast were evaluated by the difference between the point of maximum luminosity and minimum luminosity as function of the irradiation time (Figure 2.10 lower column). The decrease in contrast indicates membrane leakage.

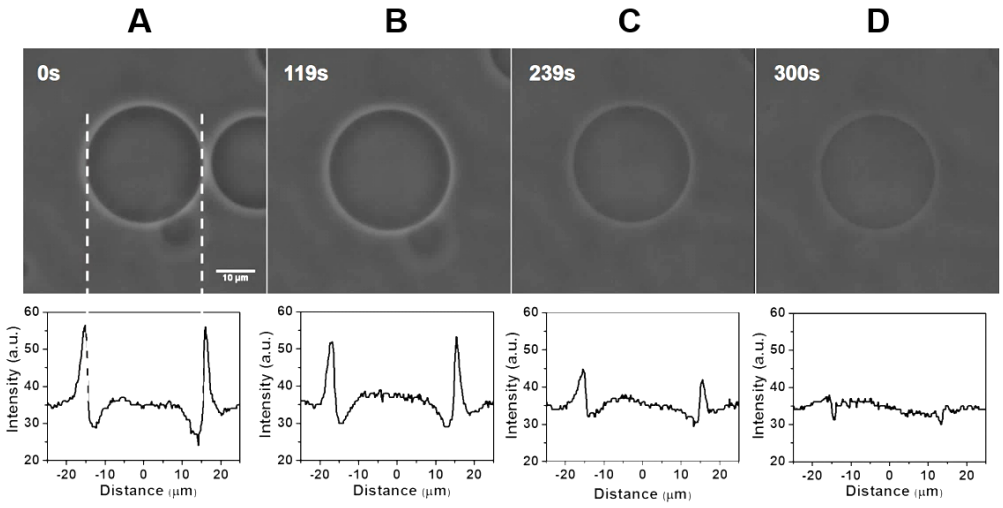

Figure 2.10. (Upper line) Phase contrast optical microscopy images of the giant vesicles (GUVs) and (Lower line) intensity profiles across the equator of GUVs as a function of time (in seconds) during photoactivation with 0.7 µM $TPPS_{2a}$. The scale bars are 10 µm.

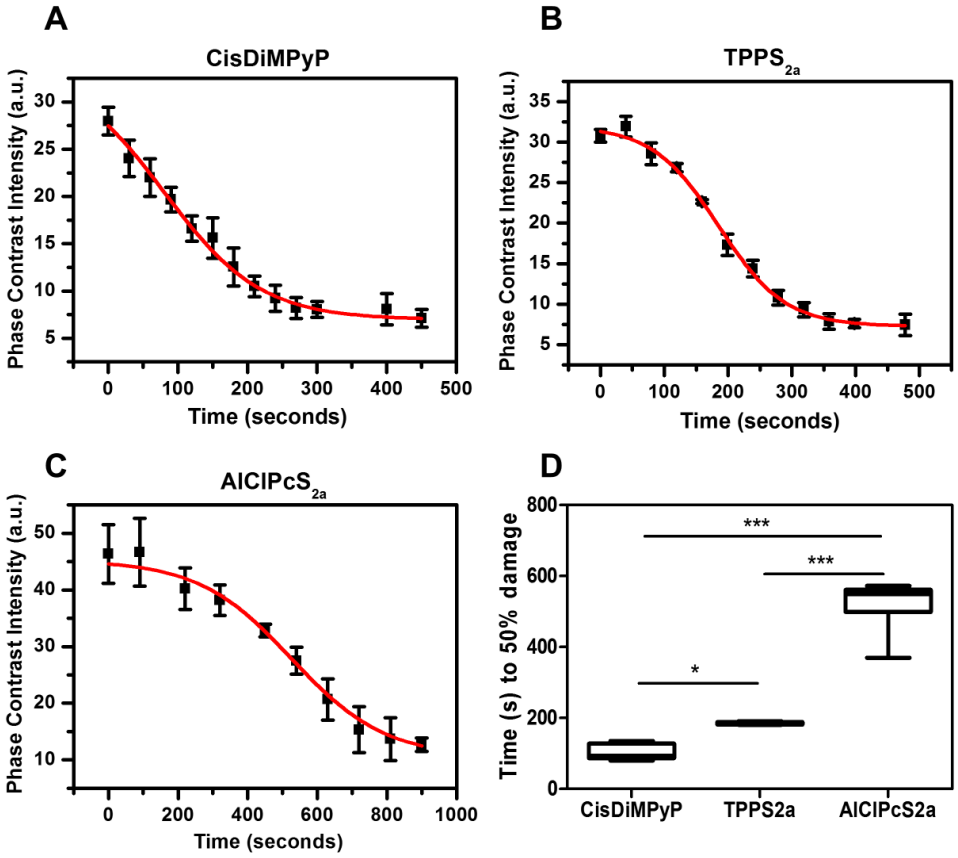

Figure 2.11. Phase-contrast intensity decay of DOPC-GUVs during photoirradiation in the presence of (A) 0.7 µM CisDiMPyP (B) 0.7 µM $TPPS_{2a}$ and (C) 0.7 µM $AlClPcS_{2a}$. Each point corresponds to the average of at least six vesicles and standard deviation (SD) is represented by the error bars. (D) Time (in seconds) to reach 50% photodamage induced in the GUVs by each photosensitizer. Box plots shows minimum to maximum values (*$p<0.05$ and ***$p<0.001$ are considered statistically significant). [DOPC]=2.5 mM, 0.2 M sucrose inside vesicle, 0.2 M glucose outside vesicle. Irradiation carried out using the Zeiss Filter Set 05 for porphyrins (excitation BP 395-440 nm, beam splitter FT 460nm, emission LP 470nm, 135 µW/cm^2) and the Zeiss Filter Set 32 for phthalocyanine (excitation BP 665/45 nm, beam splitter FT 695nm, emission BP 725/50nm, 135 µW/cm^2). The number of photons absorbed by the different photosensitizers were normalized.

PpNetNI induced membrane leakage in the dark even at low concentration (0.3 µM). Thus, by using GUVs assays we evaluated only the efficiency of photoinduced membrane damage of three other amphiphilic photosensitizers: CisDiMPyP, $TPPS_{2a}$, $AlClPcS_{2a}$. Nevertheless, the increase in membrane permeability (or phase contrast decay) by sucrose (inner pool) and glucose (outer solution) exchange was clearly observed by the fading of membrane contrast of the GUVs (Figure 2.11) in all studied photosensitizers (Figure 2.11A,

Figure 2.11B and Figure 2.11C), the elapsed time to observe a 50% optical contrast loss was 104 ± 22 seconds, 184 ± 4 seconds and 534 ± 37 seconds for CisDiMPyP, $TPPS_{2a}$, $AlClPcS_{2a}$., respectivately (Figure 2.11D).

Taken together, these findings showd that the photodynamic efficiency in membranes (erythrocytes and GUVs) of amphiphilic photosensitizers is directly associated with the efficiency of membrane binding whose descending order was: CisDiMPyP > $TPPS_{2a}$ > PpNetNI ≥ $AlPcS_{2a}$. This is in agreement with literature, which show that a stronger membrane interaction is correlated not only with greater membrane damage but also with more effective photo-induced damage of whole cells and/or organisms (Bacellar et al. 2014; Fabio M. Engelmann et al. 2007; Ben Amor, Bortolotto, and Jori 2000). As example, Bacellar *et al*. used a series of phenothiazinium, containing different degrees of hydrophobicity and demonstrated that the higher PS-membrane interaction was correlated to more membrane leakage (Bacellar et al. 2014). Also, Pavani and coworkers demonstrated the direct relationship between the porphyrins membrane binding and the efficiency in killing eukaryotic cells (Figure 2.12) (Pavani, Iamamoto, and Baptista 2012).

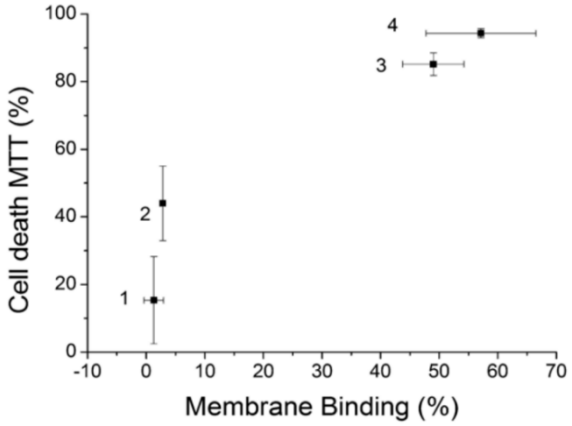

Figure 2.12. Cell death versus membrane binding measured in multilamellar vesicles. 1: TMePyP, 2: Zn-TMePyP, 3: TC18PyP and 4: Zn-TC18PyP. Reprinted by permission from John Wiley and Sons (Pavani, Iamamoto, and Baptista 2012).

To further investigate this premise, we selected two photosensitizers (CisDiMPyP and $TPPS_{2a}$) to evaluate the biological effects in a human cell line, which is presented in details on the next chapter (Chapter 3). The choice of CisDiMPyP and $TPPS_{2a}$ for the further studies in eukaryotic cells is because they may be more efficient to PDT due to the larger membrane binding and better photoactivity compared to others amphiphilic photosensitizers studied. At the same time, CisDiMPyP and $TPPS_{2a}$ exhibit similar structures and photophysical properties (same ϕ_F and ϕ_Δ), but different charges which allow the evaluation of the effect of charges in the photodynamic efficiency.

2.4. CONCLUSION

Within the series of amphiphilic photosensitizers studied by us, we found that the different peripheral groups do not significantly affect the photophysical properties of porphyrins. However, the phthalocyanine chromophore exhibits different photophysical properties from the porphyrins. The photophysical data indicates that the porphyrins have low fluorescence quantum yields and are efficient generators of $^1O_2$, while the phthalocyanine presents a two-fold higher fluorescence quantum yield and generates $^1O_2$ less efficient compared to the porphyrins.

Even though peripheral groups do not significantly affect the photophysical properties of the photosensitizers, it was shown to have a direct impact on the PS-membrane interaction and the photo-induced membrane damage. It was found that the photodynamic efficiency is correlated to the efficiency of membrane binding (The descending order of their efficiency is CisDiMPyP > $TPPS_{2a}$ > PpNetNI ≥ $AlPcS_{2a}$). We choose two photosensitizers with larger interaction and highest ability of photodamage and photophysical properties and molecular structure (CisDiMPyP and $TPPS_{2a}$) to further evaluate the biological effects in eukaryotic cells (Chapter 3).

CHAPTER 3

MODULATING PDT EFFICIENCY BY THE CHARGE OF PHOTOSENSITIZER

It has been demonstrated that the specificity of photosensitizers inside eukaryotic cells can increase the photodynamic effect. When a photosensitizer is localized in a strategic target, the required PDT dose (PS concentration and light dose) is much smaller than when the PS is not specific. By using two porphyrins with similar structure but bearing opposite charges, it became clear that the affinity to different organelles induces distinct mechanisms of cell death. Our results provide insights about the choice of target and cell death mechanism upon PDT as well as about the rational design of new drugs for organelle-target therapies.**

** The work described in this chapter is adapted from submitted paper to *Scientific Reports*. "Enhanced efficiency of cell death by lysosome-specific photodamage." Tayana M. Tsubone, Waleska K. Martins, Christiane Pavani, Helena C. Junqueira, Rosangela Itri and Maurício S. Baptista.
This work was presented orally on *International Photodynamic Association (IPA)* in May 2015 at Rio de Janeiro – Brazil and in *Tsukuba Global Science Week* in September 2016 at Tsukuba - Japan.

3. MODULATING PDT EFFICIENCY BY THE CHARGE OF PHOTOSENSITIZER

3.1. INTRODUCTION

The search for better new-photosensitizers usually focuses on a higher absorption in the red region ("therapeutic window") and/or a higher efficiency in the generation of singlet oxygen (Bonnett 1995; Pushpan et al. 2002; Derosa and Crutchley 2002). Even though these are important parameters of PS for PDT application, other factors such as the tendency of intracellular location and the modes of cell death can be more decisive in the final photodynamic efficiency in eukaryotic cells and thus should also be considered when planning the molecular structure of a new photosensitizer. As already mentioned in Chapter 1, the work of Oliveira *et al*. demonstrated exactly this point: although methylene blue produces a higher amount of ROS than crystal violet, crystal violet has a better efficiency of killing cells compared to methylene blue (Chapter 1 - Figure 1.5) due to a highly specific localization of crystal violet in mitochondria (Oliveira et al. 2011). However, all these parameters (PS structure, reactive oxygen species generated, cellular uptake, subcellular localization and consequences of specific photodamage) are not usually evaluated together, sometimes missing the complete picture of an ideal PS-structure.

Therefore, this work will discuss how and why the net charges of the porphyrin rings can define the PDT efficiency and the type of the cell death mechanism by characterizing their intracellular sites of photodamage, their ability to decrease viability and proliferation of HeLa cells, and their consequences in terms of cell death mechanisms. Finally, by using photosensitizers bearing opposite charges (CisDiMPyP and $TPPS_{2a}$ – see structures in Chapter 2 – Figure 2.2), we answer whether mitochondria or lysosomes may be the best intracellular target of photo-oxidation to kill specific cancer cells.

3.2. METHODOLOGY

3.2.1. Cells and culture conditions

The human cervical adenocarcinoma cell line (HeLa – ATCC CCL-2) was cultured in Dulbecco's Modified Eagle medium (DMEM) supplemented with 10% (v/v) fetal bovine serum (FBS) and 1% (v/v) penicillin/streptomycin. HeLa cells were maintained in a humid incubator (ThermoScientific) at 37ºC under an atmosphere of 5% carbon dioxide (CO_2).

3.2.2. Cellular uptake of photosensitizers in HeLa cells

HeLa cells ($2x10^5$ cells/well) were seeded in 12-well plates (Corning), incubated for 18 hours for attachment to the bottom of the well and then treated with photosensitizers (5 μM) in 1 mL DMEM (1% (v/v) FBS) during 3 hours in the dark, 5% CO_2 at 37ºC. After this period, 0.5 mL of the supernatant solution (free PS) was removed from the well and diluted with 0.5 mL Triton X-100 10% (v/v) for spectroscopic investigation. The remaining supernatant was discarded and the adhered cells were washed twice with PBS buffer and finally lysed in 1.0 mL Triton X-100 5% (v/v) (bound PS). The Triton X-100 solubilizes the cell membranes and at the same time avoids PS aggregation. The absorption spectra of supernatant and cell lysate were put in cuvettes of 1.0 cm optical path length. The absorption spectra wererecorded using a Shimadzu UV-2400-PC spectrophotometer and the PS uptake in cells was calculated as described by equation 3.1.

$$\%\ Cellular\ uptake = 100\ \frac{Abs\ cell}{Abs\ cell + (2x\ Abs\ supernatant)} \qquad \text{Equation 3.1}$$

where *Abs cell* is the absorbance of photosensitizer uptake by cells and *Abs supernatant* is absorbance of PS solution in the supernatant. The absorbance wavelength used in the calculation was 424 nm and 418 nm for CisDiMPyP and $TPPS_{2a}$, respectively. A correction factor of 2 was added to *Abs supernatant* to correct for 2-fold dilution of the solution.

3.2.3. Photosensitization in HeLa cells

Cells were seeded ($2.8x10^4$ cells/well) in a 48-well plate (Corning), incubated 18 hours for attachment to the flask and then treated with porphyrins CisDiMPyP (50 nM-300 nM) or $TPPS_{2a}$ (5 nM-100 nM) in 1% (v/v) FBS DMEM media for 3 hours in the dark, 5% CO_2 at 37ºC. Next, HeLa cells were washed twice with PBS. 300 µL of PBS was refilled and the cells were submitted to irradiation for 15 minutes using a light emitting diode system (LED), emitting at 522 ± 20 nm, up to a final light dose of 2.1 J/cm^2 (see spectrum overlay of porphyrins absorption and LED emission at Figure 3.1). After irradiation, the cells were incubated in 1% (v/v) FBS DMEM media until the further measurements. For autophagy monitoring experiments, 2 nM baflomicin-A1 (BAF) or 5 mM 3-methyladenine (3-MA) were added immediately after irradiation.

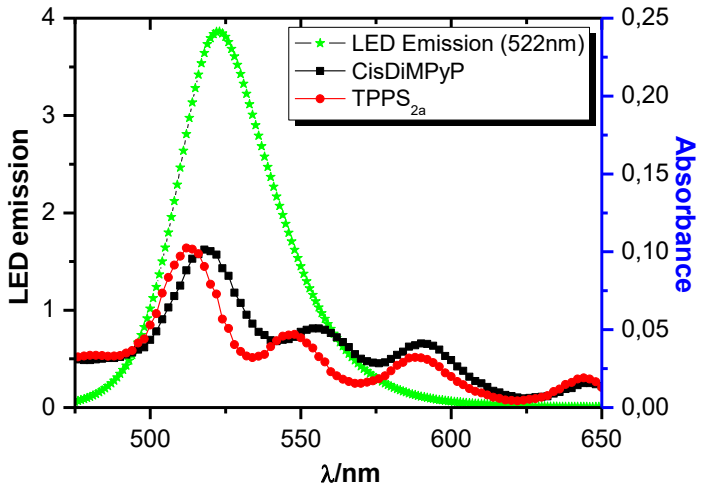

Figure 3.1. Overlay of LED emission and absorption spectra of both porphyrins.

3.2.4. Cell viability assays

3.2.4.1. MTT assay

After irradiation, HeLa cells were washed again with PBS. FBS DMEM media 1% (v/v) was added added and the cells were incubated for 3 and 48 hours in the dark, 5% CO_2 at 37ºC. The cell survival was determined by an MTT assay 3-(4,5-dimethylthiazol-2-yl)-2,5-

diphenyltetrazolium bromide, where cells were incubated with 0.15 mg/mL of MTT for 2 hours in an incubator (5% CO_2 at 37ºC). Formazan crystals were solubilized in dimethyl sulfoxide (DMSO) and quantified by measuring the absorption at 550 nm (Infinite M200 plate reader-Tecan). The percentage of viable cells was calculated relative to the absorbance of the control cells (taken as 100% viability).(Meerloo, Kaspers, and Cloos 2011)

3.2.4.2. Clonogenic assay

Immediately after irradiation, control and photosensitized cells were detached by tripsinization and counted. 500 cells per well were placed in a 6-well plate and incubated during 8 days at 5% CO_2 at 37ºC. Then, HeLa cells were washed with PBS and incubated with 6% (v/v) glutaraldehyde solution for 20 minutes followed by incubation with crystal violet in PBS (0.5% w/v) for 20 minutes. The crystal violet solution was removed by washing the well under tap water. The colonies greater than 50 cells were visually counted.(Franken et al. 2006).

3.2.5. Subcellular localization and site-specific photodamage

3.2.5.1. Colocalization fluorescence microscopy

HeLa cells ($1x10^5$ cells/well in a 6-well plate) were incubated with porphyrins (1μM in DMEM supplemented with 1% FSB) for 3 hours at 37ºC, 5% CO_2. DAPI, MitoTracker® Green FM and LysoTracker® Green DND-26 were used as probes for nuclei, mitochondria and lysosomes, respectively. MitoTracker® Green FM (150 nM) and LysoTracker® Green DND-26 (150 nM) were added after 150 minutes of PS-incubation, then the cells were incubated for another 30 min. Microscope slides were prepared by adding ready-to-use Prolong Diamond Antifade Mountant with DAPI and analyzed under the confocal microscope (Zeiss™ Axiovert 200 LSM 510 Laser and Confocor Modules). Porphyrin fluorescence images were then recorded using 514 nm laser for excitation and a 600-800 nm bandpass filter for emission. The excitation/emission of MitoTracker® Green and LysoTracker® Green were 488 nm

/505-530 nm, and that of DAPI was 358 nm/420 nm (longpass filter). Fluorescence images were obtained using a confocal Zeiss (LSM 510). Images were analyzed using *Image J* software and calculation of colocalization between photosensitizer and organelle-probe were performed using the *Manders overlay coefficient (MOC)* plugin of *Image J*.

3.2.5.2. Mitochondrial membrane depolarization analysis by flow cytometry

Three hours after the irradiation, the treated and control cells (HeLa) were incubated with rhodamine 123 (200 nM) for 15 minutes (37ºC, 5% CO_2). Then, HeLa cells were washed twice with PBS, detached through trypsinization procedure and centrifuged at 600g for 5 minutes at 4ºC. Pellet cells were re-suspended in buffer and then cytofluorometric analyzed by *FACS VERSE BD*® using excitation at 488 nm and emission at 527 ± 32 nm (FL1). Results were analyzed using *FlowJo* software.

3.2.5.3. Evaluation of organelle photodamage

Three hours after irradiation with either 100 nM CisDiMPyP or 30 nM $TPPS_{2a}$, the treated and control cells (HeLa) were incubated with 1 µM *MitoTracker® Red CM-H_2XRos* (MTR) or 200 nM *LysoTracker® Red* (LTR) during 30 minutes (37ºC, 5% CO_2). We analyzed 4,6-diamidino-2-phenylindole (DAPI) counterstained slides under confocal microscope (ZeissTM Axiovert 200 LSM 510 Laser and Confocor Modules) equipped with 63x objective. Images were analyzed using *Image J* software.

3.2.6. Investigation of the photoinduced cell death mechanism

3.2.6.1. Annexin V-FITC/PI double-labeled flow cytometry

Three hours after irradiation, the treated and control cells (HeLa) were detached through trypsinization, washed and centrifuged twice with PBS and re-suspended in 400 µL of binding buffer. Four µL of a 50 µg/mL Annexin V-FITC (final concentration 0.5 µg/mL to each sample) were added and 8 µL of a 100 µg/mL propidium iodide (final concentration 2 µg/mL

to each sample), followed by incubation at room temperature in the dark for 10 min. Finally, fluorescence emission was analyzed by cytofluorometry in an *FACS VERSE BD®*. For Annexin V-FITC the excitation was at 488 nm, theemission at 527 ± 32 nm (FL1) and for Propidium iodide (PI) excitation was at 633 nm and emission at 660 ± 22 nm (FL3). At least 20,000 events were collected in each analysis and data was analyzed by *FlowJo* software.

3.2.7. Immunofluorescence staining

***Caspase/Cathepsin*:** Three hours after irradiation, the treated and control cells (HeLa) were fixed and submitted to permeabilization with 0.3 % (v/v) Triton X-100 and blockage, followed by incubation with primary rabbit or mouse monoclonal antibodies against, respectively, caspase-3 active form (CASP3, Cell Signaling Technology) or Cathepsin B (CTSB, Abcam). Next, the primary antibody was revealed using goat secondary antibodies (Alexa 488) from Molecular probes (Eugene, OR, USA).

Cathepsin/p62: 48 hours after irradiation according to the the same sample preparation as described above, but applying a double-staining against Cathepsin B (CTSB, Abcam®) and ubiquitin binding protein sequestosome 1 (SQSTM1/p62, Cell Signaling Technology) the primary antibody was revealed using goat secondary antibodies specific to mouse IgG CTSB (Alexa 488) and rabbit P62 (Alexa 633), both from Molecular Probes. We analyzed 4,6-diamidino-2-phenylindole (DAPI) counterstained slides under confocal microscope (ZeissTM Axiovert 200 LSM 510 Laser and Confocor Modules) equipped with a Plan-Apochromat 63X/1.40 oil DIC M27 objective. Images were analyzed using *Image J* software.

3.2.8. Acridine orange and propidium iodide double staining

Three and 48 hours after irradiation, HeLa cells were washed with PBS and incubated with AO/PI solution (1 µg/mL each dye in PBS) for 10 minutes at 5% CO_2 and 37ºC.(Abdel Wahab et al. 2009) A positive control for autophagy inhibition, i.e., 60 µM Chloroquine (CQ)

was used for comparison.(Mizushima, Yoshimori, and Levine 2010; Mizushima 2004; Agholme et al. 2012) Images were acquired under a fluorescence microscope Axiovert 200 (Carl Zeiss) equipped with Zeiss Filter Set 09, which provided excitation in the 450-490 nm range and emission above 515 nm. The ratio between red and green fluorescence (AO/PI double staining) was calculated by analyzing at least six different images from random areas of two independent experiments. ImageJ Software was used to separate green and red channels.

3.2.9. Quantification of autophagy arbitrary units (AAU)

To quantify cell death associated with autophagy, this was quantified in terms of numeric arbitrary autophagy units – AAU by equation 3.2 (Waleska K. Martins et al. 2013):

$$AAU = \frac{x_a}{[x_b + x_c]/2} \qquad \text{Equation 3.2}$$

Where x_a, x_b and x_c are the survival rates measured by NR, CV and MTT assays respectively (Waleska K. Martins et al. 2013). This strategy is based on a parallel evaluation of NR-uptake, weighted by the average of cell survival measured by MTT and CV (Crystal Violet) assays. The MTT reduction method was conducted as described above. To quantify lysosomal content after photosensitization, HeLa cells were stained with NR (60 μg/mL) by incubation for 2 hours at 37°C. After washing, NR was then diluted with an alcoholic-based 1% (v/v) acetic acid fixing solution and measured at 540 nm. Subsequently, these fixed cells after washing with water were used for CV assay. Finally, following washing of fixed-cells stained with Crystal Violet at 0.02% (w/v) for 5 minutes at room temperature, we diluted CV with 0.1 M sodium citrate in 50% (v/v) ethanol, and recorded absorbance values at 585 nm (Waleska K. Martins et al. 2013). The detection of MTT, NR and CV absorbance was performed using the microplate reader Infinite® 200 PRO (Tecan).

3.2.10. Western Blot

48 hours after irradiation, HeLa cells were lysed [lysis buffer-20 mM PIPES, 100 mM NaCl, 1 mM EDTA, 10% (w/v) sacarose, 0.1% (v/v) CHAPS, 0.1% (v/v) Triton X-100, 1 mM PMSF, 2 μM Pepstatin A, 50 μM digitonin]. 20 μg of the total proteins were separated in 12% (w/v) acrylamide gels and transferred to PVDF membranes (GE healthcare). PVDF membranes (0.45 μm pore) were blocked with 5% (w/v) BSA in 0.01% (v/v) TBS-T (Tween 20 in TBS) for one hour at room temperature, followed by incubation with primary antibodies against LC3B (Cell Signaling Technology) and α-tubulin (Sigma Aldrich) in 0.01% (v/v) TBS-T with 2.5% (w/v) BSA overnight at 4ºC. Next, PVDF membranes were washed three times with 0.01% (v/v) TBS-T for 10 minutes and then incubated with secondary antibodies (anti-rabbit HRP for LC3B and anti-mouse HRP for α-tubulin) diluted in 0.01% (v/v) TBS-T with 2.5% (w/v) BSA for one hour at room temperature. Again, PVDF membranes were washed three times with 0.01% (v/v) TBS-T for 10 minutes and revealed using SuperSignal West Pico Chemiluminescent Substrate. Data acquisition was performed by using the Alliance 6.7-89WL/20M chemiluminescence detection system. Images were analyzed using NineAlliance 9.717.00b software and the LC3 data were normalized to α-tubulin band intensities.

3.2.11. Statistics

To perform comparative statistical analysis, we first analyzed the variance between the groups of samples. Next, we analyzed statistical differences by a parametric or non-parametric T-student test for pair-wise comparisons. In case of multiple comparisons, we performed a one-way analysis of variance (ANOVA) with Dunnett's T3 or Bonferroni post-hoc tests, depending on the homogeneity of variance. The statistical analyses were performed using the *IBM SPSS Statistic* software. Data were obtained in most of the experiments from three independent experiments, in some cases only two independent experiments (n = 6) were available. Results

are expressed as mean values ± standard deviation (SD). As statistically significant, we considered P-values lower than 0.05 (*), lower than 0.01 (**) and lower than 0.001 (***).

3.3. RESULTS AND DISCUSSION

3.3.1. Uptake and phototoxicity in HeLa cells

The uptake of CisDiMPyP by HeLa cells (26% ± 2) was about 35 % larger than that of $TPPS_{2a}$ (16.6% ± 2.4) (Figure 3.2). In Chapter 2, it was demonstrated that there are the two major contributions to the PS internalization: the positive charge of CisDiMPyP is promoting a stronger interaction with the cytoplasmic membrane by electrostatic attraction and the dipolar interactions, which are present in both porphyrins. The uptake in cells therefore follows the same trend as found for the interaction with membranes (Chapter 2 - Figure 2.6) confirming this hypothesis.

The phototoxicity of porphyrins in HeLa cells was assessed by MTT and clonogenic assays (Figure 3.2B and Figure 3.2C). None of the porphyrins caused a decrease of viability or proliferation in the dark, thus confirming no dark-cytotoxicity. $TPPS_{2a}$ showed to be more phototoxic compared to CisDiMPyP (Figure 3.2B and Figure 3.2C). The lethal concentration to cause 50% of cell death (LC_{50}) estimated for CisDiMPyP (100 nM) was at least 3-fold higher than for $TPPS_{2a}$ (30 nM).

It is worth mentioning that $TPPS_{2a}$ is more efficient in terms of photo-damaging HeLa cells regardless of its lower internalization. In order to compare the cell killing efficiency per molecule of PS, we considered the concentration of PS that is actually internalized at the LC_{50}, which is 4.5 nM for $TPPS_{2a}$ and 25 nM for CisDiMPyP. Thus, the cell killing efficiency per molecule of $TPPS_{2a}$ is around 5 times larger than of CisDiMPyP.

$TPPS_{2a}$ and CisDiMPyP have similar ϕ_Δ values (Chapter 2 - Table 2.2), consequently the greater molecular photo-efficiency observed for $TPPS_{2a}$ in HeLa cells cannot be explained by an excess amount of $^1O_2$. It does not correlate neither with cell uptake nor with the efficiency

of membrane binding/damaging. This fact is intriguing because it goes against several paradigms in this field, i.e.: a stronger membrane binding results in greater cell damage (Bacellar et al. 2015; Fabio M. Engelmann et al. 2007), a higher amount of PS incorporation of similar PSs in the cell results in a greater efficiency of photo-induced cellular damage (Bacellar et al. 2015; Fabio M. Engelmann et al. 2007; Ben Amor, Bortolotto, and Jori 2000). We observed a lack of relationship between the efficiency of cell killing (Figure 3.2) with the other parameters mentioned above (binding membrane, photodamage in membanes) (Chapter 2 – Figure 2.6 and Table 2.2). We hypothesize that the observed differences may be due to the different intracellular localization and induction of distinct cell death mechanisms (Rodriguez et al. 2009; Fabris et al. 2001; Tardivo et al. 2005; Bacellar et al. 2015).

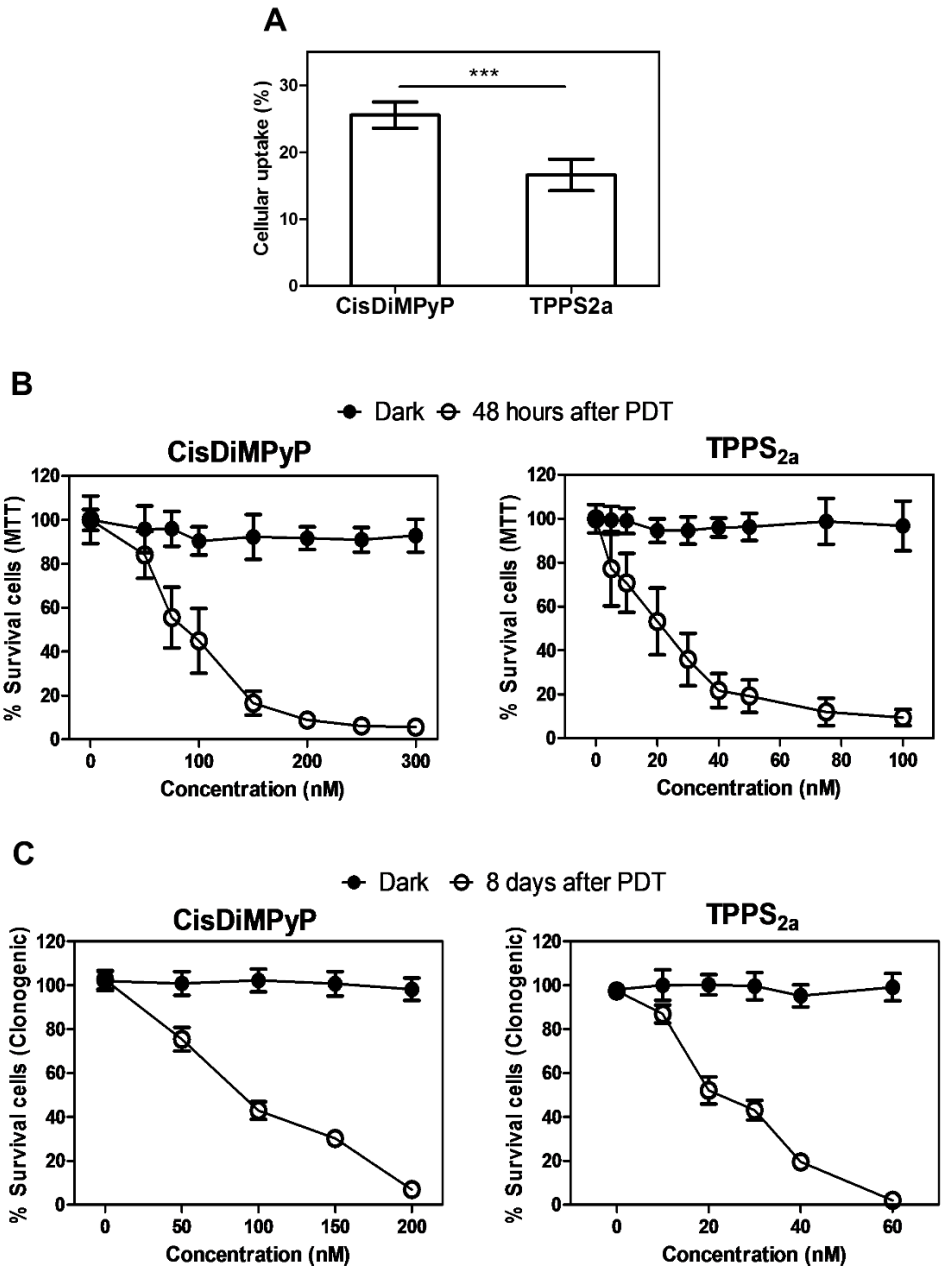

Figure 3.2. **(A)** Uptake of $TPPS_{2a}$ and CisDiMPyP in HeLa cells after 3 hours incubation in the dark. [Porphyrins]=5 µM, $5x10^4$ cells/cm^2 in DMEM culture medium 1% FBS, pH 7.4, Bars represent mean ± SD of three independent experiments (n = 9, ***$p<0.001$ are considered statistically significant). **(B)** MTT assay. Cell viability in the dark and 48 hours after irradiation as a function of the PS concentration. Each point represents the mean ± SD of three independent experiments (n = 9). **(C)** Clonogenic assay. Survival cells in the dark and 8 days after irradiation as a function of PS concentration determined by clonogenicity. Each point represents the mean ± SD (n = 4). **(A, B and C)** Incubation of HeLa cells with porphyrins for 3 hours in DMEM with 1% FBS. **(B and C)** After incubation with PS, irradiation was performed in PBS using a LED system emitting at 522 ± 20 nm with a light dose of 2.1 J/cm^2.

3.3.2. Porphyrins-charge governing intracellular localization and subcellular photodamage

In order to characterize the different locations of these PS in the intracellular environment, we initially tried lysosome and mitochondria co-localization protocols (Table 3.1 and Figure 3.3). CisDiMPyP showed a higher tendency to accumulate in mitochondria, while $TPPS_{2a}$ accumulates more in lysosomes, as revealed by the raw percentage data of co-localization with Lysotracker® and Mitotracker® (Figure 3.3), as well as by the ratio of raw percentages for each PS (M/L values - Table 3.1). This result was somehow expected, because positively charged PSs in general are known to accumulate in mitochondrial membranes and negatively charged PSs in lysosomal membranes (Horobin, Stockert, and Rashid-Doubell 2015; Yue et al. 2011; Kristian Berg et al. 1990; Dummin, Cernay, and Zimmermann 1997). However, the experimental conditions of these co-localization protocols were not ideal, because we could only obtain well-resolved fluorescence images of PS intracellular localization at PS concentrations, which were a lot higher than the LC_{50} (one order of magnitude). At these high concentrations, the PS saturates not only the primary accumulation sites but also other lower affinity sites. The relatively low percentages of co-localization in mitochondria and in lysosome by both PSs (<50%, Table 3.1) attest this fact. Because we could not precisely characterize PS location in the 30-100 nM range directly by fluorescence images, we then relied on protocols aiming to characterize the specific damages in mitochondria and lysosomes at the LC_{50}.

Table 3.1. Co-localization percentage of porphyrins with Mitotracker® green and Lysotracker® green after 3h incubation in HeLa cells.

Overlay (PS/organelle)	**LysoTracker® (L)**	**MitoTracker® (M)**	**M/L**
CisDiMPyP	20% ± 2	38% ± 5	1.9 ± 0.2
$TPPS_{2a}$	39% ± 4	30% ± 5	0.7 ± 0.1

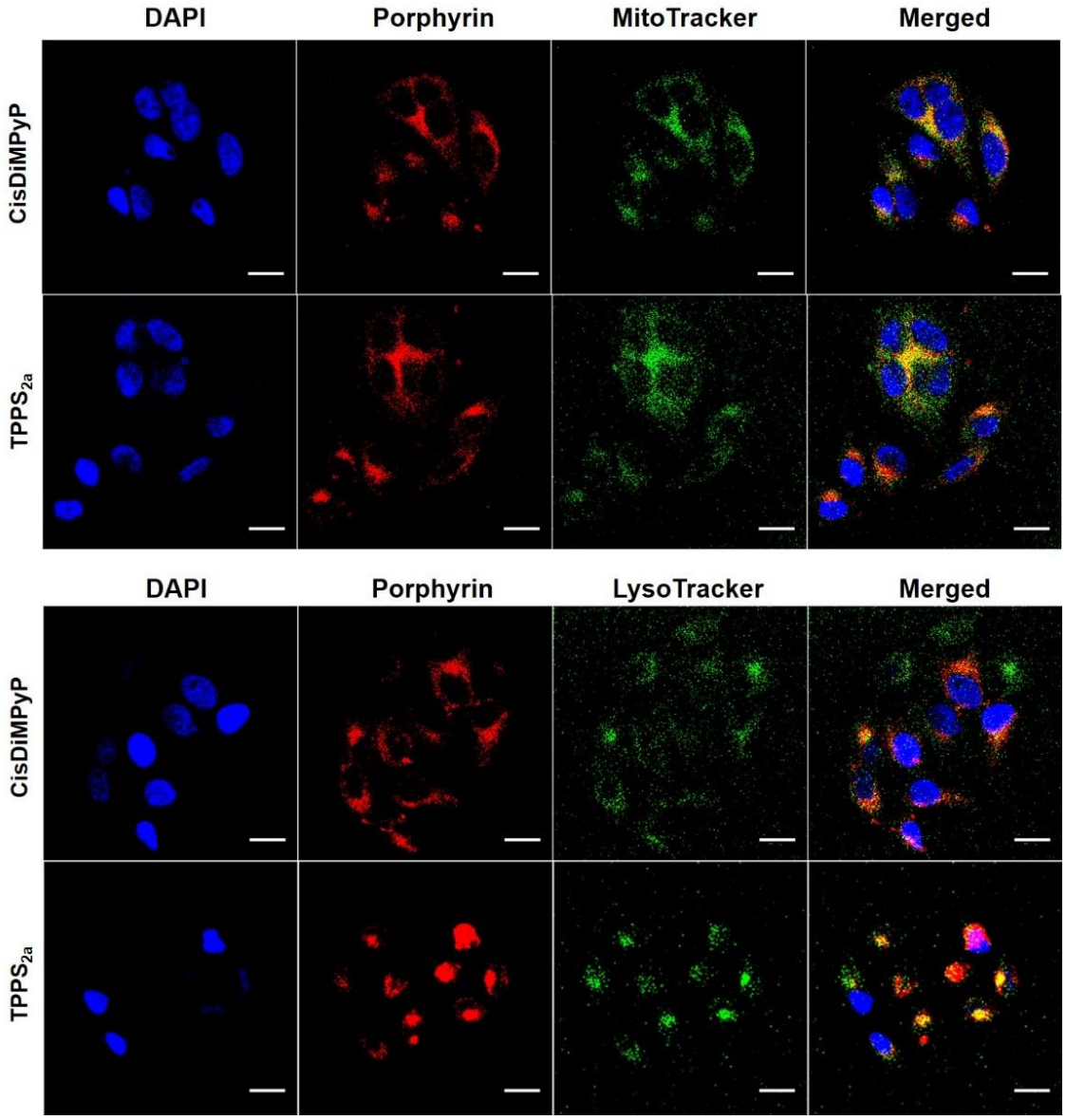

Figure 3.3. **(A)** Confocal fluorescence microscopy images of HeLa cells with blue fluorescence of nucleus (DAPI), red fluorescence of porphyrins (1 μM) and green fluorescence of mitochondria (150 nM MitoTracker®). Right column shows the overlay from three channels (blue, red and green). **(B)** Confocal fluorescence microscopy images of HeLa cells with blue fluorescence of nucleus (DAPI), red fluorescence of porphyrins (1 μM) and green fluorescence of lysosomes (150 nM LysoTracker®). Right column shows the overlay from three channels (blue, red and green). Scale bars corresponds to 20 μm.

The experiments were performed 3 hours after irradiating cells, previously treated with either 30 nM of $TPPS_{2a}$ or 100 nM of CisDiMPyP. The loss of mitochondrial transmembrane inner potential ($\Delta\Psi m$) was evaluated by means of fluorescence intensity of Rhodamine 123 (Rh123) using flow cytometry. The subcellular photodamage was evaluated by staining

mitochondria with *MitoTracker® Red CM-H_2XRos* (MTR) and lysosomes with *LysoTracker® DND-99 Red* (LTR). Cathepsin B, which is a lysosomal enzyme released in the cytosol when the lysosome is damaged, was characterized by immunostaining. The early activation of apoptosis was evaluated by immunoassays against the activated-form of caspase-3 (Figure 3.5 and Figure 3.6).

Upon CisDiMPyP photosensitization, there is a remarkable decrease in Rh123 fluorescence (FITC-A+ 59.4), indicating a loss of ΔΨm, while in the case of $TPPS_{2a}$-treated cells, the Rh123 fluorescence (FITC-A+ 75.1) (and consequently ΔΨm) remained at the same level as the control (Figure 3.4).

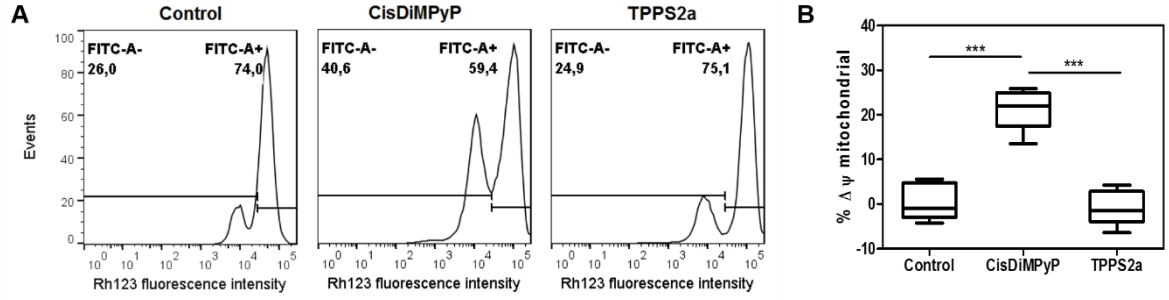

Figure 3.4. **(A)** Flow cytometry histograms of rhodamine 123 (Rh123) fluorescence, 3 hours after irradiation, in control cells and in HeLa cells treated with 30 nM $TPPS_{2a}$, 100 nM CisDiMPyP (left) and irradiated (2.1 J/cm^2 at 522nm). **(B)** Percentage of mitochondrial membrane potential ($\Delta\psi_m$) depolarization in comparison with control cells. $\Delta\psi_m$ values were calculated from the data shown in the left figure. Box plots correspond to minimum and maximum values of at least two independent experiments (n = 6, ***$p<0.001$ are considered statistically significant).

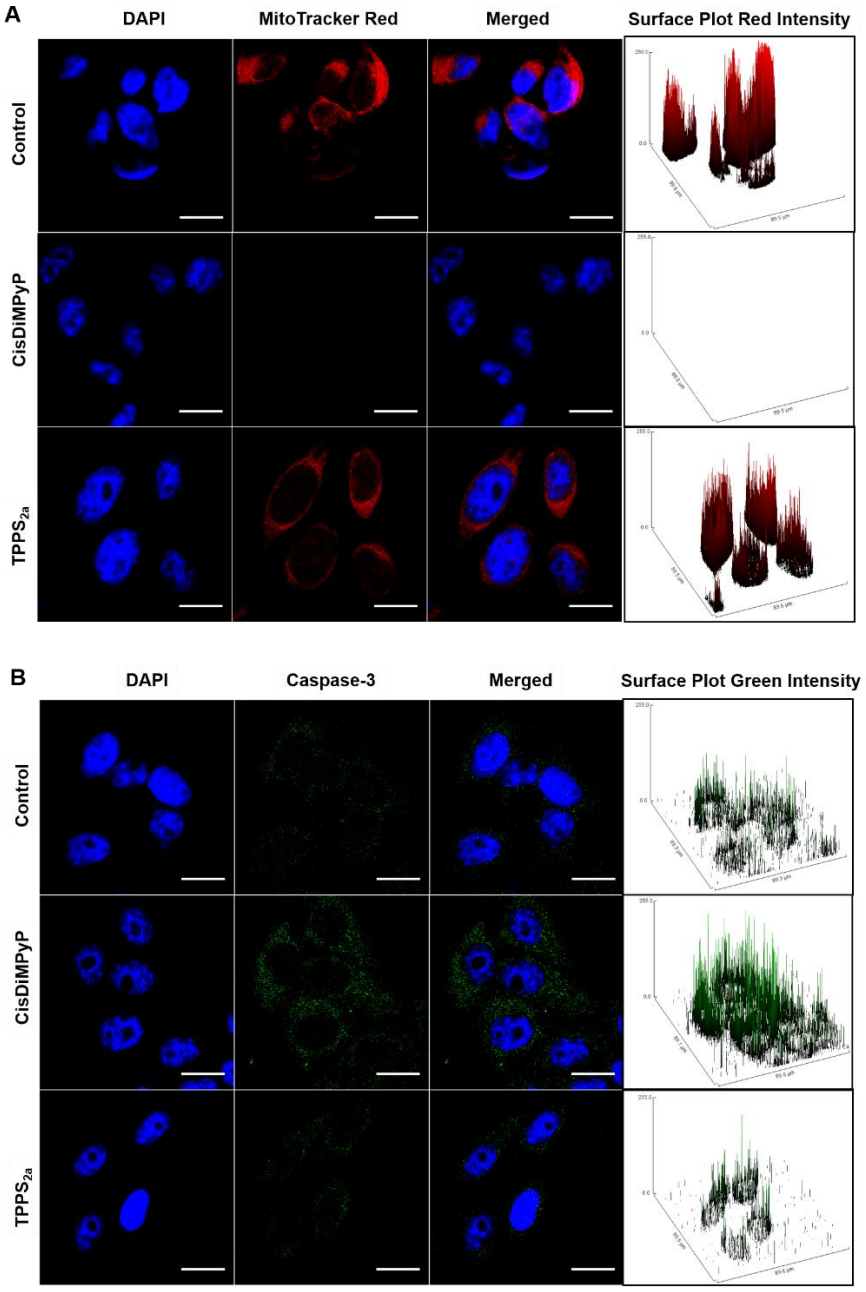

Figure 3.5. **(A)** Fluorescence images obtained 3 hours after irradiation of control HeLa cells, and cells incubated with 100 nM CisDiMPyP or 30 nM $TPPS_{2a}$ and irradiated. First column: blue fluorescence of nucleus DAPI staining; second column: red fluorescence of MitoTracker® Red, staining actively-respiring mitochondria; third column: both channels (blue and red) merged; Fourth column: surface plots of red intensity from MitoTracker®. Scale bar of 20 μm. **(B)** Fluorescence images obtained 3 hours after irradiation of control HeLa cells, and of cells incubated with 100 nM CisDiMPyP or 30 nM $TPPS_{2a}$. First column: blue fluorescence of DAPI nucleus staining; second column: green fluorescence of cleaved caspase-3 antibody; third column: both channels (blue and green) merged; fourth column: surface plots of green intensity from cleaved caspase-3 antibody. Scale bar of 20 μm.

There was also a significant loss of MTR-fluorescence intensity in CisDiMPyP-treated cells, which is a consequence of mitochondrial damage and decrease in $\Delta\Psi m$, contrasting the MTR-fluorescence images observed for $TPPS_{2a}$ and control cells (Figure 3.5A). Surface plot profiles and quantification of fluorescence intensity support these findings (Figure 3.5A, right panels). Several literature reports have shown that mitochondrial photodamage may trigger apoptosis (Spring et al. 2015; Bacellar et al. 2015; C. A. Morton et al. 2013; Pavani, Iamamoto, and Baptista 2012; David Kessel and Luo 1998; Mroz et al. 2011; D. Kessel and Luo 2001). Based on this premise, we also measured the profile of activated caspase-3, which is the major modulator of the apoptotic cascade (Figure 3.5B). Only CisDiMPyP-photosensitized cells showed a noticeable increase in the levels of caspase-3 (Figure 3.5B). It is clear that unlike $TPPS_{2a}$, CisDiMPyP at the LC_{50} promptly accumulates within mitochondria and upon photo-activation causes severe damage in this organelle membrane.

In contrast to CisDiMPyP, $TPPS_{2a}$ triggered remarkable photodamage in lysosomes. $TPPS_{2a}$-photosensitized cells were not stained by lysosomotropic LTR, while CisDiMPyP-photosensitized cells showed similar levels of LTR staining as control cells (Figure 3.6A). Supporting this finding, the level cytosolic Cathepsin B (CTSB release) was higher for $TPPS_{2a}$ than for CisDiMPyP and control cells, indicating an increase of lysosome membrane permeability (LMP) after photosensitization (Figure 3.6B). The lack of lysotracker staining and the diffuse pattern of cathepsin staining are characteristic markers of LMP (Boya and Kroemer 2008). Therefore, at the LC_{50}, $TPPS_{2a}$ caused significant damage in lysosomes.

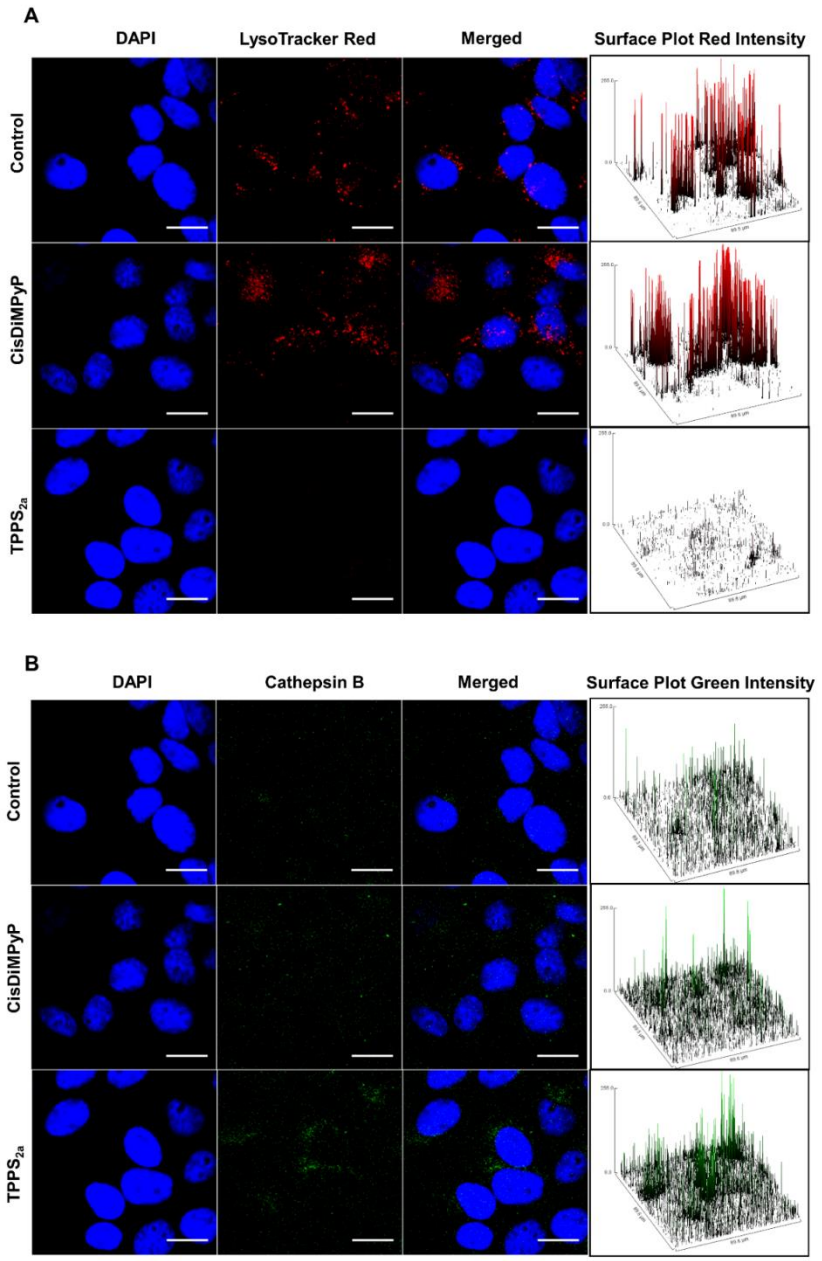

Figure 3.6. Fluorescence images obtained 3 hours after photosensitization of control HeLa cells and of cells incubated with 100 nM CisDiMPyP and 30 nM $TPPS_{2a}$. **(A)** First column: blue fluorescence of DAPI staining nucleus; second column: red fluorescence of LysoTracker® Red staining lysosomes; third column: both channels (blue and red) merged; Fourth column: surface plots of red fluorescence from LysoTracker®. Scale bar of 20 μm. **(B)** First column: blue fluorescence of DAPI staining nucleus; second column: green fluorescence of cathepsin B anti-body; third column: both channels (blue and green) merged; fourth column: surface plots of green intensity from cathepsin B antibody. Scale bar of 20 μm. Incubation of HeLa cells with porphyrins for 3 hours in DMEM with 1% FBS followed by irradiation with LEDs emitting at 522 ± 20 nm and light dose 2.1 J/cm^2.

3.3.3. Consequences of the organelle-specific photodamage

At this point, our findings indicated that the cell killing capacity changed remarkably, depending on the PS ability of targeting specific intracellular organelles membranes. We hypothesize that such differences are correlated to the type of cell death mechanism triggered by the specific damages induced in mitochondria or in lysosomes by the photosensitized oxidations produced by CisDiMPyP and $TPPS_{2a}$, respectively. Therefore, we investigated the modes of cell death by assessing the main biochemical hallmarks as illustrated in Figure 3.7.

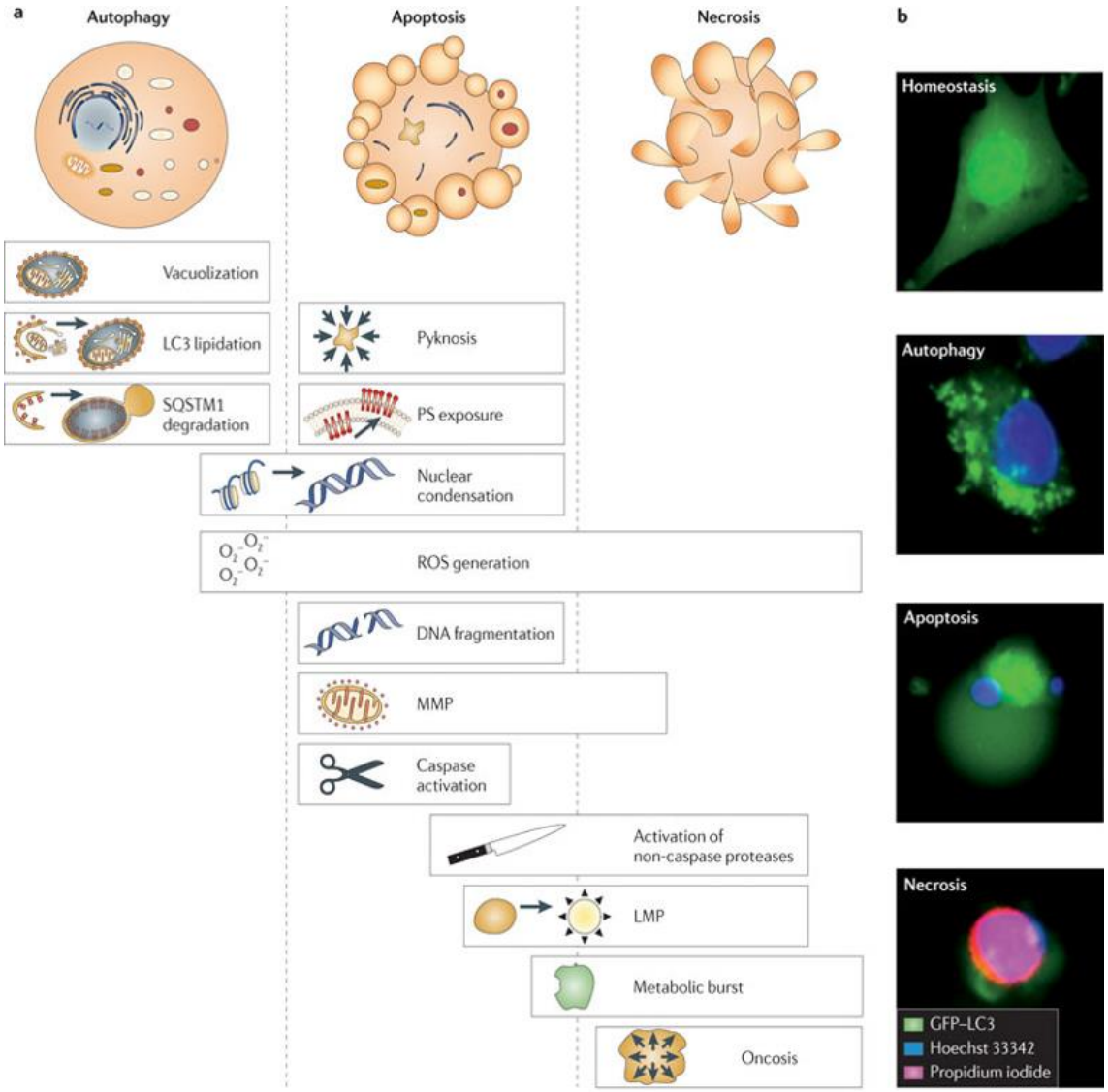

Figure 3.7. Molecular characteristics of autophagy, apoptosis and necrosis. (a) Autophagy, which is phenotypically detectable by acid vacuoles (vacuolization), LC3-II in the autophagosomal membrane (LC3 lipidation) and adaptor proteins (P62-SQSTM1) linked to

LC3-II. Apoptosis is morphologically characterized by nuclear condensation and pyknosis followed by DNA fragmentation. Also, biochemical changes such as phosphotisylserine exposure in the plasma membrane occur, as well as mitochondrial membrane permeabilization (MMP) and caspase cascade activation. Necrosis typically manifests with oncosis and shares some features with apoptosis. (b) Fluorescence microscopy for the detection of multiple cell death modes: human osteosarcoma U2OS cells stably expressing a green fluorescent protein (GFP)–LC3 chimaera were kept in control conditions (homeostasis) or treated for 12 hours with 1 μM of rapamycin (an autophagic stimulus) or 1 μM of staurosporine, either alone (triggering apoptosis) or together with 20 μM of Z-VAD-fmk (leading to necrosis). Cells were then co-stained with the nuclear dye Hoechst 33342 and the exclusion dye propidium iodide. Reprinted by permission from Macmillan Publishers Ltd (Kepp et al. 2011).

3.3.3.1. Consequences of mitochondrial photodamage by CisDiMPyP

In order to further evaluate the cytotoxic effects of both porphyrins we characterized the viability of HeLa cells 3 hours after irradiation. Cells previously incubated with 100 nM of CisDiMPyP suffered a significant decrease in cell viability (68% ± 3) compared to $TPPS_{2a}$-photosensitized cells (93% ± 1) (Figure 3.8A). Therefore, just after irradiation the phototoxicity of CisDiMPyP is actually greater than that of $TPPS_{2a}$, suggesting a more acute phototoxicity. Accordingly, by AO/PI double staining assays, it was clear that CisDiMPyP-photosensitized cells have a larger percentage of membrane permeabilization (PI incorporation), which was not present in $TPPS_{2a}$-photosensitized cells (Figure 3.8B). Note also that in CisDiMPyP-photosensitized cells nuclear dissolution occurred, indicative of pyknosis (blue arrow in Figure 3.8B), a common hallmark of late apoptotic or/and necrotic cells (David Kessel and Luo 1998; Oleinick, Morris, and Belichenko 2002; Ana P. Castano, Demidova, and Hamblin 2004). Interestingly, these results are considerably different from those measured 48 h and 8 days after photosensitization (Figure 3.2B and Figure 3.2C), which showed $TPPS_{2a}$ toxicity being several times larger than that of CisDiMPyP.

The morphological features of the cells shown in Figure 3.8B suggests apoptosis/necrosis in the Hela cells after the CisDiMPyP photosensitization. To further investigate this suggestion, we performed cytofluorometric analysis on by using Annexin V-FICT/PI approach. Scatter-plots revealed a significant larger percentage of PI(+)/AV(+) cells, which indicates late

apoptosis or necro-apoptosis, in CisDiMPyP-treated cells (47 ± 4%) in comparison with control (15 ± 3%) and $TPPS_{2a}$-treated (24 ± 4%) cells. The positive control for apoptotic cell death that we employed in this experiment, i.e. Staurosporine, induced 42 ± 2% of PI(+)/AV(+) cells, which is similar to the value observed for CisDiMPyP-treated cells. This typical apoptotic phenotype was observed neither in $TPPS_{2a}$-treated cells nor in control cells (Figure 3.8C and Figure 3.8D).

Therefore, by targeting mainly mitochondrial membranes, photoactivation of CisDiMPyP triggers the intrinsic caspase-dependent pathway, killing cells by a combination of apoptosis and necrosis. This acute toxicity right after irradiation (3 h) is a common response in the case of mitochondrial photodamage, as has been reported for several other PSs (D. Kessel and Luo 2001; Mroz et al. 2011; David Kessel and Luo 1998). The percentage of live cells (45.6% ± 1.9), which was ascribed to irradiating cells previously treated with 100 nM of CisDiMPyP according to AV/PI approach (Figure 3.8C) is basically the same as the cell viability measured at 48 hours after the acute toxic effect (LC_{50}, see Figure 3.2B). Therefore, CisDiMPyP photosensitization induces an acute damage killing a large fraction of the cells. However, cells did not die during the following hours after irradiation. The number of live cells determined 3 hours after photosensitization with 30nM of $TPPS_{2a}$ is similar to the control (Figure 3.8) and a lot larger than the 50% of cell survival determined 48 hours after irradiation (LC_{50}). Accordingly, $TPPS_{2a}$-phototoxicity seem to rely on the loss of cellular homeostasis in a time-dependence manner, unlike CisDiMPyP, which modulated cell death in a more promptly-acute way.

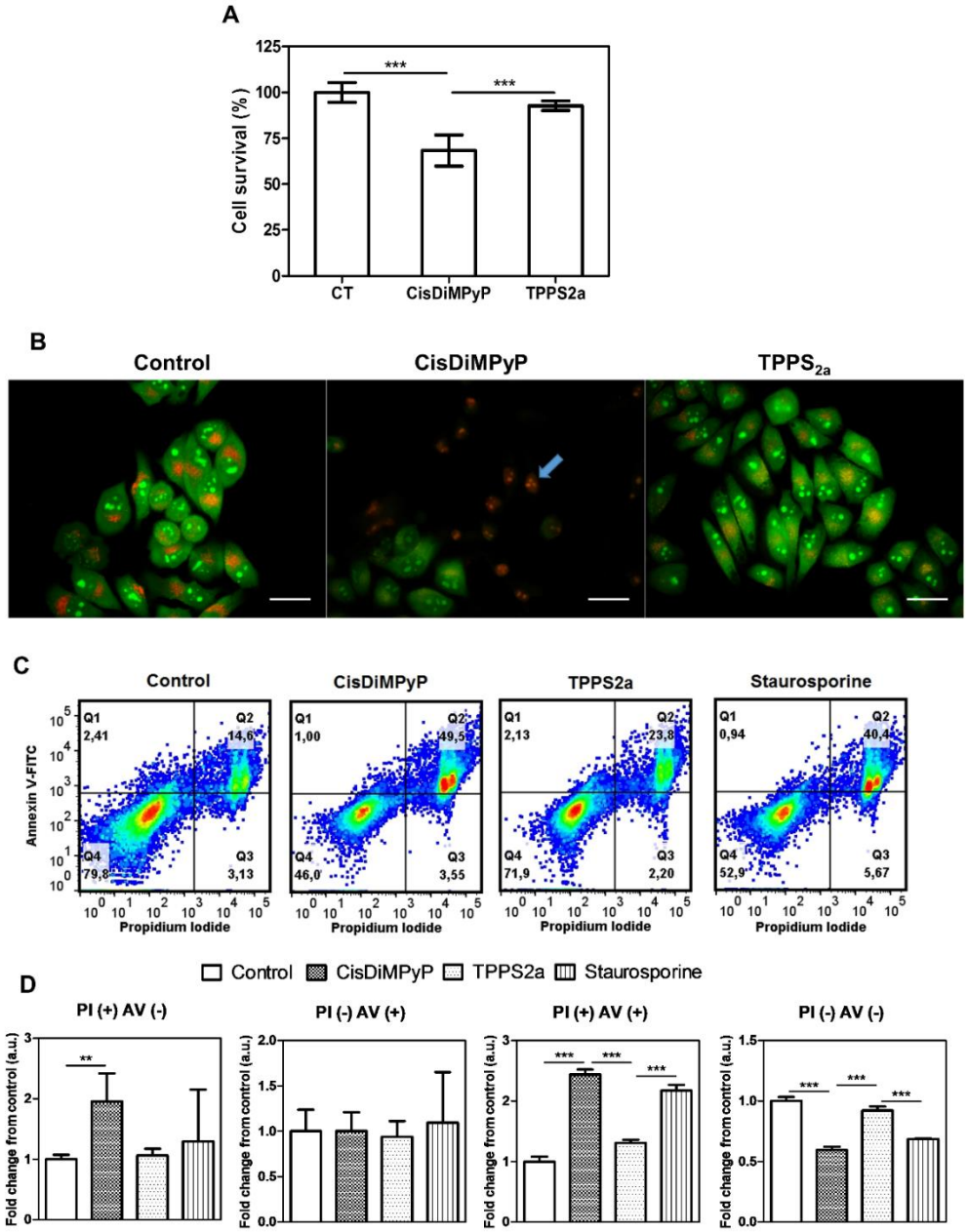

Figure 3.8. **(A)** Cell viability (by MTT assay) of control and cells incubated with 100 nM of CisDiMPyP and 30 nM of $TPPS_{2a}$, 3 hours after irradiation. Bars represent the mean ± SD of at least three independent experiments (n = 6, ***p<0.001 is considered statistically significant). **(B)** AO/PI double staining micrographs obtained 3 hours after irradiation of control cells and cells incubated with 100 nM of CisDiMPyP or with 30 nM of $TPPS_{2a}$. Scale bar is 50 μm. **(C)** Pseudo-color scatter-plots showing gating in 4 populations, according to positive and negative responses to Annexin V-FITC and Propidium iodide of non-treated cells (control) and of cells treated with: 100 nM CisDiMPyP, or 30 nM $TPPS_{2a}$, or 1 μg/mL Staurosporine. **(D)** Fold change in comparison with the control of the 4 gated populations showed in **(C)**. **(A, B, C and D)** HeLa cells were incubated with porphyrins in DMEM (1% FBS) for 3 hours, and then irradiated with LEDs emitting at 522 ± 20 nm and light dose 2.1 J/cm^2.

3.3.3.2. Consequences of lysosomal photodamage by $TPPS_{2a}$

As already discussed, 3 hours after photosensitization $TPPS_{2a}$ caused lysosomal instability (Figure 3.6). Some reports described that lysosome-targeted PDT usually induces apoptotic cell death, which is associated with the permeabilization of the lysosomal membrane and release of cathepsins, the cleavage of apoptotic effectors (Reiners et al. 2002; D. Kessel and Luo 2001). However, in our studies we observed neither Annexin V-FITC binding (Figure 3.8C and Figure 3.8D), nor caspase-3 activation (Figure 3.5C) and PI incorporation (Figure 3.8B), indicating that apoptosis is not playing a role in the case $TPPS_{2a}$-induced cell death. We cannot suppose that the absence of apoptotic response after lysosome permeabilization is a consequence of the absence of Bid (cathepsin-mediated cleavage of Bid catalyzes an apoptotic response), since HeLa cells have shown to have active Bid and to engage in apoptosis induced by lysosome membrane permeabilization (Cirman et al. 2004; Köhler et al. 2008). We hypothesize that $TPPS_{2a}$ is triggering cell death by inhibiting autophagy, which is an important biological process responsible for the maintenance of cellular homeostasis. By triggering lysosomal impairment, $TPPS_{2a}$ could suppress the autophagic flux, which in turn causes autophagy-associated cell death, as has been recently shown by Kessel and co-authors (David Kessel 2015).

In order to uncover the role of $TPPS_{2a}$-modulated lysosomal impairment, we performed experimental protocols aiming to monitor autophagy (Klionsky et al. 2016; W.K. Martins et al. 2015). Thus, 48 hours after irradiation we stained HeLa cells with the lysosomotropic dye acridine orange (AO). As revealed by the orange/red fluorescence dots present in $TPPS_{2a}$-photosensitized cells, but not in cells photosensitized with CisDiMPyP, there was a remarkable accumulation of acid vacuoles (Figure 3.9A-i). The AO red/green fluorescence fold, which is proportional to the ratio of acidic vacuoles to the total cell staining, increased in the order: control in absence of porphyrins (1.0 ± 0.1) < CisDiMPyP (1.2 ± 0.4) < $TPPS_{2a}$ (1.7 ± 0.2) ≤

Chloroquine (2.0 ± 0.1) (Figure 3.9A-ii). Indeed, the level of accumulation of acidic vacuoles observed in $TPPS_{2a}$-photosensitized cells is similar to that observed in cells treated with chloroquine, which is a known inhibitor of the autophagy flux (Figure 3.9A-ii).

Additionally, we compared the level of *autophagy arbitrary units* (AAU), which is an indicator of the magnitude of autophagy-associated cell death (AAU is calculated by comparing the viability measured by three independent methods, NR, CV and MTT) (Waleska K. Martins et al. 2013), in cells incubated with either CisDiMPyP or $TPPS_{2a}$ and irradiated (Figure 3.9B). While dark controls have relatively stable levels of AAU, an increase in AAU was observed as a function of $TPPS_{2a}$ concentration, while in CisDiMPyP-photosensitized cells there was a decrease in the AAU level. This finding indicates that autophagy is not correlated with the decrease in cell viability as CisDiMPyP concentration increases (Figure 3.9B). In the case of $TPPS_{2a}$ there was a remarkable accumulation of lysosomotropic vacuoles (i.e. increase of AAU), which significantly and strongly correlate with decrease in cell survival as $TPPS_{2a}$ concentration increased (W.K. Martins et al. 2015).

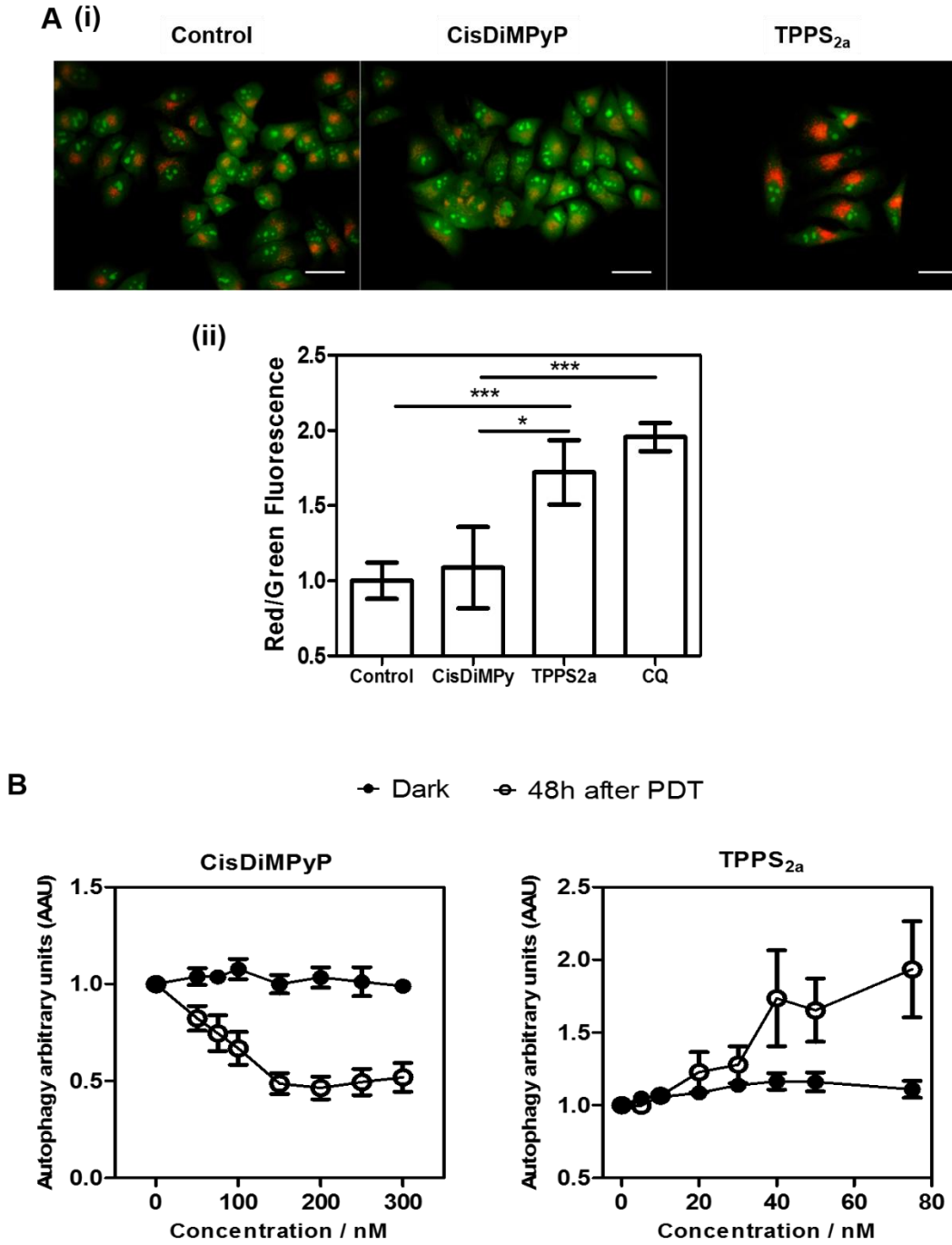

Figure 3.9. **(A) (i)** Micrographs obtained 48 hours after irradiation of control cells and of cells incubated with 100 nM of CisDiMPyP or with 30 nM of $TPPS_{2a}$, using AO/PI double staining. Scale bar of 50 µm. **(ii)** Bars represent red and green fluorescence ratio of AO/PI double staining from micrographs of cells showed in the left and of cells treated with 60 µM of Chloroquine (CQ). (n = 6, **p<0.03 and ***p<0.001). **(B)** Autophagy arbitrary units calculated 48 hours after the irradiation of cells previously incubated with either CisDiMPyP or $TPPS_{2a}$ as function of porphyrin concentration (nM).

As illustrated in Figure 3.7, autophagy is typically detectable by LC3 lipidation and adaptor proteins (P62-SQSTM1) linked to LC3-II. Thus, we estimated the autophagic flux in terms of LC3 by western blotting assay 48 hours after cell irradiation (Figure 3.10i). LC3-II accumulates in $TPPS_{2a}$- photosensitized cells, regardless of autophagy inhibition by BAF (Figure 3.10ii), attesting that there was autophagy inhibition (Klionsky et al. 2016).

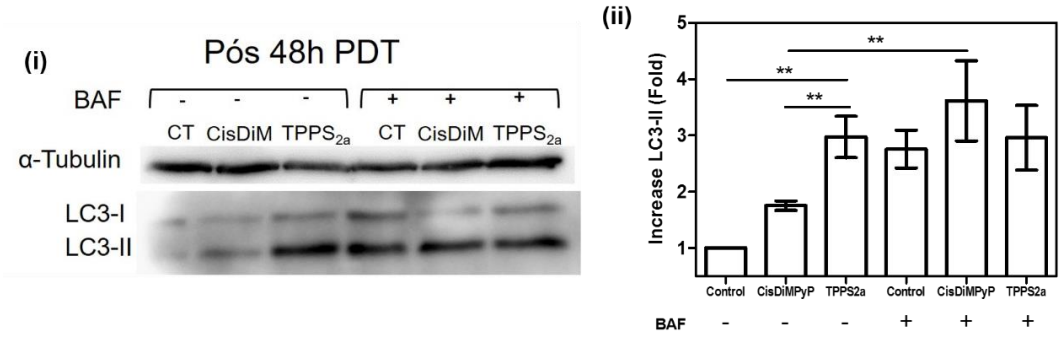

Figure 3.10. **(i)** Expression levels of LC3I and LC3-II by western blot analysis of control cells and of cells previously incubated with 100 nM of CisDiMPyP or 30 nM of $TPPS_{2a}$, 48h after irradiation in the absence or presence of 5 nM of baflomicyn-A1 (BAF). **(ii)** Bars represent the results from 2 independents experiments and indicate the relative amounts of LC3-II (%) normalized by baseline expression of α-tubulin and the standard deviation (SD) is represented by error bars (n = 4, **p<0.03 and ***p<0.001).

Next, we also evaluated the recruitment of adaptor molecules such as P62/SQSTM1, which represents a selective degradation signal in mammalian cells (Pankiv et al. 2007; Bjørkøy et al. 2009) (Figure 3.11A). The labeling of the endogenous P62/SQSTM1 in the cytosol of $TPPS_{2a}$-photosensitized cells significantly increased 48 hours after irradiation, compared to control and CisDiMPyP-photosensitized cells (Figure 3.11B), regardless of autophagy inhibition by BAF. In the case of CisDiMPyP, recruitment of endogenous P62/SQSTM1 happens only in the presence of BAF, which is a condition with parallel damage in mitochondria and lysosome, previously described to cause strong autophagy inhibition (W.K. Martins et al. 2015). Moreover, confocal microscopy revealed a larger recruitment of lysosomal enzymes (cathepsin B) for $TPPS_{2a}$-photosensitized cells compared with those photosensitized with CisDiMPyP (Figure 3.11C).

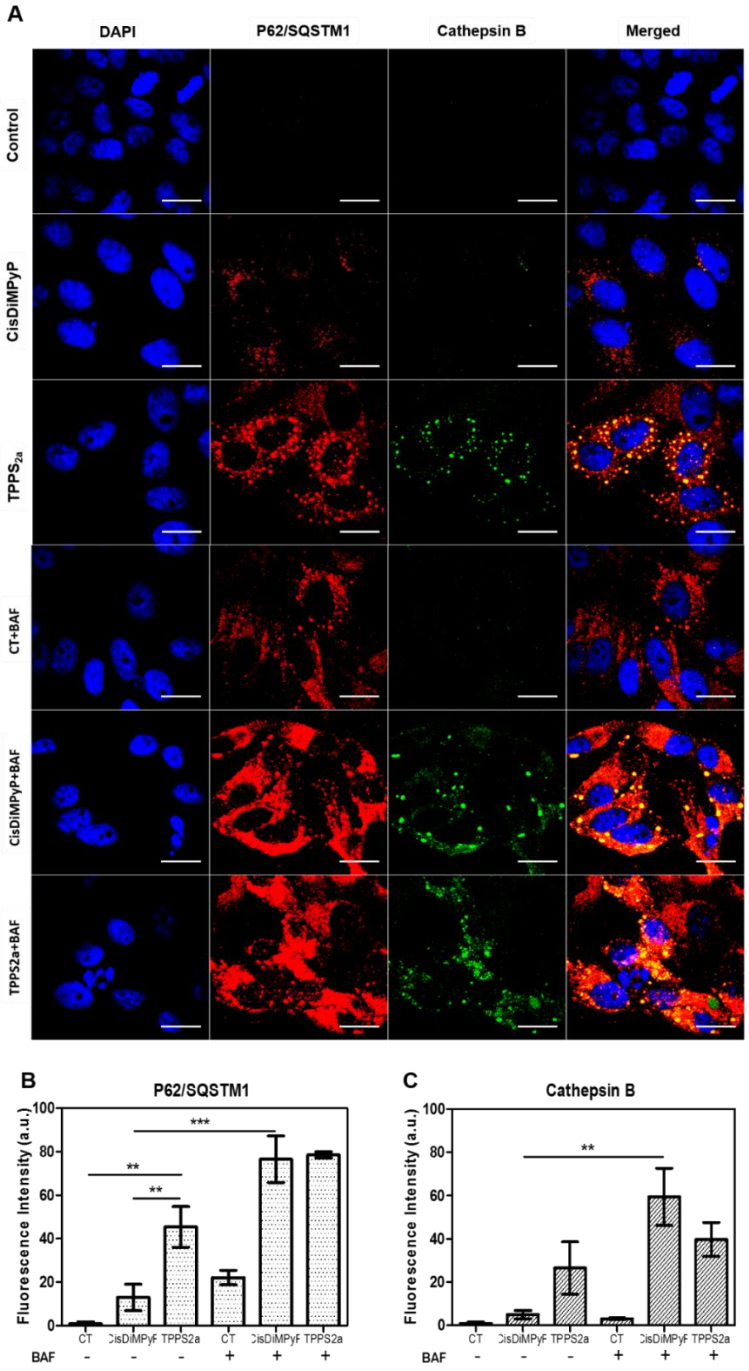

Figure 3.11. **(A)** Images of HeLa cells non-treated (Control) and treated with photosensitizers (100 nM CisDiMPyP or 30 nM $TPPS_{2a}$) and 2 nM baflomycin-A1 (BAF) followed by immunostaining for P62/SQSTM1 (red fluorescence) and cathepsin B (green fluorescence). The scale bars are 20 µm. **(B)** Fluorescence intensity of P62/SQSTM1 (red fluorescence) and **(C)** cathepsin B (green fluorescence) from control cells and of cells previously incubated with 100 nM of CisDiMPyP or 30 nM of $TPPS_{2a}$ in the absence or presence of 2 nM of baflomycin-A1 (BAF). Bars correspond the mean ± SD of at least two independent experiments (n = 6, **p<0.03 and ***p<0.001 are considered statistically significant).

Autophagy can be a dual-function process, facilitating both, protecting against cell death and/or promoting cell death. Its role was examined by using an inhibitor of phosphatidylinositol 3-kinases (PI3K): 3-methyladenine (3-MA). The inhibition of autophagy by 3-MA provides protection against the loss of viability in $TPPS_{2a}$-photosensitized HeLa cells (Figure 3.12), suggesting that the impairment of autophagic pro-survival functions is responsible for a more efficient long-term phototoxicity. Contrasting this result, the effect of 3-MA was absent in CisDiMPyP-photosensitized cells (Figure 3.12). Taken together, these results showed that $TPPS_{2a}$ inhibited autophagic flux resulting in autophagy-associated cell death.

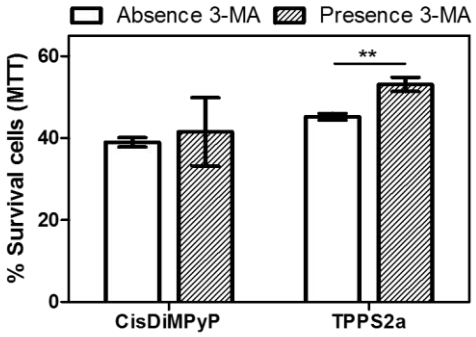

Figure 3.12. Effect of autophagy inhibition by 3-MA. Cell viability 48h after irradiation of cells previously treated with 100 nM of CisDiMPyP or 30 nM of $TPPS_{2a}$ in the absence or presence of 5mM of 3-MA. The viability of cells exposed to 3-MA alone was 52 ± 2% compared to untreated control cells, then cell survival data in presence of 3-MA were normalized to control exposed to 3-MA. Bars correspond the mean ± SD (n = 6, **$p<0.03$ is considered statistically significant).

3.4. CONCLUSION

The net charge of the PS plays a major role in the efficiency and mechanism of cell death. Amphiphilic cationic compounds are known to accumulate in mitochondrial membranes because of the negative electrochemical potential (~ -180 mV) of this organelle. Mitochondrial oxidative stress leads to a decrease in cellular ATP and to several signaling responses, which can trigger cell death trough apoptotic and/or necrotic pathways (Bacellar et al. 2015; Pavani, Iamamoto, and Baptista 2012; David Kessel and Luo 1998), in short-time periods (few hours)

after irradiation. This scenario was in fact observed after irradiating cells previously incubated with CisDiMPyP (Figure 3.13). Although the acute toxicity of CisDiMPyP was larger (compared with $TPPS_{2a}$), surviving cells seem to recover fairly well and behave as control cells some days after irradiation. On the other hand, amphiphilic anionic compounds usually localize preferentially in lysosomes (Kristian Berg et al. 1990; Woodburn et al. 1991; K. Berg and Moan 1994). Upon photo-stimulation, $TPPS_{2a}$ caused remarkable lysosomal impairment and triggered the regulated cell death associated with autophagy, which manifested itself days after irradiation, by causing cell death and proliferation decrease with a higher efficiency at extremely low PS concentration (Figure 3.13). Therefore, by targeting lysosomes, instead of mitochondria, we provided insights into a more effective PDT protocol. This information is in agreement with a previous literature report with a mechanistic explanation (Rodriguez et al. 2009). Cells photoactived with $TPPS_{2a}$ show the absence of active caspase-3, lower levels of apoptosis, damage in the lysosomal membrane, interruption in the final stage of autophagy involving fusion of autophagosomes and lysosomes, proliferation of autophagosomes (accumulation of acidic vacuoles and increased levels of LC3-II and P62/SQSTM1), inability of cells to recycle proteins and other components, leading to autophagy-associated cell death.

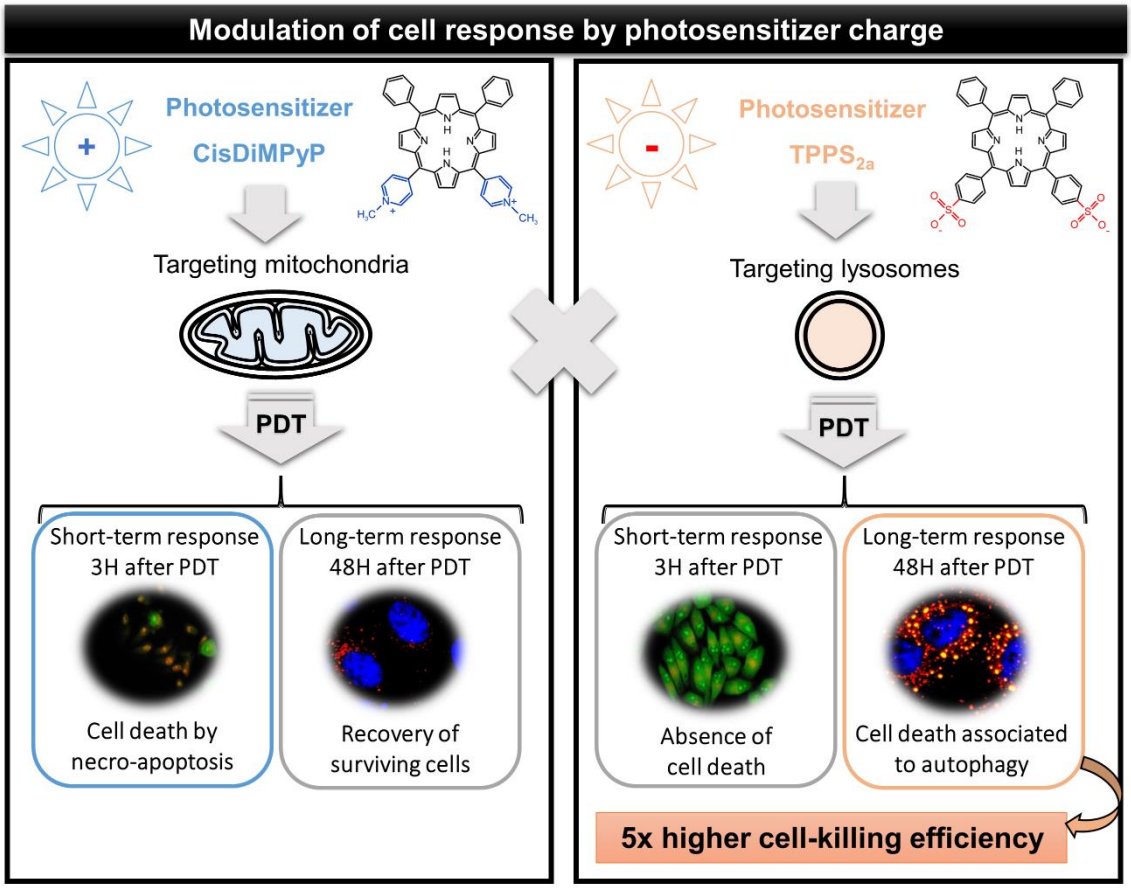

Figure 3.13. Scheme showing consequence of photodamaging cells with porphyrins containing opposite charges.

By addressing the relationship between the chemical structure of the PS, the site of intracellular damage and the mechanism of photo-induced cell death, we showed that PSs can be planned to precisely target organelles and to specifically trigger regulated cell death mechanisms. This work stands as a proof of concept that lysosomal membrane damage and induction of autophagy-associated cell death is long-lasting and a more effective way to decrease cell proliferation. Conceivably, this knowledge will help in the rational design of new drugs for organelle-target therapies.

CHAPTER 4

ENHANCED PDT EFFICIENCY PROVIDED BY TYROSINE-DERIVED NANOSPHERES

Third-generation photosensitizers aim to improve bioavailability. They consist of first and second generation PS, conjugated to or packaged within carrier molecules such as polymers. In this chapter, we demonstrate that tyrosine-derived nanospheres (Tyrospheres) can encapsulate amphiphilic photosensitizers in monomeric form, improving their photophysical and photochemical properties. Our data indicate the great potential of Tyrospheres in PDT as nanocarrier.[‡]

[‡] The work described in this chapter is in the final stage of writing for submission. Tyrosine-derived nanospheres as carrier of porphyrins in Photodynamic Therapy. Tayana M. Tsubone, Zheng Zhang, Ritu Goyal, Joachim Kohn and Maurício S. Baptista.
This work was presented orally on *10th World Biomaterials Congress (WBC)* in May 2016 at Montréal – Canada.

4. ENHANCED PDT EFFICIENCY PROVIDED BY TYROSINE-DERIVED NANOSPHERES

4.1. INTRODUCTION

As already commented in Chapter 1, even though the extended delocalized aromatic π electron system of photosensitizers allows efficient light absorption, the same π electron system may favor π-π stacking and hydrophobic interactions, therefore forming aggregates in aqueous media. One the one hand, hydrophobicity is a desirable characteristic of PS to improve their affinity to lipid bilayers, as already pointed out in Chapter 2. On the other hand, this feature leads to a poor water solubility, contributing to its aggregation tendency (Brown, Shillcock, and Jones 1976). This affects the bioavailability of the photosensitizer and hampers its ROS generation ability, causing a reduction of the PDT efficiency. Thus, attempts have been made to create suitable carrier systems that can transport photosensitizers in a stable monomeric form without altering their spectroscopic properties, without decreasing their activity, and without causing toxicity.

Most of the delivery systems are based on nanostructures such as liposomes, dendrimers and polymers. Polymeric micelles have been shown to have a good PDT outcome because of their targeting ability and pharmacokinetic functions, which can be controlled by their composition, size, surface charge, morphology and hydrophobicity (Avci, Sibel Erdem, and Hamblin 2014; Lucky, Soo, and Zhang 2015; Chatterjee, Fong, and Zhang 2008). Typically, polymeric micelles are formed by self-assembly of amphiphilic block copolymers, in which the inner core holds hydrophobic compounds and the hydrophilic shell provides protection of loaded drugs from the external environment.

Among various biocompatible polymer blocks used to form the inner core of micelles that are also occurring naturally, the most commonly used is poly(amino acids) (Khan et al. 2011; Nair and Laurencin 2007). Kohn´s group has revealed the applicability of tyrosine-

derived polymers with various applications in the biomedical field (e.g. bone regeneration, drug delivery, 3D printed scaffold) due to a number of favorable properties (Bourke and Kohn 2003). For instance, the poly(ethylene glycol)-block-oligo(desaminotyrosyltyrosine octyl ester suberate)-block-poly(ethylene glycol) (abbreviated as PEG_{5K}-b-oligo(DTO-SA)-b-PEG_{5K}) exhibits a glass transition temperature (T_g) of 21ºC which provides a sufficient flexibility of copolymer to self-assemble into a dynamic and soluble structure under physiological conditions (Larisa Sheihet et al. 2005; Nardin, Bolikal, and Kohn 2004). Also, PEG_{5K}-b-oligo(DTO-SA)-b-PEG_{5K} (also named Tyrospheres or Tyrosine-derived nanospheres) presents a significantly low critical aggregation concentration (cac ~ 0.26 µg/mL at 37ºC) (Larisa Sheihet et al. 2005; Nardin, Bolikal, and Kohn 2004) when compared with other polymeric micelles commercially available, as for example F127 (cac ~ 0.025 g/L at 35ºC) and P123 (cac ~ 0.001 g/L at 35ºC) (Alexandridis, Holzwarth, and Hatton 1994). This implies that Tyrosine-derived nanospheres are very stable upon strong dilution, a desirable feature in case intravenous administration and distribution in the blood volume. Because the advantages that Tyrospheres offer (i.e. biodegrability, biocompatibility, high loading capacity, easily micellize yielding, extremely stable micelles), we consider them very attractive as carriers for photosensitizers.

A great part of PDT treatments is directed at the treatment of superficial tumors (e.g. in the skin) or other non-oncological skin conditions. Tyrospheres have already been patented in USA and are used for the delivery of several drugs, including topical application methods. They have been used for the delivery of paclitaxel (a chemotherapeutic agent), Vitamin D3 and Betamethasone dipropionate (for treatment of psoriasis) (Kilfoyle et al. 20012; Kilfoyle 2011). The authors showed that Tyrospheres deliver twice the amount of active substance to the epidermis than commercially available cream (Batheja et al. 2011; Kilfoyle et al. 20012). This may probably be, because tyrosine-derived nanospheres facilitate the transport of lipophilic substances to deeper layers of skin (L. Sheihet et al. 2008).

Together with the advantages of Tyrospheres, mentioned above, we were encouraged to investigate the possibility of the use of Tyrospheres as nanocarriers for amphiphilic photosensitizers (CisDiMPyP and $TPPS_{2a}$).

4.2. METHODOLOGY

4.2.1. Preparation of photosensitizer-loaded TyroSpheres

Photosensitizers were encapsulated in tyrosine-derived nanospheres (Tyrospheres) by a self-assembly technique according to previously established protocols (L. Sheihet et al. 2008; Larisa Sheihet et al. 2012; Larisa Sheihet et al. 2007). The polymer PEG-oligo(DTO-SA)-PEG was synthesized and gently supplied by Kohn´s group (*New Jersey Center for Biomaterials – Rutgers University*). Then, 60 mg of PEG-oligo(DTO-SA)-PEG was dissolved in 400 µL dimethylformamide (DMF) and mixed with 300 µL of 1 mg/mL photosensitizer (CisDiMPyP or $TPPS_{2a}$) in DMF. This solution was added drop-wise to 14.3 mL of deionized water under constant stirring. The resulting suspension was passed through 0.22 µm PVDF filters and ultra-centrifuged for 3 hours at 65,000 rpm and 18ºC. The supernatant was removed and the pellet of nanospheres was washed twice with PBS and re-suspended in 1 mL PBS at 25ºC, diluted to 3 mL using PBS, and filtered again through 0.22 µm PVDF filters (L. Sheihet et al. 2008; Larisa Sheihet et al. 2012; Larisa Sheihet et al. 2007).

4.2.2. Characterization of photosensitizer-loaded TyroSpheres

The nanospheres containing PS were characterized by their particle size, size distribution, zeta potential, and binding and loading efficiency. The hydrodynamic diameters and polydispersity index of the Tyrospheres with or without porphyrins were obtained using dynamic light scattering, as previously described (L. Sheihet et al. 2008). The stability of the nanosphere size was monitored also by dynamic light scattering (DLS) as a function of the time,

whereas time zero is just after the Tyrosphere preparation. To determine binding and loading efficiency a predetermined aliquot (50 μL) of PS-loaded Tyrosphere suspension was dissolved in 2 mL methanol. The absorbance spectrum of PS extracted from polymer was measured using UV-Vis spectrophotometer and values of binding and loading efficiency were calculated by equation 4.1 and 4.2 (Larisa Sheihet et al. 2007; L. Sheihet et al. 2008).

$$Binding\ Efficiency = \frac{\text{Amount of PS in TyroSpheres}}{\text{Amount of PS in Initial Feed}}\ x\ 100\% \qquad \text{(Equation 4.1)}$$

$$Loading\ Efficiency = \frac{\text{Amount of PS in TyroSpheres}}{\text{Amount of Polymer in TyroSpheres}}\ x\ 100\% \qquad \text{(Equation 4.2)}$$

Mean value ± SD were acquired from three independent experiments with at least 3 identical samples in each experiment (n=9).

4.2.3. Photophysical properties of PS-loaded Tyrospheres

The absorption spectrum of PS-Tyrospheres was recorded at room temperature for the wavelength range of 350 to 700 nm using a Shimadzu UV2401-PC spectrophotometer. The fluorescence emission spectrum and resonant light scattered (RLS) were registered on a Varian Cary Eclipse spectrofluorimeter. For the fluorescence emission experiments spectra were recorded in the 600-800 nm range, using an excitation wavelength of 515 nm, excitation slit 5 nm and emission slit 10 nm. Absorbance values of samples and reference solutions were kept below 0.1 at the excitation wavelength, to avoid inner filter effects. Fluorescence quantum yields (ϕ_F) of porphyrins in methanol were calculated by measuring the area under the emission spectrum and comparison with $TPPS_4$ in methanol ($\phi_F = 0.16$)(Basu 1991) as standard (equation 4.3) (D'Souza et al. 2015).

$$\phi_F^{PS} = \frac{F_{PS} \cdot \eta_{Std}^2}{F_{Std} \cdot \eta_{PS}^2} \cdot \phi_F^{Std} \qquad \text{Equation 4.3}$$

Where F is the fluorescence spectrum area, η is the refraction index and ϕ_F is the fluorescence quantum yield. The symbols reported as subscript represent the standard (Std) and photosensitizer (PS).

RLS spectra were obtained at wavelengths from 200 to 800 nm with $\Delta\lambda$ = 0 nm (synchronous mode), excitation and emission slits 2.5 nm. RLS spectra of PS-Tyrospheres were subtracted by RLS spectra of empty-Tyrospheres to eliminate the scattering signal from Tyrosine-derived nanospheres. Quartz cuvettes with a path length of 1.0 cm were used for all measurements and all experiments were performed at room temperature.

4.2.4. Singlet oxygen generation of PS-loaded Tyrospheres

A home-made setup for singlet oxygen luminescence detection was implemented by Edinburgh Instruments. It consists of a time resolved near-infrared fluorimeter with a Hamamatsu R55009 photomultiplier cooled to -80ºC. Laser excitation was performed with a Nd:YAG coupled to an OPO (Quantel laser Brilliant, 3W, Rainbow OPOTEC) set to 515 nm, delivering 5 ns pulses at 10 Hz, with a pulse energy of 2 mJ/pulse. Decays were obtained with a MSA_300 and spectra were obtained with an Edinburgh Instruments acquisition with F900 software. The singlet oxygen quantum yield (ϕ_Δ) of porphyrins in methanol was determined using $TPPS_4$ in methanol (ϕ_Δ = 0.70) as reference (R W Redmond and Gamlin 1999), while ϕ_Δ of porphyrins in PBS and Tyrospheres was calculated using $TPPS_4$ in 2% Triton X-100 (ϕ_Δ = 0.80) (R W Redmond and Gamlin 1999) as standard (equation 4.4) (Kempa et al. 2015). All photosensitizer (in solution or suspension) had an absorbance of 0.3 at 515 nm to ensure the same number of photons absorbed for all samples.

$$\phi_\Delta^{PS} = \frac{I_{PS}}{I_{Std}} . \phi_\Delta^{Std} \qquad \text{Equation 4.4}$$

I is the maximum phosphorescence intensity of the singlet oxygen decay curve and ϕ_Δ is the singlet oxygen quantum yield. Symbols as subscript refer to the standard (Std) and photosensitizer (PS).

4.2.5. Time-resolved fluorescence measurements in aqueous media

Time-resolved fluorescence measurements were performed by time-correlated single-photon counting (TCSPC) using a TimeHarp 260 PICO board (PicoQuant, Berlin, Germany). The samples were excited with a 405 nm picosecond pulsed diode laser (LDH-P-C-405, PicoQuant, Berlin, Germany) and the emission was detected with a long-pass filter 630LP. For data analysis, the SymPhoTime64 software version 2 1 3813 was used. The fluorescence lifetimes (τ_F) were obtained by deconvolution fitting.

4.2.6. Fluorescence lifetime imaging (FLIM) in living cells

The time-resolved luminescence imaging of HeLa cells incubated 3 hours with 1 μM porphyrins (free or encapsulated) was acquired using a MicroTime 200 time-resolved confocal fluorescence microscope (PicoQuant, Berlin, Germany) was used, which consists of an inverted microscope (IX 73, Olympus) equipped with an Olympus UPlanSApo 60 × /NA 1.2 water immersion objective. A pulsed diode laser (LDH-P-C-405, PicoQuant, Berlin, Germany) operating at 405 nm with a pulse width of <64 ps was used as an excitation source. For the separation of luminescence and rejection of the excitation light, a long-pass filter 630LP was used.

4.2.7. Subcellular localization

HeLa cells ($1x10^5$ cells/well at 6-well plate) were incubated with porphyrins (1μM in DMEM supplemented with 1% FSB) for 3 hours at 37ºC, 5% CO_2. DAPI, MitoTracker® Green

FM and LysoTracker® Green DND-26 were used as probes for nuclei, mitochondria and lysosomes, respectively. MitoTracker® Green FM (150 nM) and LysoTracker® Green DND-26 (150 nM) were added after 150 minutes of PS-incubation, and then the cells were incubated for another 30 min. Microscope slides were placed with ready-to-use Prolong Diamond Antifade Mountant with DAPI and analyzed under confocal microscope (Zeiss^{TM} Axiovert 200 LSM 510 Laser and Confocor Modules). Porphyrin fluorescence images were then recorded using a 514 nm laser for excitation and a bandpass filter, 600-800 nm, for emission. Note: excitation/emission of MitoTracker® Green and LysoTracker® Green were 488 nm /505-530 nm, and that of DAPI was 358 nm/460 nm. Fluorescence images were obtained using a confocal Zeiss (LSM 510). Images were analyzed using *Image J* software. The calculation of the colocalization between photosensitizer and organelle-probe was performed by *Manders overlay coefficient (MOC)* plugin from *Image J*.

4.2.8. Acridine orange and propidium iodide double staining

After 3 and 48 hours of PDT, cells were washed with PBS and incubated with AO/PI solution (1µg/mL each dye in PBS) for 10 minutes, at 5% CO_2 and 37ºC (Abdel Wahab et al. 2009) Images were acquired with a fluorescence microscope Axiovert 200 (Carl Zeiss), equipped with Zeiss Filter Set 09, which provides excitation in the 450-490 nm range and emission above 515nm. The *ImageJ* software was used to separate the green channel from the red channel in each micrograph and quantify the red and green fluorescence intensity of AO/PI double staining. Then, the ratio between red and green fluorescence of micrographs (AO/PI double staining assays) was calculated by analyzing at least four different images from random areas covering several cells of two independent experiments.

4.2.9. Cellular uptake of PS-loaded Tyrospheres in HeLa cells

HeLa cells were seeded in a 12-well plate and incubated in DMEM (1% (v/v) FBS), 5% CO_2 at 37ºC for 18 hours for attachment to the wells. Next, PS-loaded Tyrospheres were added (the final concentration of PS in the cell culture medium was 5 µM) and the cells kept for 3 hours in the dark. After this period, the supernatant solution was diluted 1:1 (v/v) with 10% (v/v) Triton X-100, while the adhered cells were washed using PBS buffer and lysed in 5% (v/v) Triton X-100. In this case, Triton X-100 was used to solubilize cell membrane and the PS. The absorption spectra of supernatant and cell lysate were recorded and the PS uptake in cells was estimated using equation 4.5.(9)

$$\%\, Uptake = 100 \,.\, \frac{Abs_C}{(Abs_C)+(2x\ Abs_S)} \qquad \text{Equation 4.5}$$

Where Abs_c is the absorbance intensity of the porphyrin in the cell lysate and Abs_s is the absorbance intensity of porphyrin in the supernatant. A correction factor of 2 was required to Abs_s due a 2-fold dilution of the suspension. At least two independent experiments were performed in triplicate (n=6).

4.2.10. Phototoxicity of PS-loaded Tyrospheres in HeLa cells

Cells ($2.8x10^4$ cells/well) were seeded in a 48-well plate and incubated for 18 hours for attachment to the wells. Then, the cells were treated with the porphyrin $TPPS_{2a}$-loaded TyroSpheres and CisDiMPyP-loaded TyroSpheres in DMEM (1% (v/v) FBS) for 3 hours in the dark, at 5% CO_2 and 37ºC. Next, the HeLa cells were washed twice with PBS and submitted to irradiation in 300 µL PBS for 15 min using a light emitting diode system (LED), emitting at 522 ± 20 nm, with final light dose of 2.1 J/cm^2. After irradiation, the cells were washed again with PBS and DMEM (1% (v/v) FBS) was added. The cells were then kept for 48 hours in the dark, at 5% CO_2 and 37ºC. The cell survival was determined by the 3-(4,5-dimethylthiazol-2-yl)-2,5-diphenyltetrazolium bromide (MTT) method (Meerloo, Kaspers, and Cloos 2011). The

cells were incubated with 0.15 mg/mL of MTT for 2 hours at5% CO_2 and 37ºC. The formed crystals were solubilized in dimethyl sulfoxide (DMSO) and quantified by absorption measurement at 550 nm using a TECAN Infinite M200 plate reader. The percentage of viable cells was calculated relative to the absorbance of the control cells (taken as 100% viability). Mean values ± standard deviation was acquired from two independent experiments, with 3 replicates per each experiment (n=6).

The values of PDT efficiency (η_{PDT}) was calculated as indicated by equation 4.6:

$$PDT\ efficiency\ (\eta PDT) = \frac{\%\ Survival\ cells}{[PS]\ incorporated\ in\ cells} \qquad \text{Equation 4.6}$$

4.2.11. Statistical analysis

To perform comparative statistical analysis, we analyzed statistical differences by a student's t-test or one-way ANOVA using GraphPrism 5.0 software. Data was obtained from at least two independent experiments (n = 6) and expressed as mean values ± standard deviation (SD). As statistically significant, we considered P-values lower than 0.05 (*), lower than 0.01 (**) and lower than 0.001 (***).

4.3. RESULTS AND DISCUSSION

4.3.1. Properties of PS-loaded Tyrospheres

The same amphiphilic porphyrins as studied in Chapter 3 (*i.e.* CisDiMPyP and $TPPS_{2a}$) were used for encapsulation in tyrosine-based triblock copolymer (see polymer structure in Figure 4.1) and formation of nanospheres. The preparation method of the PS-loaded Tyrospheres depends on the self-assembly of the tyrosine-derived copolymer in aqueous solution in such a way that the use of external stabilizers is not required, since the amphiphilic characteristic of PEG-oligo(DTO-SA)-PEG is able to stabilize the nanospheres (Zhang et al. 2014; Goyal, Macri, and Kohn 2015).

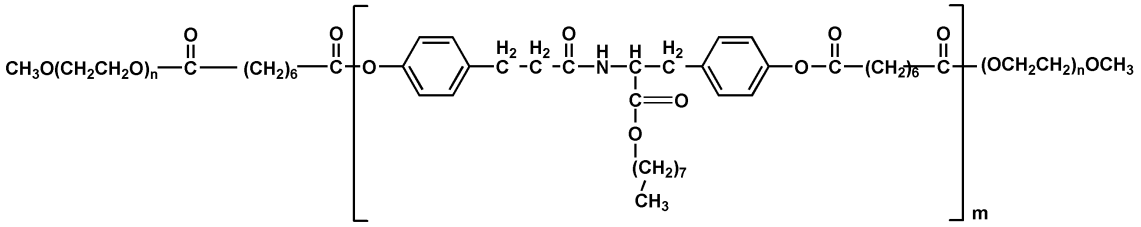

Figure 4.1. Tyrosine-derived, ABA-type poly(ethylene glycol)-b-oligo(desaminotyrosyl-tyrosine octyl ester suberate)-b-poly(ethylene glycol) triblock copolymer (PEG-oligo(DTO-SA)-PEG) used in the preparation of Tyrospheres.

The average hydrodynamic diameter of the produced nanospheres was measured by dynamic light scattered (DLS). A range of 60-70 nm with low polydispersity index (~ 0.2) – Table 4.1 was determined. The zeta potential (ξ) of the Tyrospheres was approximately zero (Table 4.1) confirming a neutral surface charge of Tyrospheres due the presence of PEG on the out shell (Larisa Sheihet et al. 2012; Goyal, Macri, and Kohn 2015). The characterization of the nanospheres showed that neither the presence of the photosensitizers nor their charge (positive or negative) significantly affects the size, size distribution and surface charge of the Tyrospheres (Table 4.1). Additionally, the stability of the nanospheres, as monitored by changes of the size and size distribution over time, showed no significant variation within 84 h at room temperature protected from light. This indicates that neither aggregation nor degradation occurs under these conditions (Figure 4.2). Note that these properties of the PS-loaded Tyrospheres are consistent with other literature reports showing that size and size distribution of Tyrospheres (size range 60-80nm and PDI <0.25) have not been affected by incorporation of different drugs or fluorescent compounds and that the formulation stability may be months (Zhang et al. 2014; Zhang et al. 2013b; Larisa Sheihet et al. 2012; L. Sheihet et al. 2008; Batheja et al. 2011).

Table 4.1. Values of size, polydispersity index (PDI), zeta potential of PS-TyroSpheres, binding and loading efficiencies.

PS-loaded TyroSpheres	Size (nm)	PDI	Zeta Potential (mV)	Binding efficiency (%)	Loading efficiency (%)
Empty- TyroSpheres	67 ± 3	0.20 ± 0.05	-0.3 ± 0.9	----	----
CisDiMPyP-TyroSpheres	63 ± 3	0.17 ± 0.04	-1.2 ± 0.7	70 ± 6	0.55 ± 0.09
TPPS$_{2a}$-Tyrospheres	63 ± 4	0.16 ± 0.04	-0.5 ± 1	67 ± 4	0.56 ± 0.08

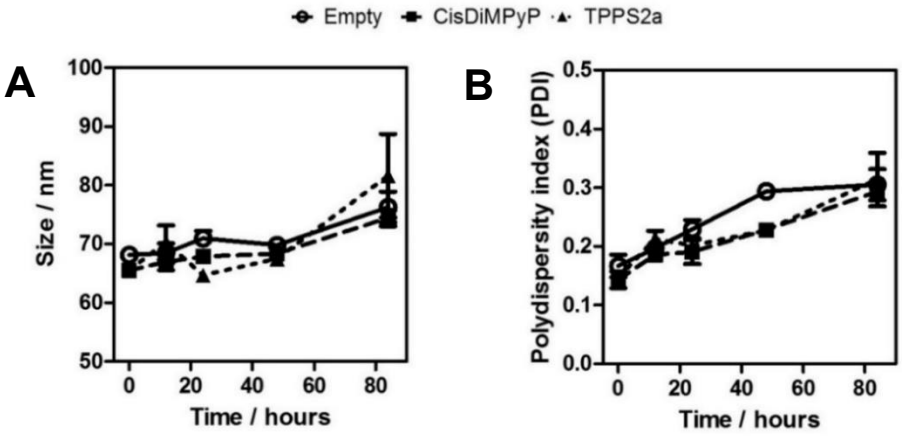

Figure 4.2. (A) Size stability of Tyrospheres in function of time encapsulating none compound (circle with solid line), CisDiMPyP (square with dashed line) and TPPS$_{2a}$ (triangle with dotted line) at room temperature. (B) polydispersity index (PDI) of Tyrospheres as a function of time, without any incorporated compound (circle with solid line), with CisDiMPyP (square with dashed line) and TPPS$_{2a}$ (triangle with dotted line) at room temperature.

The amount of encapsulated PS was evaluated by quantifying binding and loading efficiencies, which were approximately 70% and 0.5% (w/w), respectively, for both porphyrins (Table 4.1). It is noteworthy that the binding affinity was independent of the porphyrin charge, suggesting that the interaction between the amphiphilic photosensitizer and the polymer depends mainly on the hydrophobic effect. In fact, studies based on computational modeling reported that hydrophobicity and interactions such as hydrogen binding and π-π stacking are responsible for the strong interaction between amphiphilic drugs and the tyrosine-derived copolymer (Costache et al. 2010; Zhang et al. 2014).

All data together demonstrates that photosensitizers do not cause changing on the nanosphere properties such as size, charge and stability. However, we hypothesized that Tyrospheres may provide important alterations on the photosensitizers properties.

4.3.2. Influence of Tyrospheres on photophysical properties of PS

The photophysical parameters are of key interest to evaluate the potential of a photosensitizer formulation aiming at a PDT application. The absorption spectra (Figure 4.3A) show a broadening, an intensity decrease and a maximum wavelength shift of the Soret band (400-450 nm) of both porphyrins in PBS, typical for porphyrin aggregates (Robert F Pasternack et al. 1971; Brown, Shillcock, and Jones 1976). However, in a polar solvent (e.g. methanol) or when encapsulated in Tyrospheres, both porphyrins present a sharp Soret band (Figure 4.3A) indicating that molecules are mostly monomeric (Bajema, Gouterman, and Meyer 1968).

The photosensitizers showed a lower fluorescence intensity in PBS compared to methanol and when encapsulated in Tyrospheres (Figure 4.3B). Although porphyrins exhibit low fluorescence quantum yields ($\phi_F \sim 0.16$) due other competitive relaxation processes (Joseph R. Lakowicz 2006), it was possible to note that Tyrospheres provide approximately 2-fold increase in fluorescence quantum yields (ϕ_F) with respect to aqueous media (Figure 4.3D). It suggests the monomerization of compounds by encapsulation in the nanospheres.

Further evidence for porphyrin aggregation in aqueous media was found by resonance light scattering (RLS) spectroscopy which is a technique extremely sensitive and suitable to explore chromophore aggregation (R F Pasternack and Collings 1995). The presence of a scattering signal, characteristic for aggregates, was detected at 457 nm and 485 nm for CisDiMPyP and $TPPS_{2a}$, respectively, in PBS (Figure 4.3C). However, after being encapsulated in the Tyrospheres there is no more resonant light scattering in any of the porphyrins (Figure 4.3C) confirming that the Tyrospheres are able to keep photosensitizers monomeric.

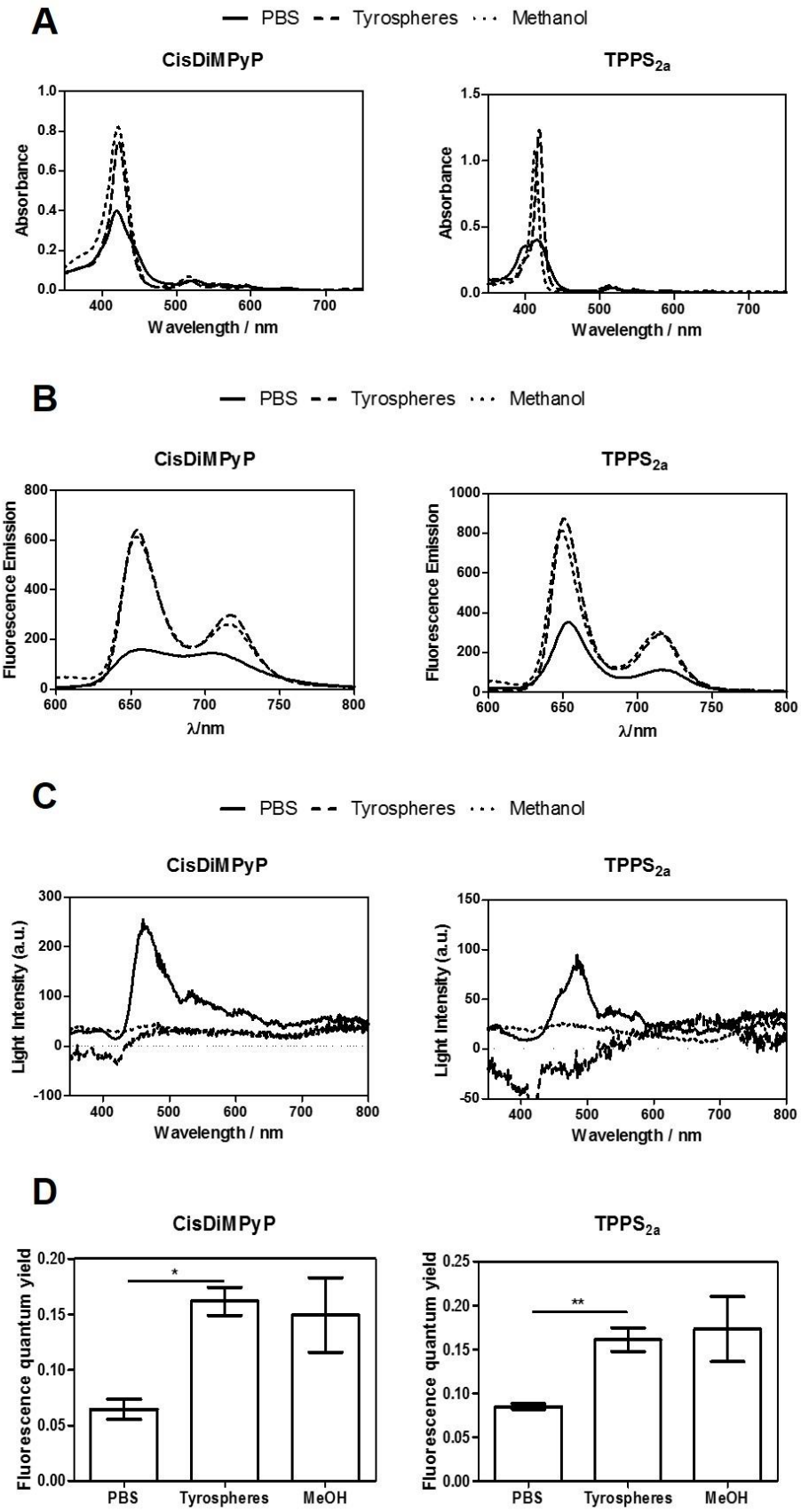

Figure 4.3. **(A)** Absorption spectrum of CisDiMPyP (5μM) and $TPPS_{2a}$ (3μM) in PBS (solid line), Tyrospheres (dashed line) and methanol (dotted line). Empty Tyrospheres were

used as baseline at the same concentration as the PS-loaded Tyrospheres in order to compensate for scattered light. **(B)** Fluorescence emission of CisDiMPyP and $TPPS_{2a}$ in PBS (solid line), Tyrospheres (dashed line) and methanol (dotted line). **(C)** Resonance light scattering spectrum (RLS) of CisDiMPyP and $TPPS_{2a}$ in PBS (solid line), Tyrospheres (dashed line) and methanol (dotted line). **(D)** Fluorescence quantum yield (ϕ_F) values of porphyrins in PBS, Tyrospheres and methanol (MeOH). Bars correspond the mean ± SD and *p<0.05, **p<0.01 are considered statistically significant.

4.3.3. Importance of Tyrospheres on singlet oxygen generation of PS

The PDT effects of PS-free and PS-loaded Tyrospheres depends on their ability to generate singlet oxygen ($^1O_2$) (Tada and Baptista 2015; Robert W Redmond and Kochevar 2006; Tanielian, Heinfuch, and Pascal 1995). Then, in order to evaluate the impact of Tyrospheres on photosensitizers photochemical properties, the amount and lifetime of singlet oxygen ($^1O_2$) was quantified by the phosphorescence emission spectra. Figure 4.4A shows that both PS, after encapsulation in Tyrospheres, exhibit a higher phosphorescence intensity at 1275nm compared to the PS in PBS. It means that the generation of singlet oxygen for the PS-loaded Tyrospheres is higher than for the free PS in PBS. In fact, the singlet oxygen quantum yield (ϕ_Δ) values were higher to PS-loaded Tyrospheres (similar to organic solvent, e.g. methanol) than to the free ones (Figure 4.4B). This is in accordance to the previous findings (section 4.3.2) and the literature, reporting that porphyrins are monomeric inside the nanospheres (Ding et al. 2011; Tada et al. 2010; Tanielian, Heinfuch, and Pascal 1995). Therefore, encapsulating porphyrins in Tyrospheres remarkably increase the efficiency in singlet oxygen generation ($^1O_2$) compared to the free ones in aqueous media.

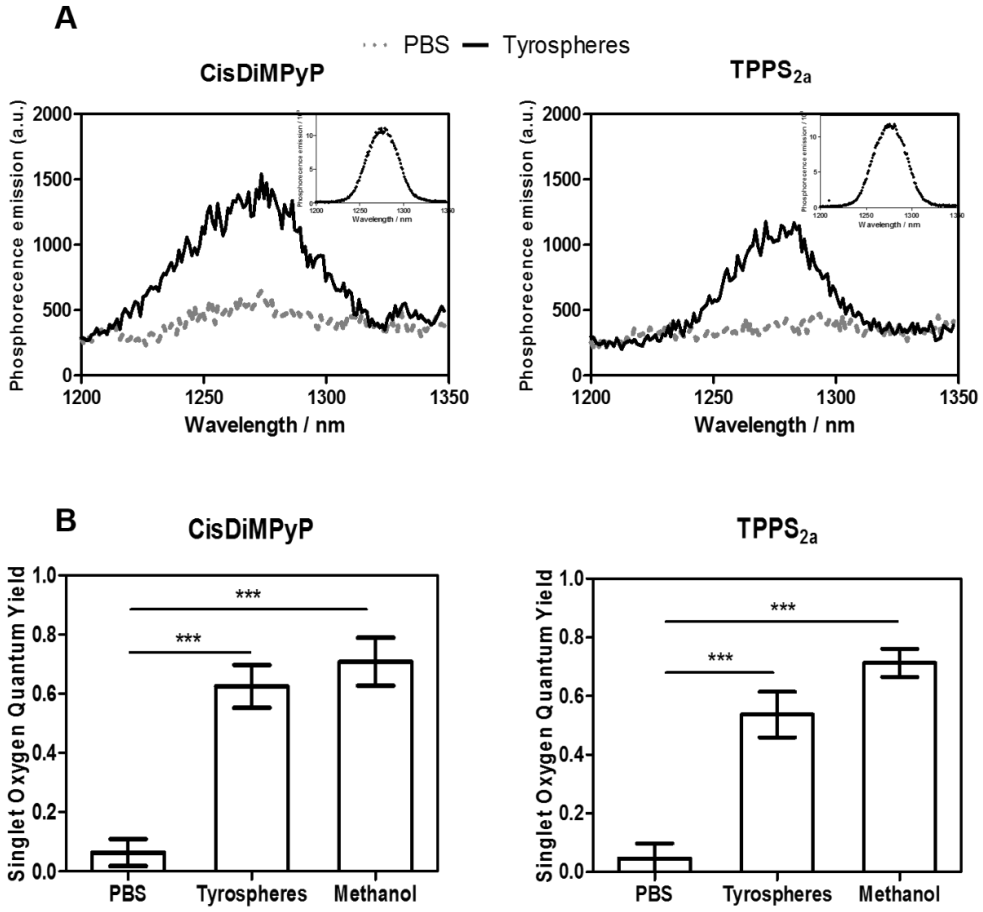

Figure 4.4. **(A)** Phosphorescence emission spectrum of singlet oxygen generated by porphyrins in aqueous media (Tyrospheres or PBS) and the insert shows the emission spectrum of PS in methanol. **(B)** Singlet oxygen quantum yield (ϕ_Δ) for each PS in PBS, Tyrospheres and methanol. Bars correspond the mean ± SD of at least two independent experiments and ***$p<0.001$ is considered statistically significant.

4.3.4. Release of PS from Tyrospheres in living cells by time-resolved luminescence

The fluorescence lifetime of photosensitizers is extremely sensitive to physicochemical effects, such as aggregation and the interaction of the photosensitizer with a polymer coating or cytosol in a cell. Furthermore, changes in fluorescence lifetimes indicate changes of the photophysical parameters and may also be indicative of changes of the intersystem crossing rate which finally affects the efficiency of the photodynamic effect (Berezin and Achilefu 2010; Xu et al. 2015; Simon et al. 2015). Therefore, we investigated the photosensitizer fluorescence

lifetimes in both aqueous solution and living cells by time correlated single photon counting (TCSPC) and fluorescence lifetime imaging microscope (FLIM).

The fluorescence lifetime of PS-loaded Tyrospheres was 10 ns and 12 ns (to CisDiMPyP and $TPPS_{2a}$, respectively), and therefore around 2 nanoseconds longer than that of the free PS in PBS solution (8 ns and 10 ns to CisDiMPyP and $TPPS_{2a}$, respectively, Table 4.2 and Figure 4.5A). This lifetime increase upon loading in nanospheres has been attributed to the PS disaggregation, as aggregation induces a self-quenching mechanism This data is in agreement with literature (Ding et al. 2011; Berezin and Achilefu 2010; Yeh et al. 2014; Simon et al. 2015) and our other results of the steady-state photophysical properties and singlet oxygen generation.

Table 4.2. Fluorescence lifetimes of porphyrins (τ_F) from free photosensitizers in PBS and PS loaded Tyrospheres in aqueous media.

PS		***A_1***	***τ_F (ns)***	***X^2***
Free	CisDiMPyP	0.6 ± 0.2	8.8 ± 0.5	0.97
	$TPPS_{2a}$	1.1 ± 0.2	10.4 ± 0.3	1.01
Tyrospheres	CisDiMPyP	0.42 ± 0.08	10.2 ± 0.7	1.05
	$TPPS_{2a}$	0.4 ± 0.2	12.3 ± 0.5	1.04

The fluorescence lifetimes in living cells showed a bi-exponential decay (Table 4.3). The longer fluorescence lifetimes (τ_1) was attributed to porphyrins since their values were close to that one which characterized the compounds in solution (Table 4.2). The shorter lifetimes (τ_2) were designed be auto-fluorescence from cells once these values were identical to the shorter lifetimes of control cells (without photosensitizers or with empty-Tyrospheres) – Table 4.3. Due the fact that the interesting point for monitoring photosensitizer environment is longer fluorescence lifetimes (τ_1), it will be highlighted in the discussion.

Table 4.3. Fluorescence lifetimes of porphyrins (τ_F) from photosensitizers free and in Tyrospheres in living cells.

PS		***A_1***	***A_2***	***τ_1 (ns)***	***τ_2 (ns)***	***X^2***
Free	HeLa Control	0.4 ± 0.1	1.4 ± 0.4	5.1 ± 0.2	1.65 ± 0.07	1.01
	CisDiMPyP	10 ± 3	13.2 ± 9.2	7 ± 1	1.8 ± 0.3	1.05
	$TPPS_{2a}$	51 ± 20	28.9 ± 7.9	8.0 ± 0.3	2.1 ± 0.1	1.03
Tyrospheres	Empty	0.22 ± 0.01	0.84 ±0.07	5.1 ± 0.2	1.64 ± 0.05	1.01
	CisDiMPyP	2.8 ± 3.9	2.9 ± 2.4	7.8 ± 0.7	1.9 ± 0.2	1.02
	$TPPS_{2a}$	2.8 ± 1.1	2.3 ± 0.9	10.7 ± 0.9	2.0 ± 0.3	1.03

Interestingly, a slight decrease of the fluorescence lifetime (2 ns) of the PS-loaded Tyrospheres was observed after 3 hours of incubation in HeLa cells (Figure 4.5A). This change detected after incubation in living cells can be due to the different microenvironment found by photosensitizer, where the interaction PS with polymer is changed to the interaction with intracellular substrates (Wang et al. 2013; Berezin and Achilefu 2010; Xu et al. 2015). It suggests that both porphyrins are released from Tyrospheres after interaction with living cells. Such changes could also be seen in the false-coloured FLIM images in Figure 4.5B, indicating that both porphyrins were released from nanospheres. Noteworthy, fluorescence lifetime imaging microscopy (FLIM) on living HeLa cells revealed that photosensitizers (free or encapsulated) localizes at the cytoplasm and it was ever detected at the cell nuclei (Figure 4.5B).

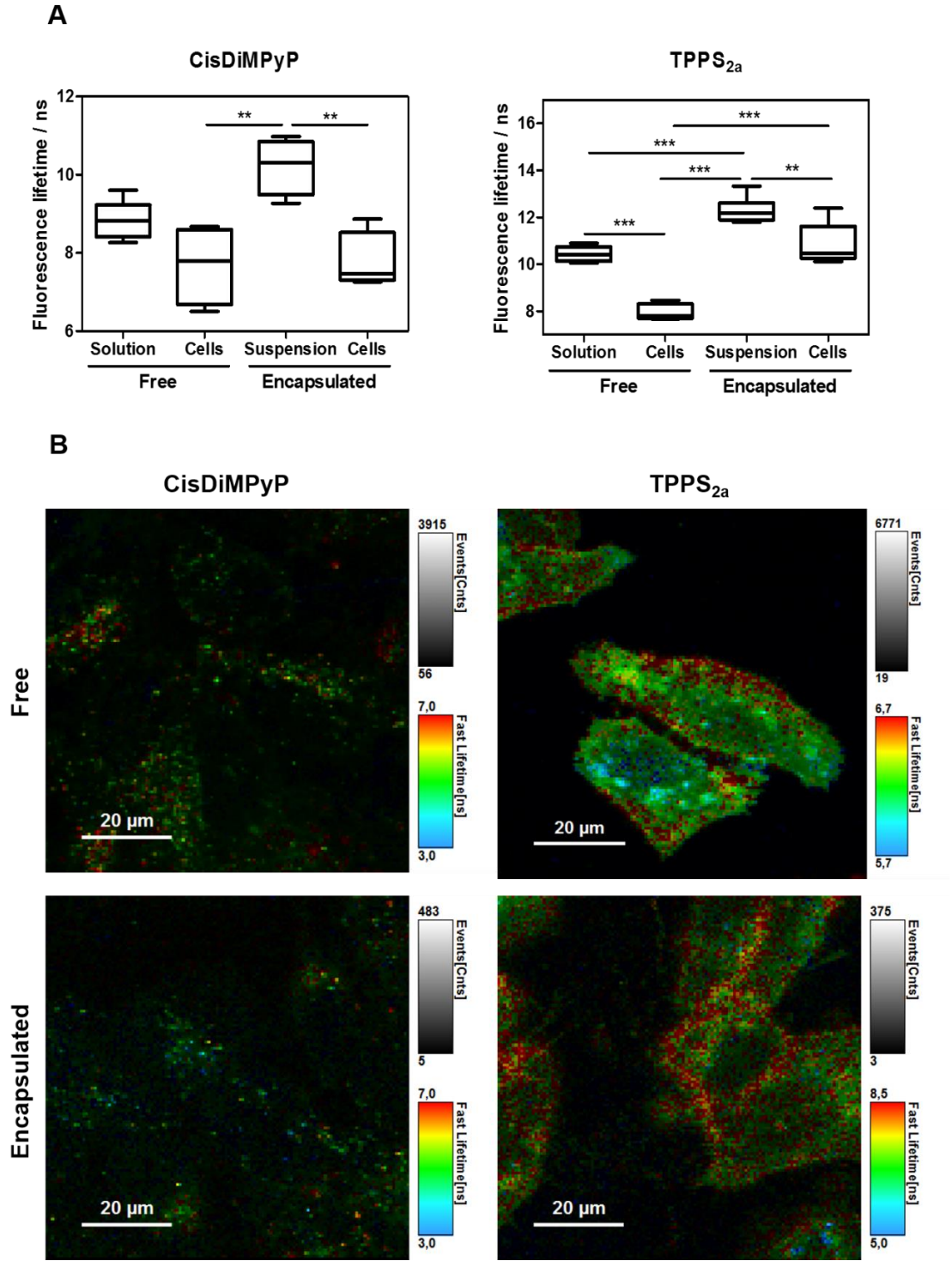

Figure 4.5. **(A)** Fluorescence lifetimes (τ_F) of photosensitizers (free or encapsulated) before (solution) and after incubation (3 hours) in living HeLa cells. Box plot correspond to the minimum and maximum values, including the mean. **p<0.01, ***p<0.001 are considered statistically significant. **(B)** Fluorescence lifetime imaging microscopy (FLIM) of HeLa cells incubated for 3 hours with CisDiMPyP (free or in Tyrospheres) and $TPPS_{2a}$ (free or in Tyrospheres). λ_{exc} = 405nm and emission with filter long pass 630nm. The scale bar is 20 µm.

4.3.5. Tyrospheres keeping subcellular localization and cell death mechanism of PS

Another important key parameter for the photodynamic efficiency is the PS intracellular localization which may avoid generation of reactive oxygen species in a non-specific and inefficient way (Oliveira et al. 2011; Deda et al. 2013). Then, we investigated the effect of encapsulation on the specific sites of subcellular localization. For this, red fluorescence of porphyrins was monitored with green fluorescence of organelle-probe (lysosomes or mitochondria) by confocal fluorescence images (Figure 4.6A and Figure 4.6B) and the percent values of colocalization were calculated (Figure 4.6C).

Results demonstrate that Tyrospheres do not influence the intracellular localization with respect to free compounds. CisDiMPyP and CisDiMPyP-loaded TyroSpheres accumulate two times more (M/L = 1.9 ± 0.1 for free and M/L = 1.9 ± 0.3 to Tyrospheres) in mitochondria than lysosomes while $TPPS_{2a}$ and $TPPS_{2a}$-loaded TyroSpheres localize two times more (M/L = 0.76 ± 0.05 for free and M/L = 0.55 ± 0.05 to Tyrospheres) in lysosomes than in mitochondria (Figure 4.6D-left). Therefore, the accumulation tendency of the free PS is partly maintained. However, the total percentage of PS localized in lysosomes or mitochondria (M+L in Figure 4.6D-right) of the free photosensitizers is considerably higher compared to the Tyrospheres incorporated PS (M+L decreases from 58% ± 4 to 31% ± 4 and from 69% ± 4 to 45% ± 3 in the case of CisDiMPyP and $TPPS_{2a}$, respectively).

The influence of Tyrospheres on the mechanism of cell death was investigated using acridine orange (AO) and propidium iodide (PI) assays (Figure 4.7). Results demonstrate that cells treated with CisDiMPyP-loaded TyroSpheres had dead cells stained with PI (white arrow) 3 hours after PDT (Figure 4.7) suggesting necrosis/apoptosis as mechanism of cell death (David Kessel and Luo 1998; Oleinick, Morris, and Belichenko 2002). Forty-eight hours after PDT, treatment with $TPPS_{2a}$-loaded TyroSpheres indicated an increased amount of red fluorescence (blue arrow) which represent enhancement of acids organelles (Figure 4.7). Contrast between

treatments has been clearly on bars graph suggesting cell death related to autophagy due the larger amount of acids organelles (Du et al. 2014; Lihuan et al. 2014). Similar results were observed to the free form of PS (discussed in Chapter 3) revealing that encapsulating process do not alter cell death mechanism induced by PS. This is not a surprise once the subcellular localization was also kept even after encapsulation.

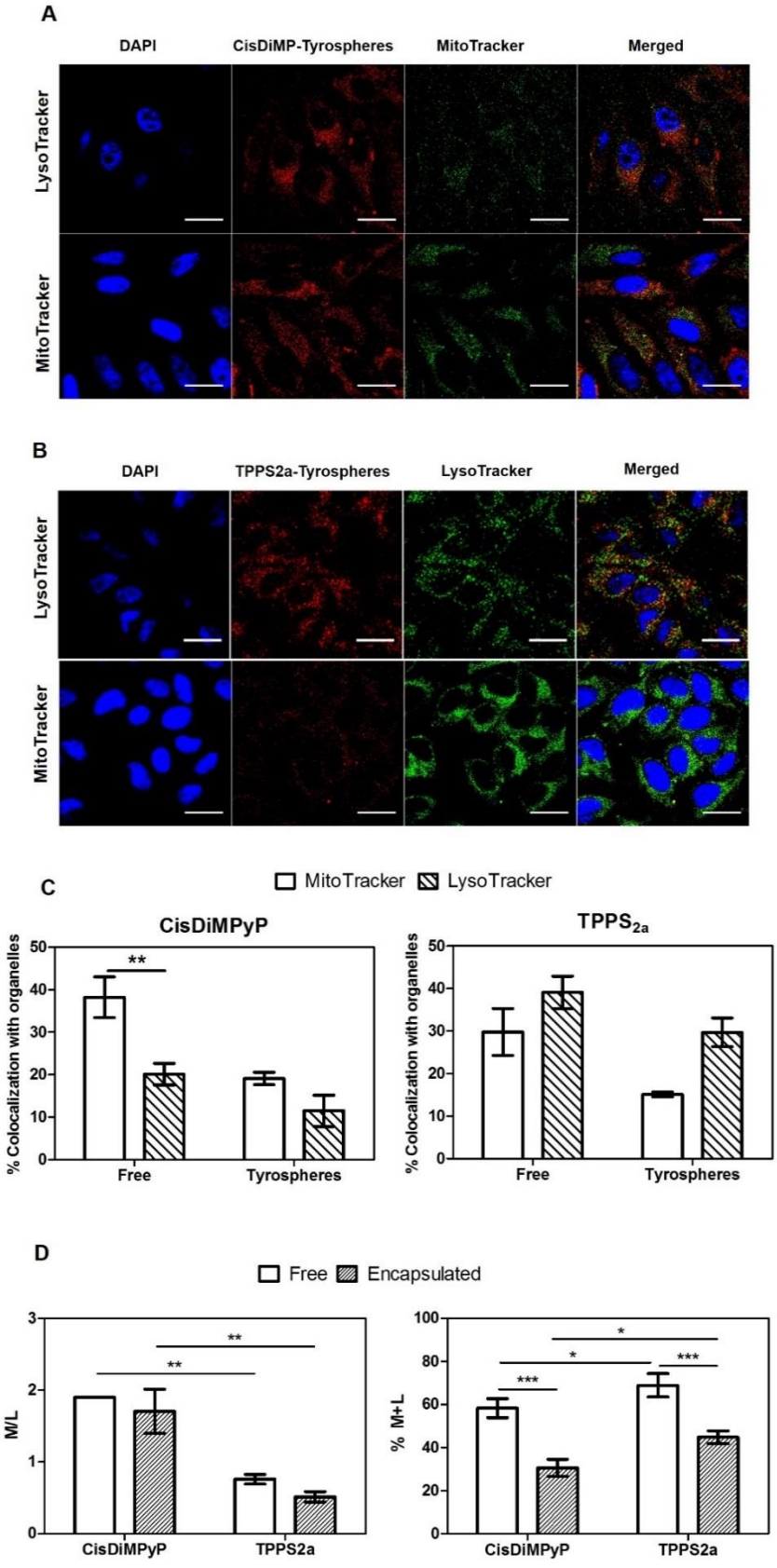

Figure 4.6. **(A)** Confocal fluorescence microscopy images of HeLa cells with blue fluorescence of nucleus (DAPI), red fluorescence of CisDiMPyP encapsulated in Tyrospheres

and green fluorescence of organelle-probe (MitoTracker® or LysoTracker®). Right column shows the overlay from three channels (blue, red and green). Scale bar corresponds to 20 µm. **(B)** Confocal fluorescence microscopy images of HeLa cells with blue fluorescence of nucleus (DAPI), red fluorescence of $TPPS_{2a}$ encapsulated in Tyrospheres and green fluorescence of organelle-probe (MitoTracker® or LysoTracker®). Right column shows the overlay from three channels (blue, red and green). Scale bar corresponds to 20 µm **(C)** Bars correspond to the mean ± SD from calculated percent of colocalization between red fluorescence of porphyrins and green fluorescence of organelle-probe to each case (porphyrin free or encapsulated in Tyrospheres). **(D)** On left: Bars represent the mean ± SD of the mitochondria and lysosomes ratio (M/L) to each porphyrin (free and encapsulated in Tyrospheres). On right: Bars represent the mean ± SD of total percentage of localization in lysosomes and mitochondria (% M+L) to each porphyrin (free and encapsulated in Tyrospheres). *p<0.05, **p<0.01, ***p<0.001 are considered statistically significant.

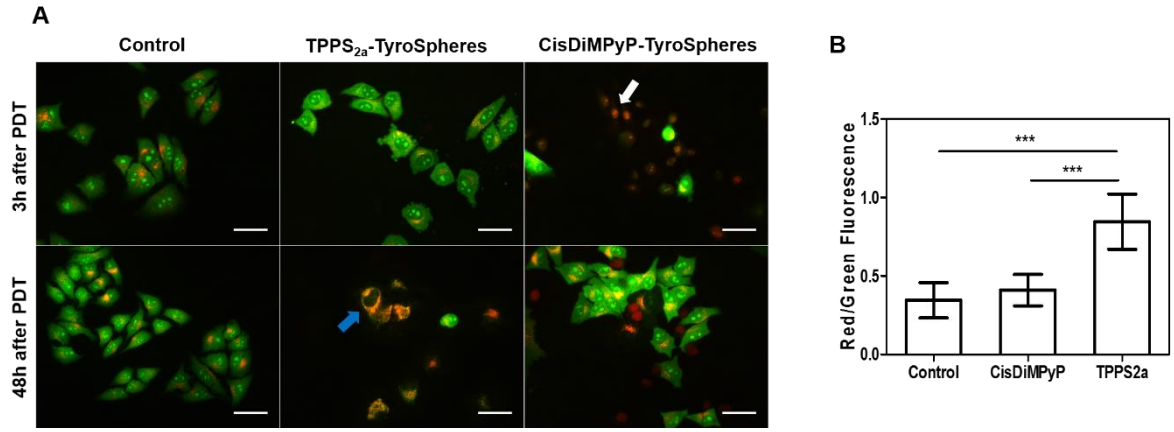

Figure 4.7. **(A)** Micrographs obtained 3 and 48 hours after PDT in HeLa cells treated without porphyrins (control), incubated with 100 nM CisDiMPyP-loaded Tyrospheres or with 30 nM $TPPS_{2a}$-loaded Tyrospheres, using AO/PI double staining. Scale bar of 20 µm. **(B)** Bars represent red and green fluorescence ratio from micrographs of HeLa cells 48 hours after PDT with PS-loaded Tyrospheres. ***p<0.001 are considered statistically significant.

4.3.6. Tyrospheres providing enhanced photodynamic activity of PS

The cellular uptake of porphyrins in the free form and loaded in Tyrospheres was measured in HeLa cells after 3 hours of incubation. PS-loaded Tyrospheres presented reduced uptake (6-fold lower to CisDiMPyP and 4-fold lower to $TPPS_{2a}$) with respect to free compounds (Figure 4.8A). This result suggests that cellular interaction and uptake occur by different mechanism for photosensitizer free and encapsulated in Tyrospheres. The reduced PS uptake in cells upon incorporation in nanospheres has also been observed in other similar experimental systems (Deda et al. 2013; Silva et al. 2016).

Phototoxicity was measured 48h post-irradiation in cells incubated for 3 hours with PS-free or PS-loaded Tyrospheres. None of the PS (encapsulated or free) showed cytotoxicity in the dark under similar experimental conditions (Figure 4.8B). The photoinduced cell death gradually increased in a concentration dependent manner for both porphyrins in the free form and incorporated in Tyrospheres (Figure 4.8B). The PS-loaded Tyrospheres seem to result in a similar cell killing efficiency than PS-free (Figure 4.8B). However, this initial interpretation of the raw data does not reflect the amount of PS that is actually internalized in each condition. Therefore, considering the value of incorporated porphyrin, the calculated PDT efficiencies (η_{PDT}) (Figure 4.8C) increased for both photosensitizers (3-fold to CisDiMPyP and 5-fold to $TPPS_{2a}$) after encapsulated in Tyrospheres (Figure 4.8C). This indicates that PS-loaded Tyrospheres have a larger phototoxic effect compared to the same amount of free PS. It seems to be not related to tyrosine-derived nanospheres cytotoxicity, since empty-Tyrospheres have not shown any cytotoxic effects (Figure 4.9).

We therefore demonstrate an enhanced PDT activity of PS-loaded Tyrospheres in HeLa cells in comparison to free PS. The Tyrospheres are able to improve photophysical properties, the generation of singlet oxygen and release their cargo into the intracellular environment, preserving the biological consequences of each photosensitizer.

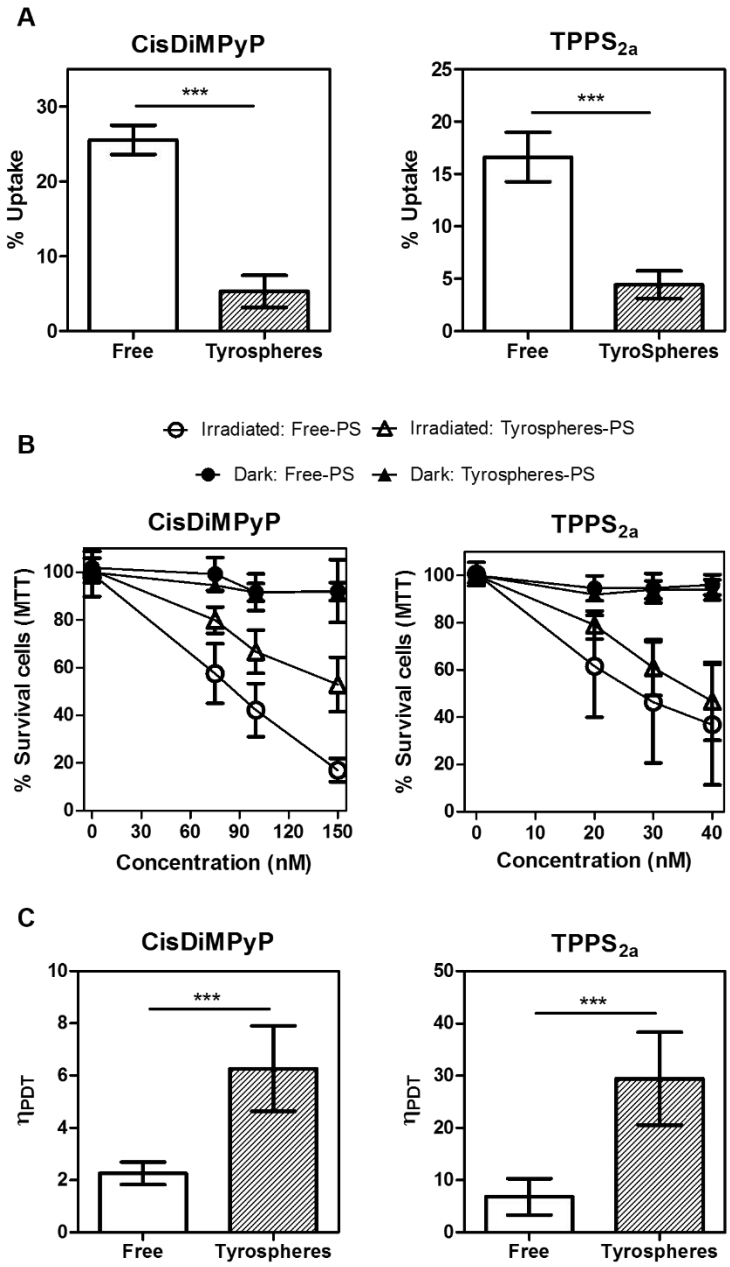

Figure 4.8. **(A)** Uptake of free phorphyrins or encapsulated in Tyrospheres after 3 hours of incubation in HeLa cells. Porphyrins 5 µM and $5x10^4$ cells/cm^2 in DMEM culture medium 1% FBS. Bars represent the mean ± SD of at least two independent experiments (***$p<0.001$ are considered statistically significant). **(B)** Percentage of surviving cells, 48 hours after PDT as a function of PS (free or encapsulated) concentration, determined by MTT. Each point represents the mean ± SD of at least three independent experiments. Incubation of HeLa cells with porphyrins for 3 hours in DMEM with 1% FBS in the dark. Following the incubation the samples were irradiated in PBS using a LED system emitting at 522±20nm, light dose of 2.1 J/cm^2. **(C)** Bars correspond to the mean ± SD of PDT efficiencies (η_{PDT}) for each photosensitizer (free or encapsulated) in the LC_{50} corrected by their respective cellular uptake levels (***$p<0.001$ are considered statistically significant).

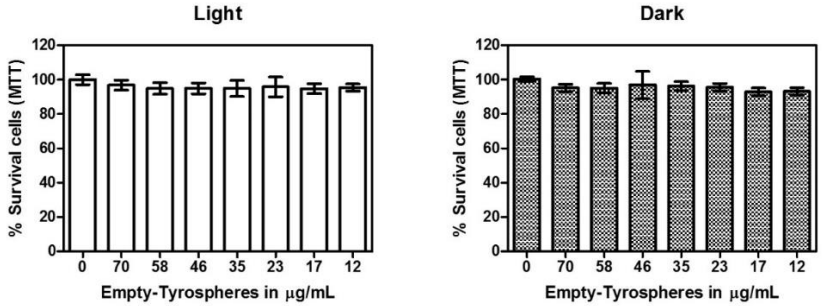

Figure 4.9. Cell viability of HeLa cells incubated for 3 hours with empty-TyroSpheres under the same conditions used to fabricate PS-loaded Tyrospheres.

4.4. CONCLUSION

This work evaluates potential application of Tyrospheres as a nanocarrier system for photosensitizers used in Photodynamic Therapy (PDT). PS-loaded Tyrospheres form stable nanospheres with identical structure and stability compared to unloaded ones. Tyrosine-derived nanospheres provide greatly enhanced physical-chemical properties of both CisDiMPyP and $TPPS_{2a}$, improving their photophysical properties and causing a large increase in the yield of singlet oxygen generation. Fluorescence lifetime image microscopy (FLIM) suggests that photosensitizers are released from nanospheres inside cells, allowing their distribution in mitochondria and lysosome as the same way that free porphyrins. Also, PS-loaded Tyrospheres presented similar characteristics of cell death to free porphyrins as already discussed in Chapter 3, confirming that Tyrospheres do not change the subcellular localization neither biological consequences. Interesting, in addition to keeping subcellular localization and cell death mechanism, the PDT efficiencies (η_{PDT}) to PS-loaded Tyrospheres were larger compared to the free compounds demonstrating a significant improvement in the photoactivity efficiency. All data together indicate the great potential of Tyrospheres in Photodynamic Therapy as nanocarrier and their role to improve photophysical properties, increase singlet oxygen generation, keep biological consequences and enhance photodynamic efficiency of the photosensitizers.

CHAPTER 5

CONCLUSION AND FUTURE PERSPECTIVE

A general conclusion of the work described in previous chapters as well as suggestions for future work are given in this chapter.

5. CONCLUSION AND FUTURE PERSPECTIVE

PDT has been receiving substantial attention of the academic and industrial communities, aiming at the development of new applications in medicine and correlated fields (cosmetics, veterinary, etc). Even though several photosensitizers have been tested and approved by regulatory agencies for the treatment of oncological and non-oncological diseases, PDT treatments are still not prominent in routine clinical practice and less known than well-established treatments (e.g. chemotherapy, radiotherapy, surgery). It is not an easy task to prove the medical benefits of PDT compared to conventional treatments, when commercial interests are in place. In fact, pharmaceutical companies, favor to sell medicines alone instead of selling medicines together with photons. This thesis provides new insights on the molecular level about strategies to enhance the PDT efficiency. One of the main strategies is to maximize the intrinsic efficiency of the photosensitizers to make to protocols more accurate and reliable. This thesis provides some insights at molecular level (not clinical or *in vivo*) about strategies to enhance the PDT efficiency.

Chapter 2 was dedicated to an in-depth study of the importance of the molecular amphiphilicity of differently charged PS to achieve a high degree of PS-membrane interaction. Most notably, it was found that the negatively-charged amphiphilic molecule ($TPPS_{2a}$) was also able to interact efficiently with negative membranes – which has previously been assumed to rather be a property of positively-charged amphiphilic molecules. It is probable that, in the case of amphiphilic molecules, the main forces driving PS-membrane interaction involve the hydrophobic and dipolar interactions and not only electrostatics. Overall, the efficiency of membrane photodamage exhibits a good correlation with the ability of the PS binding to membranes. The order of photodamage efficiency in the studied molecules was: CisDiMPyP > $TPPS_{2a}$ > PpNetNI > $AlPcS_{2a}$. The two best PS in terms of binding/photodamage (CisDiMPyP and $TPPS_{2a}$) were selected for further investigations on eukaryotic cells.

In Chapter 3, we demonstrated that the cell killing efficiency of $TPPS_{2a}$ is larger than CisDiMPyP, even the cellular uptake and the membrane binding efficiency of $TPPS_{2a}$ is lower. This was intriguing because previous results from our and other labs had confirmed that the efficiency of membrane binding and of intracellular accumulation was correlated with the efficiency of cell, tissue and animal killing. The detailed studied of the intracellular damage caused by $TPPS_{2a}$ and CisDiMPyP confirmed that the first target mainly lysosomes and the last mitochondria. Therefore, our data indicates that lysosome is a better intracellular target than mitochondria. By studying the mechanisms of cell death, it is shown that the lysosome damage caused by photoactivation of $TPPS_{2a}$ triggers cell death associated to autophagy in a long-term response compared to the acute promptly mitochondria damage, which results in the classical apoptotic/necrotic cell death. Our data therefore question two important concepts in PDT: (i) higher ability of PS-membrane interaction causes stronger phototoxicity and (ii) mitochondria is the most efficient target to induce photoinduce cell killing. Moreover, LC_{50} values exhibited in this work was on the nanomolar magnitude, while known PS molecules found in literature are on the order of micromolar.

Since cancer cells can upregulate autophagy to survive under metabolic and microenvironmental stress, the inhibition of autophagy pathway can be crucial and strategical to improve results of therapies (White 2015). Thus, we have found that photodamaging lysosomes impair the autophagic flux removing the ability of cytoprotection and decreases the ability of cells to survive and proliferate in a more efficient way than a more acute damage in mitochondria.

Another technology based on photosensitized oxidations, which is named Photochemical Internalization (PCI), also uses endosomes/lysosomes as target of photosensitizers (Selbo et al. 2010; Norum et al. 2009). Usually, photosensitizers used in PCI are negatively-charged amphiphilic molecules such as $TPPS_{2a}$ in order to release chemotherapeutics, proteins, acid

nucleic or other macromolecules with inefficient ability to escape of lysosomes (Figure 5.1). The enhanced efficiency of PCI is attributed to the delivery of these compounds from lysosomes to cytosol avoiding their degradation inside lysosomes (Figure 5.1). However, our data showed that an enhanced PDT effect can be observed only by the fact of using a lysosomal-photosensitizer (in this case $TPPS_{2a}$) due to impairment of autophagy after lysosome photodamage. Therefore, future works could elucidate if cell death associated to autophagy could be correlated to the better efficacy observed in PCI protocols.

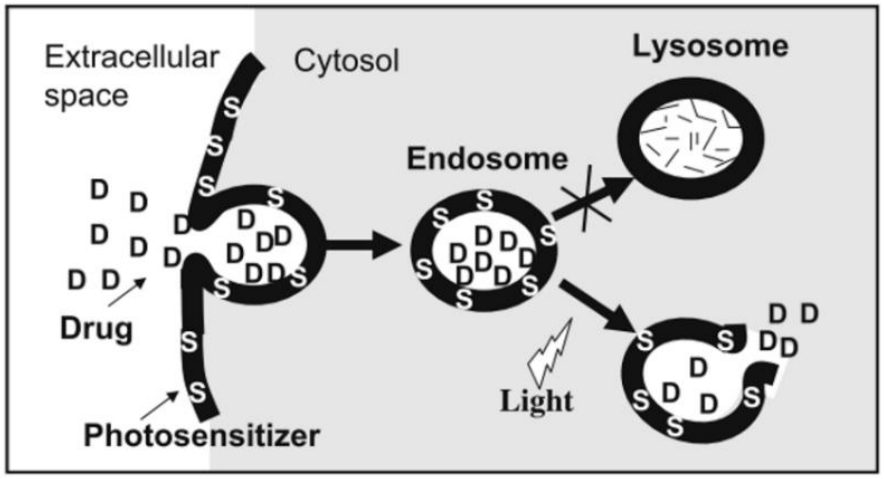

Figure 5.1. Schematic illustration of the PCI process. Reprinted with permission from Elsevier (Norum et al. 2009).

In Chapter 4, it was demonstrated the use of polymeric nanospheres made by tyrosine-derived polymer also increase the efficiency in PDT. In fact, Tyrospheres kept photosensitizers in a monomeric form, upgrading their photophysical properties and causing a large increase in the singlet oxygen generation when compared to free photosensitizers. Because of this, a significant improvement in the photoactivity efficiency was observed.

It was clear that using Tyrospheres as nanocarriers improve the photodynamic efficacy, however it still needs to be understood how Tyrospheres delivery PS into cells. Although this type of ABA-type amphiphilic triblock copolymers that self-assemble into nanospheres were

intentionally designed to degrade via the hydrolysis of ester bonds, experimental data have already demonstrated that there is no degradation of the polymer in the presence of enzymes (e.g. carboxylesterase) that cleave carboxylic ester, thioester and amine ester linkages (Kilfoyle 2011). Then, future works could explain how occurs the release mechanism of Tyrospheres.

6. REFERENCES

Abdel Wahab, Siddig Ibrahim, Ahmad Bustamam Abdul, Adel Sharaf Alzubairi, Manal Mohamed Elhassan, and Syam Mohan. 2009. "In Vitro Ultramorphological Assessment of Apoptosis Induced by Zerumbone on (HeLa)." *Journal of Biomedicine and Biotechnology* 2009. doi:10.1155/2009/769568.

Abounit, Kadija, Tiziano M Scarabelli, and Roy B Mccauley. 2012. "Autophagy in Mammalian Cells." *World Journal of Biological Chemistry* 3 (1): 1–6. doi:10.4331/wjbc.v3.i1.TOPIC.

Agholme, Lotta, Maria Agnello, Patrizia Agostinis, Julio a Aguirre-ghiso, Hyung Jun Ahn, Ouardia Ait-mohamed, Jay E Brenman, et al. 2012. "Guidelines for the Use and Interpretations of Assays for Monitoring Autophagy." *Autophagy* 8 (4): 445–544.

Agostinis, Patrizia, Esther Buytaert, Hilde Breyssens, and Nico Hendrickx. 2004. "Regulatory Pathways in Photodynamic Therapy Induced Apoptosis." *Photochemical & Photobiological Sciences : Official Journal of the European Photochemistry Association and the European Society for Photobiology* 3 (8): 721–29. doi:10.1039/b315237e.

Alexandridis, Paschalis, Josef F Holzwarth, and T Alan. Hatton. 1994. "Micellization of Poly(ethylene Oxide)-Poly(propylene Oxide)-Poly(ethylene Oxide) Triblock Copolymers in Aqueous Solutions: Thermodynamics of Copolymer Association." *Macromolecules* 27 (9): 2414–25. doi:10.1021/ma00087a009.

Ali, Hasrat, and Johan E van Lier. 1999. "Metal Complexes as Photo- and Radiosensitizers." *Chemical Reviews* 99 (9): 2379–2450. doi:10.1021/cr980439y.

Ambroz, M, A Beeby, Aj Macrobert, Msc Simpson, Rk Svensen, and D Phillips. 1991. "Preparative, Analytical and Fluorescence Spectroscopic Studies of Sulfonated Aluminum Phthalocyanine Photosensitizers." *J Photochem Photobiol B: Biol* 9: 87–95. http://discovery.ucl.ac.uk/84806/.

Andrzejak, Michelle, Michael Price, and David H. Kessel. 2011. "Apoptotic and Autophagic Responses to Photodynamic Therapy in 1c1c7 Murine Hepatoma Cells." *Autophagy* 7 (9): 979–84. doi:10.4161/auto.7.9.15865.

Angelova, Miglena I, and Dimiter S Dimitrov. 1986. "Liposome Electro Formation." *Faraday Discuss. Chem. SO* 81: 303–11.

Ashkenazi, Avi, and Vishva M Dixit. 1998. "Death Receptors: Signaling and Modulation." *Science (New York, N.Y.)* 281 (5381): 1305–8. doi:10.1126/science.281.5381.1305.

Auler, H., and G. Banzer. 1942. "Untersuchungen Über Die Rolle Der Porphyrine Bei Geschwulstkranken Menschen Und Tieren." *Z. Krebsforsch.* 53: 65–72.

Avci, Pinar, S. Sibel Erdem, and Michael R. Hamblin. 2014. "Photodynamic Therapy: One Step Ahead with Self-Assembled Nanoparticles." *Journal of Biomedical Nanotechnology* 10 (9): 1937–52. doi:10.1166/jbn.2014.1953.

Babilas, Philipp, Stephan Schreml, Michael Landthaler, and Rolf Markus Szeimies. 2010. "Photodynamic Therapy in Dermatology: State-of-the-Art." *Photodermatology Photoimmunology and Photomedicine* 26 (3): 118–32. doi:10.1111/j.1600-0781.2010.00507.x.

Bacellar, Isabel O L, Christiane Pavani, Elisa M. Sales, Rosangela Itri, Mark Wainwright, and Mauricio S. Baptista. 2014. "Membrane Damage Efficiency of Phenothiazinium Photosensitizers." *Photochemistry and Photobiology* 90: 801–13. doi:10.1111/php.12264.

Bacellar, Isabel O L, Tayana M Tsubone, Christiane Pavani, and Mauricio S Baptista. 2015. "Photodynamic Efficiency : From Molecular Photochemistry to Cell Death," 20523–59. doi:10.3390/ijms160920523.

Bajema, Larry, Martin Gouterman, and Beat Meyer. 1968. “Spectra of Porphyrins.” *Journal of Molecular Spectroscopy* 27: 225–35. doi:10.1016/0022-2852(68)90032-5.
Baptista, Mauricio S, Jean Cadet, Paolo Di Mascio, Ashwini A. Ghogare, Alexander Greer, Michael R. Hamblin, Caroline Lorente, et al. 2017. “Type I and II Photosensitized Oxidation Reactions: Guidelines and Mechanistic Pathways.” *Photochemistry and Photobiology* 38 (1): 42–49. doi:10.1111/php.12716.
Basu, Sekbar. 1991. “Fluorescence Enhancement of Tetrakis (Sulfonatophenyl) Porphyrin in Homogeneous and Micellar Solutions.” *J Photochem Photobiol A:Chem* 56: 339–47.
Batheja, Priya, Larisa Sheihet, Joachim Kohn, Adam J. Singer, and Bozena Michniak-Kohn. 2011. “Topical Drug Delivery by a Polymeric Nanosphere Gel: Formulation Optimization and in Vitro and in Vivo Skin Distribution Studies.” *Journal of Controlled Release* 149 (2). Elsevier B.V.: 159–67. doi:10.1016/j.jconrel.2010.10.005.
Beesoo, Rima, Vidushi Neergheen-Bhujun, Ranjeet Bhagooli, and Theeshan Bahorun. 2014. “Apoptosis Inducing Lead Compounds Isolated from Marine Organisms of Potential Relevance in Cancer Treatment.” *Mutation Research* 768 (March). Elsevier B.V.: 84–97. doi:10.1016/j.mrfmmm.2014.03.005.
Ben Amor, T, L Bortolotto, and G Jori. 2000. “Porphyrins and Related Compounds as Photoactivatable Insecticides. 3. Laboratory and Field Studies.” *Photochemistry and Photobiology* 71 (2): 124–28. doi:10.1562/0031-8655(2000)071<0124:SIPPAR>2.0.CO;2.
Berezin, M Y, and S Achilefu. 2010. “Fluorescence Lifetime Measurements and Biological Imaging.” *Chem. Rev.* 110 (5): 2641–84. doi:10.1021/cr900343z.
Berg, K., and J. Moan. 1994. “Lysosomes as Photochemical Targets.” *International Journal of Cancer* 59 (6): 814–22. doi:10.1002/ijc.2910590618.
Berg, Kristian, André Western, Jerry C Bommer, and Johan Moan. 1990. “Intracellular Localization of Sulfonated Meso-Tetraphenylporphines in a Human Carcinoma Cell Line.” *Photochemistry and Photobiology* 52 (3). Blackwell Publishing Ltd: 481–87. doi:10.1111/j.1751-1097.1990.tb01789.x.
Biswas, Swati, Preeti Kumari, Prit Manish Lakhani, and Balaram Ghosh. 2016. “Recent Advances in Polymeric Micelles for Anti-Cancer Drug Delivery.” *European Journal of Pharmaceutical Sciences* 83: 184–202. doi:10.1016/j.ejps.2015.12.031.
Bjørkøy, Geir, Trond Lamark, Serhiy Pankiv, Aud Øvervatn, Andreas Brech, and Terje Johansen. 2009. “Chapter 12 Monitoring Autophagic Degradation of p62/SQSTM1.” *Methods in Enzymology* 451 (C): 181–97. doi:10.1016/S0076-6879(08)03612-4.
Bonnett, Raymond. 1995. “Photosensitizers of the Porphyrin and Phthalocyanine Series for Photodynamic Therapy.” *Chemical Society Reviews*.
Bourke, Sharon L, and Joachim Kohn. 2003. “P Olymers Derived from the Amino Acid L - Tyrosine : Polycarbonates , Polyarylates and Copolymers with Poly (Ethylene Glycol).” *Advanced Drug Delivery Reviews* 55: 447–66.
Boya, P, and G Kroemer. 2008. “Lysosomal Membrane Permeabilization in Cell Death.” *Oncogene* 27: 6434–51. doi:10.1038/onc.2008.310.
Bressler, Neil M, and Susan B Bressler. 2000. “Photodynamic Therapy with Verteporfin (Visudyne): Impact on Ophthalmology and Visual Sciences.” *Iovs* 41 (3): 624–28.
Brown, S B, M Shillcock, and P Jones. 1976. “Equilibrium and Kinetic Studies of the Aggregation of Porphyrins in Aqueous Solution.” *The Biochemical Journal* 153 (2): 279–85. http://www.pubmedcentral.nih.gov/articlerender.fcgi?artid=1172573&tool=pmcentrez&rendertype=abstract.
Buchholz, Julia, Barbara Kaser-Hotz, Tania Khan, Carla Rohrer Bley, Katja Melzer, Reto A. Schwendener, Malgorzata Roos, and Heinrich Walt. 2005. “Optimizing Photodynamic

Therapy: In Vivo Pharmacokinetics of Liposomal Meta-(Tetrahydroxyphenyl) Chlorin in Feline Squamous Cell Carcinoma." *Clinical Cancer Research* 11 (20): 7538–44. doi:10.1158/1078-0432.CCR-05-0490.

Buytaert, Esther, Geert Callewaert, Nico Hendrickx, Luca Scorrano, Dieter Hartmann, Ludwig Missiaen, Jackie R Vandenheede, Ingeborg Heirman, Johan Grooten, and Patrizia Agostinis. 2006. "Role of Endoplasmic Reticulum Depletion and Multidomain Proapoptotic BAX and BAK Proteins in Shaping Cell Death after Hypericin-Mediated Photodynamic Therapy." *The FASEB Journal* 20 (6): 756–58. doi:10.1096/fj.05-4305fje.

Buytaert, Esther, Michael Dewaele, and Patrizia Agostinis. 2007. "Molecular Effectors of Multiple Cell Death Pathways Initiated by Photodynamic Therapy." *Biochimica et Biophysica Acta - Reviews on Cancer* 1776 (1): 86–107. doi:10.1016/j.bbcan.2007.07.001.

Cadet, J, and P D Mascio. 2006. "Peroxides in Biological Systems." *The Chemistry of Peroxides, Parts 1&2* 2: 915–1000.

Caetano, Wilker, Paula S. Haddad, Rosangela Itri, Divinomar Severino, Vinicius C. Vieira, Mauricio S. Baptista, André P. Schröder, and Carlos M. Marques. 2007. "Photo-Induced Destruction of Giant Vesicles in Methylene Blue Solutions." *Langmuir* 23 (17): 1307–14. doi:10.1021/la061510v.

Castano, Ana P., Tatiana N. Demidova, and Michael R. Hamblin. 2004. "Mechanisms in Photodynamic Therapy: Part One - Photosensitizers, Photochemistry and Cellular Localization." *Photodiagnosis and Photodynamic Therapy* 1 (2004): 279–93. doi:10.1016/S1572-1000(05)00007-4.

Castano, Ana Paula, Tatiana N. Demidova, and Michael R. Hamblin. 2005. "Mechanisms in Photodynamic Therapy: Part Two - Cellular Signaling, Cell Metabolism and Modes of Cell Death." *Photodiagnosis and Photodynamic Therapy* 2 (1 SPEC. ISS.): 1–23. doi:10.1016/S1572-1000(05)00030-X.

Chang, Hsin-I, and Ming-Kung Yeh. 2012. "Clinical Development of Liposome-Based Drugs: Formulation , Characterization , and Therapeutic Efficacy." *International Journal of Nanomedicine* 7: 49–60.

Chatterjee, Dev Kumar, Li Shan Fong, and Yong Zhang. 2008. "Nanoparticles in Photodynamic Therapy: An Emerging Paradigm." *Advanced Drug Delivery Reviews* 60 (15): 1627–37. doi:10.1016/j.addr.2008.08.003.

Cirman, Tina, Kristina Orešić, Gabriela Droga Mazovec, Vito Turk, John C. Reed, Richard M. Myers, Guy S. Salvesen, and Boris Turk. 2004. "Selective Disruption of Lysosomes in HeLa Cells Triggers Apoptosis Mediated by Cleavage of Bid by Multiple Papain-like Lysosomal Cathepsins." *Journal of Biological Chemistry* 279 (5): 3578–87. doi:10.1074/jbc.M308347200.

Conniot, João, Joana M Silva, Joana G Fernandes, Liana C Silva, Rogério Gaspar, Steve Brocchini, Helena F Florindo, and Teresa S Barata. 2014. "Cancer Immunotherapy: Nanodelivery Approaches for Immune Cell Targeting and Tracking." *Frontiers in Chemistry* 2 (November): 105. doi:10.3389/fchem.2014.00105.

Cordeiro, Rodrigo M, Ronei Miotto, and Maurício S Baptista. 2012. "Photodynamic Efficiency of Cationic Meso-Porphyrins at Lipid Bilayers: Insights from Molecular Dynamics Simulations." *The Journal of Physical Chemistry. B* 116 (50): 14618–27. doi:10.1021/jp308179h.

Costache, Aurora D, Larisa Sheihet, Krishna Zaveri, Doyle D Knight, and Joachim Kohn. 2010. "Polymer-Drug Interactions in Tyrosine-Derived Triblock Copolymer Nanospheres: A Computational Modeling Approach." *Mol Pharm* 6 (5): 1620–27. doi:10.1021/mp900114w.Polymer-Drug.

D'Souza, Sarah, Reama George, Meltem Göksel, Devrim Atilla, Mahmut Durmuş, and

Tebello Nyokong. 2015. “Enhanced Triplet State Yields in Aqueous Media of Asymmetric Zinc Phthalocyanines When Conjugated to Silver Nanoflowers.” *Polyhedron* 100: 296–302. doi:10.1016/j.poly.2015.08.017.

Darwent, James R., Peter Douglas, Anthony Harriman, George Porter, and Marie-Claude Richoux. 1982. “Metal Phthalocyanines and Porphyrins as Photosensitizers for Reduction of Water to Hydrogen.” *Coordination Chemistry Reviews* 44: 83–126.

Davies, Michael J. 2003. “Singlet Oxygen-Mediated Damage to Proteins and Its Consequences.” *Biochemical and Biophysical Research Communications* 305 (3): 761–70. doi:10.1016/S0006-291X(03)00817-9.

Deda, Daiana K., Christiane Pavani, Eduardo Caritá, Maurício S. Baptista, Henrique E. Toma, and Koiti Araki. 2013. “Control of Cytolocalization and Mechanism of Cell Death by Encapsulation of a Photosensitizer.” *Journal of Biomedical Nanotechnology* 9 (8): 1307–17. doi:10.1166/jbn.2013.1614.

Derosa, Maria C, and Robert J Crutchley. 2002. “Photosensitized Singlet Oxygen and Its Applications” 234.

Dewaele, Michael, Wim Martinet, Noemí Rubio, Tom Verfaillie, Peter a. de Witte, Jacques Piette, and Patrizia Agostinis. 2011. “Autophagy Pathways Activated in Response to PDT Contribute to Cell Resistance against ROS Damage.” *Journal of Cellular and Molecular Medicine* 15 (6): 1402–14. doi:10.1111/j.1582-4934.2010.01118.x.

Ding, Huiying, Baran D. Sumer, Chase W. Kessinger, Ying Dong, Gang Huang, David A. Boothman, and Jinming Gao. 2011. “Nanoscopic Micelle Delivery Improves the Photophysical Properties and Efficacy of Photodynamic Therapy of Protoporphyrin IX.” *Journal of Controlled Release* 151 (3): 271–77. doi:10.1016/j.jconrel.2011.01.004.

Dini, Luciana, Valentina Inguscio, Bernardetta Tenuzzo, and Elisa Panzarini. 2010. “Rose Bengal Acetate Photodynamic Therapy-Induced Autophagy.” *Cancer Biology and Therapy* 10 (10): 1048–56. doi:10.4161/cbt.10.10.13371.

Dolmans, Dennis E. J. G. J., Dai Fukumura, and Rakesh K. Jain. 2003. “Photodynamic Therapy for Cancer.” *Nature Reviews. Cancer* 3 (May): 380–87. doi:10.1038/nrc1070.

Dougherty, T J, G B Grindey, R Fiel, K R Weishaupt, and D G Boyle. 1975. “Photoradiation Therapy. II. Cure of Animal Tumors With Hematoporphyrin and Light.” *Journal of the National Cancer Institute* 55 (1): 115–21. doi:10.1093/jnci/55.1.115.

Dougherty, Thomas J., Charles J. Gomer, Barbara W. Henderson, Giulio Jori, David Kessel, Mladen Korbelik, Johan Moan, and Quian Peng. 1998. “Photodynamic Therapy.” *Journal of the National Cancer Institute* 90 (12): 889–905.

Du, Lihuan, Ning Jiang, Guozeng Wang, Yiwei Chu, Wei Lin, Jing Qian, Yuanfang Zhang, Jingcun Zheng, and Gang Chen. 2014. “Autophagy Inhibition Sensitizes Bladder Cancer Cells to the Photodynamic Effects of the Novel Photosensitizer Chlorophyllin e4.” *Journal of Photochemistry and Photobiology B: Biology* 133. Elsevier B.V.: 1–10. doi:10.1016/j.jphotobiol.2014.02.010.

Dummin, H., Th Cernay, and H. W. Zimmermann. 1997. “Selective Photosensitization of Mitochondria in HeLa Cells by Cationic Zn(II)phthalocyanines with Lipophilic Side-Chains.” *Journal of Photochemistry and Photobiology B: Biology* 37 (3): 219–29. doi:10.1016/S1011-1344(96)07416-7.

Engelmann, Fabio M., Ildemar Mayer, Dino S. Gabrielli, Henrique E. Toma, Alicia J. Kowaltowski, Koiti Araki, and Mauricio S. Baptista. 2007. “Interaction of Cationic Meso-Porphyrins with Liposomes, Mitochondria and Erythrocytes.” *Journal of Bioenergetics and Biomembranes* 39: 175–85. doi:10.1007/s10863-007-9075-0.

Engelmann, Fábio M., S. V O Rocha, Henrique E. Toma, Koiti Araki, and Maurício S. Baptista. 2007. “Determination of N-Octanol/water Partition and Membrane Binding of Cationic Porphyrins.” *International Journal of Pharmaceutics* 329: 12–18.

doi:10.1016/j.ijpharm.2006.08.008.
Ezzeddine, Rima, Anwar Al-Banaw, Artak Tovmasyan, James D Craik, Ines Batinic-Haberle, and Ludmil T Benov. 2013. “Effect of Molecular Characteristics on Cellular Uptake, Subcellular Localization, and Phototoxicity of Zn(II) N-Alkylpyridylporphyrins.” *The Journal of Biological Chemistry* 288 (51): 36579–88. doi:10.1074/jbc.M113.511642.
Fabris, Clara, Giuliana Valduga, Giovanni Miotto, Lara Borsetto, Giulio Jori, Spiridione Garbisa, and Elena Reddi. 2001. “Photosensitization with Zinc (II) Phthalocyanine as a Switch in the Decision between Apoptosis and Necrosis.” *Cancer Research* 61: 7495–7500.
Finsen, N. R. 1901. *Phototherapy. Edward Arnold, London,*.
Foote, Christopher S. 1987. “Type I and Type II Mechanisms of Photodynamic Action.” In *Light-Activated Pesticides. ACS Symposium Series*, Chapter 2:22–38. doi:10.1021/bk-1987-0339.ch002.
———. 1991. “Definition of Type I and Type II Photosensitized Oxidation.” *Photochemistry and Photobiology* 54 (5): 659. doi:10.1111/j.1751-1097.1991.tb02071.x.
Foote, Christopher S. 1968a. “Mechanisms of Photosensitized Oxidation.” *Sciences-New York* 162 (3857): 963–70.
———. 1968b. “Photosensitized Oxygenations and the Role of Singlet Oxygen.” *Accounts of Chemical Research* 1 (6): 104–10. doi:10.1021/ar50004a002.
Frankel, E. N. 1984. “Chemistry of Free Radical and Singlet Oxidation of Lipids.” *Progress in Lipid Research* 23 (4): 197–221. doi:10.1016/0163-7827(84)90011-0.
Franken, Nicolaas a P, Hans M Rodermond, Jan Stap, Jaap Haveman, and Chris van Bree. 2006. “Clonogenic Assay of Cells in Vitro.” *Nature Protocols* 1 (5): 2315–19. doi:10.1038/nprot.2006.339.
Frohlich, Eleonore. 2012. “The Role of Surface Charge in Cellular Uptake and Cytotoxicity of Medical Nanoparticles.” *International Journal of Nanomedicine* 7: 5577–91. doi:10.2147/IJN.S36111.
Garapati, Chandrasekhar, Brandon Clarke, Steven Zadora, Charles Burney, Brent D. Cameron, Ronald Fournier, Reginald F. Baugh, and Sai H S Boddu. 2015. “Development and Characterization of Erythrosine Nanoparticles with Potential for Treating Sinusitis Using Photodynamic Therapy.” *Photodiagnosis and Photodynamic Therapy* 12 (1). Elsevier B.V.: 9–18. doi:10.1016/j.pdpdt.2015.01.005.
Garg, A. D.;, H.; Maes, E.; Romano, and P. Agostinis. 2015. “Autophagy, a Major Adaptation Pathway Shaping Cancer Cell Death and Anticancer Immunity Responses Following Photodynamic Therapy.” *Photochemical & Photobiological Sciences* 14. Royal Society of Chemistry: 1410–24. doi:10.1039/C4PP00031E.
Gerola, Adriana P., Amanda Santana, Polyana B. França, Tayana M. Tsubone, Hueder P M De Oliveira, Wilker Caetano, Elza Kimura, and Noboru Hioka. 2011. “Effects of Metal and the Phytyl Chain on Chlorophyll Derivatives: Physicochemical Evaluation for Photodynamic Inactivation of Microorganisms.” *Photochemistry and Photobiology* 87: 884–94. doi:10.1111/j.1751-1097.2011.00935.x.
Gerola, Adriana P., Tayana M. Tsubone, Amanda Santana, Hueder P M De Oliveira, Noboru Hioka, and Wilker Caetano. 2011. “Properties of Chlorophyll and Derivatives in Homogeneous and Microheterogeneous Systems.” *Journal of Physical Chemistry B* 115: 7364–73. doi:10.1021/jp201278b.
Girotti, Albert W. 2001. “Photosensitized Oxidation of Membrane Lipids: Reaction Pathways, Cytotoxic Effects, and Cytoprotective Mechanisms.” *Journal of Photochemistry and Photobiology B: Biology* 63: 103–13. doi:10.1016/S1011-1344(01)00207-X.
Glick, Danielle, Sandra Barth, and Kay F Macleod. 2010. “Autophagy: Cellular and Molecular Mechanisms.” *Journal of Pathology* 221 (1): 3–12.

doi:10.1002/path.2697.Autophagy.
Goyal, Ritu, Lauren Macri, and Joachim Kohn. 2015. “Formulation Strategy for the Delivery of Cyclosporine A: Comparison of Two Polymeric Nanospheres.” *Scientific Reports* 5 (August). Nature Publishing Group: 13065. doi:10.1038/srep13065.
Gump, Jacob M., and Andrew Thorburn. 2011. “Autophagy and Apoptosis: What Is the Connection?” *Trends in Cell Biology* 21 (7). Elsevier Ltd: 387–92. doi:10.1016/j.tcb.2011.03.007.
Hackbarth, S., J. Schlothauer, A. Preuß, C. Ludwig, and B. Röder. 2012. “Time Resolved Sub-Cellular Singlet Oxygen Detection - Ensemble Measurements versus Single Cell Experiments.” *Laser Physics Letters* 9 (6): 474–80. doi:10.7452/lapl.201110146.
Hackbarth, Steffen, Jan Schlothauer, Annegret Preu??, and Beate R??der. 2010. “New Insights to Primary Photodynamic Effects - Singlet Oxygen Kinetics in Living Cells.” *Journal of Photochemistry and Photobiology B: Biology* 98 (3). Elsevier B.V.: 173–79. doi:10.1016/j.jphotobiol.2009.11.013.
Henderson, B W, and T J Dougherty. 1992. “How Does Photodynamic Therapy Work?” *Photochemistry and Photobiology* 55 (1): 145–57. doi:10.1111/j.1751-1097.1992.tb04222.x.
Hirsch, T, J Xiang, D T Chao, S J Korsmeyer, J F Scaife, A Colell, A Morales, et al. 1998. “Caspases: Enemies Within.” *Science* 281 (August): 1312–16. doi:10.1126/science.281.5381.1312.
Horobin, Richard W, Jc Stockert, and H Rashid-Doubell. 2015. “Uptake and Localization Mechanisms of Fluorescent and Colored Lipid Probes. Part 3. Protocols for Predicting Intracellular Localization of Lipid Probes Using QSAR Models.” *Biotechnic & Histochemistry* 90 (4): 255–63. doi:10.3109/10520295.2010.515489.
Hoye, Adam T., Jennifer E. Davoren, Peter Wipf, Mitchell P. Fink, and Valerian E. Kagan. 2008. “Targeting Mitochondria.” *Accounts of Chemical Research* 41 (1): 87–97. doi:10.1021/ar700135m.
Itri, Rosangela, Helena C. Junqueira, Omar Mertins, and Maurício S. Baptista. 2014. “Membrane Changes under Oxidative Stress: The Impact of Oxidized Lipids.” *Biophysical Reviews* 6 (1): 47–61. doi:10.1007/s12551-013-0128-9.
Jensen, Timothy J., M. Graça H Vicente, Raymond Luguya, Jolanna Norton, Frank R. Fronczek, and Kevin M. Smith. 2010. “Effect of Overall Charge and Charge Distribution on Cellular Uptake, Distribution and Phototoxicity of Cationic Porphyrins in HEp2 Cells.” *Journal of Photochemistry and Photobiology B: Biology* 100 (2). Elsevier B.V.: 100–111. doi:10.1016/j.jphotobiol.2010.05.007.
Jia, Xiao, and Lee Jia. 2012. “Nanoparticles Improve Biological Functions of Phthalocyanine Photosensitizers Used for Photodynamic Therapy.” *Current Drug Metabolism* 13 (8): 1119–22. doi:10.2174/138920012802850074.
Jori, Giulio, and Stanley B Brown. 2004. “Photosensitized Inactivation of Microorganisms.” *Photochemical & Photobiological Sciences* 3 (5): 403–5. doi:10.1039/b311904c.
Joseph R. Lakowicz. 2006. *Principles of Fluorescence Spectroscopy*.
Juzeniene, Asta, Petras Juzenas, Vladimir Iani, and Johan Moan. 2002. “Topical Application of 5-Aminolevulinic Acid and Its Methylester, Hexylester and Octylester Derivatives: Considerations for Dosimetry in Mouse Skin Model.” *Photochemistry and Photobiology* 76 (3): 329–34. doi:10.1562/0031-8655(2002)076<0329:TAOAAA>2.0.CO;2.
Kandela, Rawati K, Jeremy a Bartlett, and Guilherme L Indig. 2002. “Effect of Molecular Structure on the Selective Phototoxicity of Triarylmethane Dyes towards Tumor Cells.” *Photochemical & Photobiological Sciences : Official Journal of the European Photochemistry Association and the European Society for Photobiology* 1 (5): 309–14. doi:10.1039/b110572h.

Karayianni, Maria, and Stergios Pispas. 2016. “Self-Assembly of Amphiphilic Block Copolymers in Selective Solvents.” In *Fluorescence Studies of Polymer Containing Systems*, 16:27–64. doi:10.1007/978-3-319-26788-3.

Kempa, Marta, Patrycja Kozub, Joseph Kimball, Marcin Rojkiewics, Piotr Kus, Zugmunt Gryczynski, and Alicja Ratuszna. 2015. “Physicochemical Properties of Potential Porphyrin Photosensitizers for Photodynamic Therapy.” *Spectrochimica Acta Part A : Molecular and Biomolecular Spectroscopy* 146: 249–54.

Kennedy, J. C., R. H. Pottier, and D. C. Pross. 1990. “Photodynamic Therapy with Endogenous Protoporphyrin. IX: Basic Principles and Present Clinical Experience.” *Journal of Photochemistry and Photobiology, B: Biology* 6 (1–2): 143–48. doi:10.1016/1011-1344(90)85083-9.

Kepp, Oliver, Lorenzo Galluzzi, Marta Lipinski, Junying Yuan, and Guido Kroemer. 2011. “Cell Death Assays for Drug Discovery.” *Nature Reviews. Drug Discovery* 10 (3). Nature Publishing Group: 221–37. doi:10.1038/nrd3373.

Kessel, D. 1986. “Proposed Structure of the Tumor-Localizing Fraction of HPD (Hematoporphyrin Derivative).” *Photochemistry and Photobiology* 44 (2): 193–96. http://www.ncbi.nlm.nih.gov/pubmed/2946048.

Kessel, D., and Y. Luo. 2001. “Intracellular Sites of Photodamage as a Factor in Apoptotic Cell Death.” *Journal of Porphyrins and Phthalocyanines* 5 (2): 181–84. doi:10.1002/jpp.331.

Kessel, D, and M Castelli. 2001. “Evidence That Bcl-2 Is the Target of Three Photosensitizers That Induce a Rapid Apoptotic Response.” *Photochemistry and Photobiology* 74 (2): 318–22. doi:10.1562/0031-8655(2001)074<0318:ETBITT>2.0.CO;2.

Kessel, David. 2015. “Autophagic Death Probed by Photodynamic Therapy.” *Autophagy* 11 (10): 1941–43. doi:10.1080/15548627.2015.1078960.

Kessel, David H., Michael Price, and John J. Reiners. 2012. “ATG7 Deficiency Suppresses Apoptosis and Cell Death Induced by Lysosomal Photodamage.” *Autophagy* 8 (9): 1333–41. doi:10.4161/auto.20792.

Kessel, David, and John J Reiners Jr. 2007. “Apoptosis and Autophagy After Mitochondrial or Endoplasmic Reticulum,” no. 13: 1024–28.

Kessel, David, and Yu Luo. 1998. “Mitochondrial Photodamage and PDT-Induced Apoptosis.” *Journal of Photochemistry and Photobiology B: Biology* 42: 89–95. doi:10.1016/S1011-1344(97)00127-9.

Kessel, David, and John J Reiners. 2002. “Apoptotic Response to Photodynamic Therapy versus the Bcl-2 Antagonist HA14-1.” *Photochemistry and Photobiology* 76 (3): 314–19. doi:10.1562/0031-8655(2002)076<0314:ARTPTV>2.0.CO;2.

Kessel, David, Paul Thompson, B Musselman, and C K Chang. 1987. “Chemistry of Hematoporphyrin-Derived Photosensitizers.” *Photochemistry and Photobiology* 46 (5): 0–5.

Kessel, David, M. Graça H Vicente, and John J. Reiners. 2006. “Initiation of Apoptosis and Autophagy by Photodynamic Therapy.” *Autophagy* 2 (4): 289–90. doi:10.1002/lsm.20334.

Khan, Wahid, Saravanan Muthupandian, Shady Farah, Neeraj Kumar, and Abraham J. Domb. 2011. “Biodegradable Polymers Derived from Amino Acids.” *Macromolecular Bioscience* 11 (12): 1625–36. doi:10.1002/mabi.201100324.

Kiesslich, Tobias, Juergen Berlanda, Kristjan Plaetzer, Barbara Krammer, and Frieder Berr. 2007. “Comparative Characterization of the Efficiency and Cellular Pharmacokinetics of Foscan- and Foslip-Based Photodynamic Treatment in Human Biliary Tract Cancer Cell Lines.” *Photochemical & Photobiological Sciences : Official Journal of the European Photochemistry Association and the European Society for Photobiology* 6 (6): 619–27.

doi:10.1039/b617659c.
Kilfoyle, Brian E. 2011. “Tyrosine-Derived Nanoparticles for the Topical Treatment of Psoriasis.”
Kilfoyle, Brian E., Larissa Sheihet, Zheng Zhang, Marissa Laohoo, Joachim Kohn, and Bonzena B. Michniak-Kohn. 20012. “Development of Paclitaxel-Tyrospheres for Topical Skin Treatment.” *Journal of Controlled Release* 163 (1): 18–24. doi:10.1016/j.immuni.2010.12.017.Two-stage.
Klionsky, D, Lotta Agholme, Maria Agnello, Patrizia Agostinis, Julio A Aguirre-ghiso, Hyung Jun Ahn, Ouardia Ait-mohamed, et al. 2016. “Guidelines for the Use and Interpretation of Assays for Monitoring Autophagy.” *Autophagy* 8 (April): 445–544. doi:10.4161/auto.19496.
Knop, Katrin, Anne-Françoise Mingotaud, Naram El-Akra, Frédéric Violleau, and Jean-Pierre Souchard. 2009. “Monomeric Pheophorbide(a)-Containing Poly(ethyleneglycol-B-E-Caprolactone) Micelles for Photodynamic Therapy.” *Photochemical & Photobiological Sciences* 8: 396–404. doi:10.1039/b811248g.
Köhler, Barbara, Sergio Anguissola, Caoimhin G. Concannon, Markus Rehm, Donat Kögel, and Jochen H M Prehn. 2008. “Bid Participates in Genotoxic Drug-Induced Apoptosis of HeLa Cells and Is Essential for Death Receptor Ligands’ Apoptotic and Synergistic Effects.” *PLoS ONE* 3 (7). doi:10.1371/journal.pone.0002844.
Lassalle, Henri Pierre, Dominique Dumas, Susanna Gräfe, Marie Ange D’Hallewin, François Guillemin, and Lina Bezdetnaya. 2009. “Correlation between in Vivo Pharmacokinetics, Intratumoral Distribution and Photodynamic Efficiency of Liposomal mTHPC.” *Journal of Controlled Release* 134 (2). Elsevier B.V.: 118–24. doi:10.1016/j.jconrel.2008.11.016.
Li, Buhong, Eduardo H. Moriyama, Fugang Li, Mark T. Jarvi, Christine Allen, and Brian C. Wilson. 2007. “Diblock Copolymer Micelles Deliver Hydrophobic Protoporphyrin IX for Photodynamic Therapy.” *Photochemistry and Photobiology* 83 (6): 1505–12. doi:10.1111/j.1751-1097.2007.00194.x.
Lihuan, Du, Zheng Jingcun, Jiang Ning, Wang Guozeng, Chu Yiwei, Lin Wei, Qian Jing, Zhang Yuanfang, and Chen Gang. 2014. “Photodynamic Therapy with the Novel Photosensitizer Chlorophyllin F Induces Apoptosis and Autophagy in Human Bladder Cancer Cells.” *Lasers in Surgery and Medicine* 46 (4): 319–24. doi:10.1002/lsm.22225.
Lucky, Sasidharan Swarnalatha, Khee Chee Soo, and Yong Zhang. 2015. “Nanoparticles in Photodynamic Therapy.” *Chemical Reviews* 115 (4): 1990–2042. doi:10.1021/cr5004198.
Luo, Y, C K Chang, and D Kessel. 1996. “Rapid Initiation of Apoptosis by Photodynamic Therapy.” *Photochemistry and Photobiology* 63 (4): 528–34. doi:10.1006/bbrc.1996.0547.
Maiti, Nakul C., Shyamalava Mazumdar, and N. Periasamy. 1998. “J- and H-Aggregates of Porphyrin−Surfactant Complexes: Time-Resolved Fluorescence and Other Spectroscopic Studies †.” *The Journal of Physical Chemistry B* 102 (97): 1528–38. doi:10.1021/jp9723372.
Martins, W.K., E.T. Costa, R. Miotto, R.M. Cordeiro, and M.S. Baptista. 2015. “Parallel Damage in the Mitochondrial and Lysosome Membranes Leads to Autophagic Cell Death.” *Scientific Reports* 5. Nature Publishing Group: 1–17. doi:10.1038/srep12425.
Martins, Waleska K., Divinomar Severino, Cleidiane Souza, Beatriz S. Stolf, and Maurício S. Baptista. 2013. “Rapid Screening of Potential Autophagic Inductor Agents Using Mammalian Cell Lines.” *Biotechnology Journal* 8: 730–37. doi:10.1002/biot.201200306.
Meerloo, Johan Van, Gertjan J L Kaspers, and Jacqueline Cloos. 2011. “Cell Sensitivity Assay: The MTT Assay.” *Methods Mol Biol.* 731: 237–45. doi:10.1007/978-1-61779-080-5.

Mertins, Omar, Isabel O L Bacellar, Fabrice Thalmann, Carlos M. Marques, Maurício S. Baptista, and Rosangela Itri. 2014. “Physical Damage on Giant Vesicles Membrane as a Result of Methylene Blue Photoirradiation.” *Biophysical Journal* 106 (January): 162–71. doi:10.1016/j.bpj.2013.11.4457.

Mizushima, Noboru. 2004. “Methods for Monitoring Autophagy.” *International Journal of Biochemistry and Cell Biology* 36 (12): 2491–2502. doi:10.1016/j.biocel.2004.02.005.

———. 2007. “Autophagy: Process and Function.” *Genes and Development* 21: 2861–73. doi:10.1101/gad.1599207.eralize.

Mizushima, Noboru, Tamotsu Yoshimori, and Beth Levine. 2010. “Methods in Mammalian Autophagy Research.” *Cell* 140: 313–26. doi:10.1016/j.cell.2010.01.028.

Mohammad, Ramzi M., Irfana Muqbil, Leroy Lowe, Clement Yedjou, Hsue Yin Hsu, Liang Tzung Lin, Markus David Siegelin, et al. 2015. “Broad Targeting of Resistance to Apoptosis in Cancer.” *Seminars in Cancer Biology* 35. Elsevier Ltd: S78–103. doi:10.1016/j.semcancer.2015.03.001.

Mojzisova, Halina, Stéphanie Bonneau, Philippe Maillard, Kristian Berg, and Daniel Brault. 2009. “Photosensitizing Properties of Chlorins in Solution and in Membrane-Mimicking Systems.” *Photochemical & Photobiological Sciences : Official Journal of the European Photochemistry Association and the European Society for Photobiology* 8: 778–87. doi:10.1039/b822269j.

Morton, C. A., R. M. Szeimies, A. Sidoroff, and L. R. Braathen. 2013. “European Guidelines for Topical Photodynamic Therapy Part 1: Treatment Delivery and Current Indications - Actinic Keratoses, Bowen’s Disease, Basal Cell Carcinoma.” *Journal of the European Academy of Dermatology and Venereology* 27 (5): 536–44. doi:10.1111/jdv.12031.

Morton, Colin a, Colin a Morton, S B Brown, S B Brown, S Collins, S Collins, S Ibbotson, et al. 2002. “Guidelines for Topical Photodynamic Therapy: Report of a Workshop of the British Photodermatology Group.” *The British Journal of Dermatology* 146 (4): 552–67. doi:10.1046/j.1365-2133.2002.04719.x.

Moser, J. G. 1998. “Definitions and General Properties of 2nd and 3rd Generation Photosensitizers.” In *Photodynamic Tumor Therapy: 2nd and 3rd Generation Photosensitizers*, 256.

Mroz, Pawel, Anastasia Yaroslavsky, Gitika B. Kharkwal, and Michael R. Hamblin. 2011. “Cell Death Pathways in Photodynamic Therapy of Cancer.” *Cancers* 3 (2): 2516–39. doi:10.3390/cancers3022516.

Murugan, Karmani, Yahya E. Choonara, Pradeep Kumar, Divya Bijukumar, Lisa C. du Toit, and Viness Pillay. 2015. “Parameters and Characteristics Governing Cellular Internalization and Trans-Barrier Trafficking of Nanostructures.” *International Journal of Nanomedicine* 10: 2191–2206. doi:10.2147/IJN.S75615.

Nair, Lakshmi S., and Cato T. Laurencin. 2007. “Biodegradable Polymers as Biomaterials.” *Progress in Polymer Science (Oxford)* 32 (8–9): 762–98. doi:10.1016/j.progpolymsci.2007.05.017.

Nardin, Corinne, Durgadas Bolikal, and Joachim Kohn. 2004. “Nontoxic Block Copolymer Nanospheres: Design and Characterization.” *Langmuir* 20 (26): 11721–25. doi:10.1021/la0490285.

Nishiyama, Nobuhiro, and Kazunori Kataoka. 2006. “Current State, Achievements, and Future Prospects of Polymeric Micelles as Nanocarriers for Drug and Gene Delivery.” *Pharmacology & Therapeutics* 112 (3): 630–48. doi:10.1016/j.pharmthera.2006.05.006.

Nishiyama, Nobuhiro, Yuji Morimoto, Woo Dong Jang, and Kazunori Kataoka. 2009. “Design and Development of Dendrimer Photosensitizer-Incorporated Polymeric Micelles for Enhanced Photodynamic Therapy.” *Advanced Drug Delivery Reviews* 61 (4). Elsevier B.V.: 327–38. doi:10.1016/j.addr.2009.01.004.

Norum, Ole Jacob, Pål Kristian Selbo, Anette Weyergang, Karl Erik Giercksky, and Kristian Berg. 2009. “Photochemical Internalization (PCI) in Cancer Therapy: From Bench towards Bedside Medicine.” *Journal of Photochemistry and Photobiology B: Biology* 96 (2). Elsevier B.V.: 83–92. doi:10.1016/j.jphotobiol.2009.04.012.

Ogunsipe, Abimbola, David Maree, and Tebello Nyokong. 2003. “Solvent Effects on the Photochemical and Fluorescence Properties of Zinc Phthalocyanine Derivatives.” *Journal of Molecular Structure* 650 (1–3): 131–40. doi:10.1016/S0022-2860(03)00155-8.

Oleinick, Nancy L, Rachel L Morris, and Irina Belichenko. 2002. “The Role of Apoptosis in Response to Photodynamic Therapy: What, Where, Why, and How.” *Photochemical & Photobiological Sciences : Official Journal of the European Photochemistry Association and the European Society for Photobiology* 1: 1–21. doi:10.1039/b108586g.

Oliveira, Carla S., Rozane Turchiello, Alicia J. Kowaltowski, Guilherme L. Indig, and Mauricio S. Baptista. 2011. “Major Determinants of Photoinduced Cell Death: Subcellular Localization versus Photosensitization Efficiency.” *Free Radical Biology and Medicine* 51 (4). Elsevier Inc.: 824–33. doi:10.1016/j.freeradbiomed.2011.05.023.

Olmsted, John. 1979. “Calorimetric Determinations of Absolute Fluorescence Quantum Yields.” *The Journal of Physical Chemistry* 83 (20): 2581–84. doi:10.1021/j100483a006.

Ormond, Alexandra B., and Harold S. Freeman. 2013. “Dye Sensitizers for Photodynamic Therapy.” *Materials* 6: 817–40. doi:10.3390/ma6030817.

Oseroff, A. R., D. Ohuoha, G. Ara, D. McAuliffe, J. Foley, and L. Cincotta. 1986. “Intramitochondrial Dyes Allow Selective in Vitro Photolysis of Carcinoma Cells.” *Proceedings of the National Academy of Sciences of the United States of America* 83 (24): 9729–33. doi:10.1073/pnas.83.24.9729.

Pankiv, Serhiy, Terje Høyvarde Clausen, Trond Lamark, Andreas Brech, Jack Ansgar Bruun, Heidi Outzen, Aud Øvervatn, Geir Bjørkøy, and Terje Johansen. 2007. “p62/SQSTM1 Binds Directly to Atg8/LC3 to Facilitate Degradation of Ubiquitinated Protein Aggregates by autophagy*[S].” *Journal of Biological Chemistry* 282 (33): 24131–45. doi:10.1074/jbc.M702824200.

Parkash, Jai, John H Robblee, John Agnew, Esther Gibbs, Peter Collings, Robert F Pasternack, and Julio C De Paula. 1998. “Depolarized Resonance Light Scattering by Porphyrin and Chlorophyll a Aggregates.” *Biophysical Journal* 74 (January): 2089–99.

Pasternack, R F, and P J Collings. 1995. “Resonance Light Scattering: A New Technique for Studying Chromophore Aggregation.” *Science (New York, N.Y.)* 269 (5226): 935–39. doi:10.1126/science.7638615.

Pasternack, Robert F, Peter R Huber, Boyd P, G Engasser, L Francesconi, E Gibbs, P Fasella, and G Cerio Venturo. 1971. “On the Aggregation of Meso-Substituted Water-Soluble Porphyrins.” *Journal of the American Chemical Society* 669 (1968): 4511–17. doi:10.1021/ja00768a016.

Paszko, Edyta, Carsten Ehrhardt, Mathias O. Senge, Dermot P. Kelleher, and John V. Reynolds. 2011. “Nanodrug Applications in Photodynamic Therapy.” *Photodiagnosis and Photodynamic Therapy* 8 (1): 14–29. doi:10.1016/j.pdpdt.2010.12.001.

Pavani, Christiane, Yassuko Iamamoto, and Maurício S. Baptista. 2012. “Mechanism and Efficiency of Cell Death of Type II Photosensitizers: Effect of Zinc Chelation.” *Photochemistry and Photobiology* 88 (Cm): 774–81. doi:10.1111/j.1751-1097.2012.01102.x.

Pavani, Christiane, Adjaci F Uchoa, Carla S Oliveira, Yassuko Iamamoto, and Maurício S Baptista. 2009. “Effect of Zinc Insertion and Hydrophobicity on the Membrane Interactions and PDT Activity of Porphyrin Photosensitizers.” *Photochemical & Photobiological Sciences* 8: 233–40. doi:10.1039/b810313e.

Plaetzer, Kristjan, Tobias Kiesslich, Christian Benno Oberdanner, and Barbara Krammer. 2005. “Apoptosis Following Photodynamic Tumor Therapy: Induction, Mechanisms and Detection.” *Current Pharmaceutical Design* 11 (9): 1151–65. doi:10.2174/1381612053507648.

Politzer, Ieva Ruks, Gary W. Griffin, and John L. Laseter. 1971. “Singlet Oxygen and Biological Systems.” *Chemico-Biological Interactions* 3 (2): 73–93. doi:10.1016/0009-2797(71)90088-3.

Pushpan, S K, S Venkatraman, V G Anand, J Sankar, D Parmeswaran, S Ganesan, and T K Chandrashekar. 2002. “Porphyrins in Photodynamic Therapy - a Search for Ideal Photosensitizers.” *Current Medicinal Chemistry. Anti-Cancer Agents* 2 (512): 187–207. doi:10.2174/1568011023354137.

Raab, O. 1900. “Uber Die Wirkung Fluoreszierender Stoffe Auf Infusorien.” *Zeitung Biol* 39: 524–526.

Redmond, R W, and J N Gamlin. 1999. “A Compilation of Singlet Oxygen Yields from Biologically Relevant Molecules.” *Photochemistry and Photobiology* 70 (4): 391–475. doi:10.1111/j.1751-1097.1999.tb08240.x.

Redmond, Robert W, and Irene E Kochevar. 2006. “Spatially Resolved Cellular Responses to Singlet Oxygen.” *Photochemical and Photobiology* 82: 1178–86. doi:10.1562/2006-04-14-1R-874.

Reiners, J J, J a Caruso, P Mathieu, B Chelladurai, X-M Yin, and D Kessel. 2002. “Release of Cytochrome c and Activation of pro-Caspase-9 Following Lysosomal Photodamage Involves Bid Cleavage.” *Cell Death and Differentiation* 9 (9): 934–44. doi:10.1038/sj.cdd.4401048.

Ricchelli, F. 1995. “Photophysical Properties of Porphyrins in Biological Membranes.” *Journal of Photochemistry and Photobiology B: Biology* 29: 109–18. doi:10.1016/1011-1344(95)07155-U.

Ricchelli, Fernanda, Lisa Franchi, Giovanni Miotto, Lara Borsetto, Silvano Gobbo, Peter Nikolov, Jerry C. Bommer, and Elena Reddi. 2005. “Meso-Substituted Tetra-Cationic Porphyrins Photosensitize the Death of Human Fibrosarcoma Cells via Lysosomal Targeting.” *International Journal of Biochemistry and Cell Biology* 37 (2): 306–19. doi:10.1016/j.biocel.2004.06.013.

Rodriguez, Myrian E., Pnig Zhang, Kashif Azizuddin, Grace B. Delos Santos, Song-mao Chiu, Liang-yan Xue, Jeffery C. Berlin, et al. 2009. “Structural Factors and Mechanisms Underlying the Improved Photodynamic Cell Killing with Silicon Phthalocyanine Photosensitizers Directed to Lysosomes versus Mitochondria.” *Photochemistry and Photobiology* 85 (5): 1189–1200. doi:10.1016/j.biotechadv.2011.08.021.Secreted.

Rohatgi-Mukherjee, K. K. 1978. *Fundamentals of Photochemistry*.

Roots, Ruth, and Shigefumi Okada. 1975. “Estimation of Life Times and Diffusion Distances of Radicals Involved in X-Ray-Induced DNA Strand Breaks or Killing of Mammalian Cells.” *Radiation Research* 64 (2): 306–20. doi:10.2307/3574267.

Rossi, Liane M, Paulo R Silva, Adjaci U Fernandes, Dayane B Tada, and Mauricio S Baptista. 2008. “Protoporphyrin IX Nanoparticle-Carrier: Preparation, Optical Properties and Singlet Oxygen Generation.” *Langmuir* 24 (21): 12534–12538.

Rouser, George, Sidney Fleischer, and Akira Yamamoto. 1970. “Two Dimensional Thin Layer Chromatographic Separation of Polar Lipids and Determination of Phospholipids by Phosphorus Analysis of Spots.” *Lipids* 5: 494–96. doi:10.1007/BF02531316.

Schlothauer, J., S. Hackbarth, and B. Röder. 2009. “A New Benchmark for Time-Resolved Detection of Singlet Oxygen Luminescence - Revealing the Evolution of Lifetime in Living Cells with Low Dose Illumination.” *Laser Physics Letters* 6 (3): 216–21. doi:10.1002/lapl.200810116.

Selbo, Pål Kristian, Anette Weyergang, Anders Høgset, Ole Jacob Norum, Maria Brandal Berstad, Marie Vikdal, and Kristian Berg. 2010. "Photochemical Internalization Provides Time- and Space-Controlled Endolysosomal Escape of Therapeutic Molecules." *Journal of Controlled Release* 148: 2–12. doi:10.1016/j.jconrel.2010.06.008.

Seybold, Paul G., and Martin Gouterman. 1969. "Porphyrins XIII: Fluorescence Spectra and Quantum Yields." *Journal of Molecular Spectroscopy* 31: 1–13.

Sheihet, L., P. Chandra, P. Batheja, D. Devore, J. Kohn, and B. Michniak. 2008. "Tyrosine-Derived Nanospheres for Enhanced Topical Skin Penetration." *International Journal of Pharmaceutics* 350 (1–2): 312–19. doi:10.1016/j.ijpharm.2007.08.022.

Sheihet, Larisa, Robert a. Dubin, David Devore, and Joachim Kohn. 2005. "Hydrophobic Drug Delivery by Self-Assembling Triblock Copolymer-Derived Nanospheres." *Biomacromolecules* 6 (5): 2726–31. doi:10.1021/bm050212u.

Sheihet, Larisa, Olga B. Garbuzenko, Jared Bushman, Murugesan K. Gounder, Tamara Minko, and Joachim Kohn. 2012. "Paclitaxel in Tyrosine-Derived Nanospheres as a Potential Anti-Cancer Agent: In Vivo Evaluation of Toxicity and Efficacy in Comparison with Paclitaxel in Cremophor." *European Journal of Pharmaceutical Sciences* 45 (3). Elsevier B.V.: 320–29. doi:10.1016/j.ejps.2011.11.017.

Sheihet, Larisa, Karolina Piotrowska, Robert a. Dubin, Joachim Kohn, and David Devore. 2007. "Effect of Tyrosine-Derived Triblock Copolymer Compositions on Nanosphere Self-Assembly and Drug Delivery." *Biomacromolecules* 8 (3): 998–1003. doi:10.1021/bm060860t.

Silva, Diogo, André Luiz, Francesca Moret, Elisa Gaio, Elena Reddi, Wilker Caetano, Fabiana Quaglia, and Noboru Hioka. 2016. "Pluronic Mixed Micelles as Efficient Nanocarriers for Benzoporphyrin Derivatives Applied to Photodynamic Therapy in Cancer Cells." *Journal of Photochemistry and Photobiology A : Chemistry* 314: 143–54.

Simon, Timea, Monica Potara, Ana-Maria Gabudean, Emilia Licarete, Manuela Banciu, and Simion Astilean. 2015. "Designing Theranostic Agents Based on Pluronic Stabilized Gold Nanoaggregates Loaded with Methylene Blue for Multimodal Cell Imaging and Enhanced Photodynamic Therapy." *ACS Applied Materials & Interfaces*, 150722085411004. doi:10.1021/acsami.5b04734.

Spring, Bryan Q., Imran Rizvi, Nan Xu, and Tayyaba Hasan. 2015. "The Role of Photodynamic Therapy in Overcoming Cancer Drug Resistance." *Photochem. Photobiol. Sci.* 14: 1476–91.

Sternberg, Ethan D, David Dolphin, and Christian Brickner. 1998. "Porphyrin-Based Photosensitizers for Use in Photodynamic Therapy." *Tetrahedron* 54 (447): 4151–4202. doi:S0040-4020(98)00015-5.

Suppan, Paul. 1994. *Chemistry and Light*. doi:10.1039/9781847550439-00027.

Szeimies, Rolf-markus, and Christoph Abels. 2001. "Chapter 1 History of Photodynamic Therapy in Dermatology."

Tada, Dayane B., Emanuel Suraniti, Liane M. Rossi, Carlos a P Leite, Carla S. Oliveira, Tathyana C. Tumolo, Roberto Calemczuk, Thierry Livache, and Mauricio S. Baptista. 2014. "Effect of Lipid Coating on the Interaction between Silica Nanoparticles and Membranes." *Journal of Biomedical Nanotechnology* 10 (3): 519–28. doi:10.1166/jbn.2014.1723.

Tada, Dayane B., L. L R Vono, Evandro L. Duarte, Rosangela Itri, Pedro K. Kiyohara, Maurício S. Baptista, and Liane M. Rossi. 2007. "Methylene Blue-Containing Silica-Coated Magnetic Particles: A Potential Magnetic Carrier for pHotodynamic Therapy." *Langmuir* 23 (15): 8194–99. doi:10.1021/la700883y.

Tada, Dayane B, and Mauricio S Baptista. 2015. "Photosensitizing Nanoparticles and the Modulation of ROS Generation." *Frontiers in Chemistry* 3 (May): 1–14.

doi:10.3389/fchem.2015.00033.
Tada, Dayane B, Liane M Rossi, Carlos A P Leite, Rosangela Itri, and Mauricio S Baptista. 2010. “Nanoparticle Platform to Modulate Reaction Mechanism of Phenothiazine Photosensitizers.” *Journal of Nanoscience and Nanotechnology* 10 (5): 3100–3108. doi:10.1166/jnn.2010.2165.
Tan, Cai-Ping, Yi-Ying Lu, Liang-Nian Ji, and Zong-Wan Mao. 2014. “Metallomics Insights into the Programmed Cell Death Induced by Metal-Based Anticancer Compounds.” *Metallomics : Integrated Biometal Science* 6 (5): 978–95. doi:10.1039/c3mt00225j.
Tanielian, C, G Heinfuch, and Blake Pascal. 1995. “Effect of Aggregation on the Hematoporphyrin-Sensitized Production of Singlet Molecular Oxygen.” *Photochemistry and Photobiology* 61 (2): 131–35.
Tardivo, João Paulo, Auro Del Giglio, Carla Santos De Oliveira, Dino Santesso Gabrielli, Helena Couto Junqueira, Dayane Batista Tada, Divinomar Severino, Rozane De Fátima Turchiello, and Mauricio S. Baptista. 2005. “Methylene Blue in Photodynamic Therapy: From Basic Mechanisms to Clinical Applications.” *Photodiagnosis and Photodynamic Therapy* 2: 175–91. doi:10.1016/S1572-1000(05)00097-9.
Trauner, K B, R Gandour-Edwards, M Bamberg, S Shortkroff, C Sledge, and T Hasan. 1998. “Photodynamic Synovectomy Using Benzoporphyrin Derivative in an Antigen-Induced Arthritis Model for Rheumatoid Arthritis.” *Photochemistry and Photobiology* 67 (1): 133–39.
Trauner, Kenneth B, and Tayyaba Hasan. 1996. “Photodynamic Treatment of Rheumatoid and Inflammatory Arthritis.” *Photochemistry and Photobiology* 64 (5): 740–50.
Tsubone, T. M., C. Pavani, I. O L Bacellar, and M. S. Baptista. 2017. “In Search of Specific PDT Photosensitizers Subcellular Localization and Cell Death Pathways.” In *Imaging in Photodynamic Therapy*, 149–82.
Tsubone, Tayana M, Gustavo Braga, Bruno H Vilsinski, Adriana P Gerola, Noboru Hioka, and Wilker Caetano. 2014. “Aggregation of Aluminum Phthalocyanine Hydroxide in Water/Ethanol Mixtures” 25 (5): 890–97.
Uchoa, Adjaci F., Kleber T. De Oliveira, Mauricio S. Baptista, Adailton J. Bortoluzzi, Yassuko Iamamoto, and Osvaldo a. Serra. 2011. “Chlorin Photosensitizers Sterically Designed to Prevent Self-Aggregation.” *Journal of Organic Chemistry* 76 (21): 8824–32. doi:10.1021/jo201568n.
Uchoa, Adjaci F., Carla S. Oliveira, and Mauricio S. Baptista. 2010. “Relationship between Structure and Photoactivity of Porphyrins Derived from Protoporphyrin IX.” *Journal of Porphyrins and Phthalocyanines* 14: 832–45. doi:10.1142/S108842461000263X.
Vidòczy, Tamàs. 1992. “Type I and Type II Photosensitized Reactions: Reasons for Dispute.” *Journal of Photochemistry and Photobiology, B: Biology* 14 (1–2): 139–42. doi:10.1016/1011-1344(92)85088-C.
Von Tappeiner, H., and A. Jesionek. 1903. “Therapeutische Versuche Mit Fluoreszierenden Stoffen.” *Muench Med. Wochenschr* 47: 2042–2044.
White, Eileen. 2015. “The Role for Autophagy in Cancer.” *Journal of Clinical Investigation* 125 (1): 42–46. doi:10.1172/JCI73941.Autophagy.
Wilkinson, Francis, W. Philip Helman, and Alberta B. Ross. 1993. “Quantum Yields for the Photosensitized Formation of the Lowest Electronically Excited Singlet State of Molecular Oxygen in Solution.” *J Phys Chem* 22 (1): 113–262.
Woodburn, K W, N J Vardaxis, J S Hill, a H Kaye, and D R Phillips. 1991. “Subcellular Localization of Porphyrins Using Confocal Laser Scanning Microscopy.” *Photochemistry and Photobiology* 54 (5): 725–32.
Xu, Yongkui, Ruoyu He, Dongdong Lin, Minbiao Ji, and Jiyao Chen. 2015. “Laser Beam Controlled Drug Release from Ce6–gold Nanorod Composites in Living Cells: A FLIM

Study." *Nanoscale* 7: 2433–41. doi:10.1039/C4NR05574H.
Xue, Liang Yan, Song Mao Chiu, Kashif Azizuddin, Sheeba Joseph, and Nancy L. Oleinick. 2007. "The Death of Human Cancer Cells Following Photodynamic Therapy: Apoptosis Competence Is Necessary for Bcl-2 Protection but Not for Induction of Autophagy." *Photochemistry and Photobiology* 83 (5): 1016–23. doi:10.1111/j.1751-1097.2007.00159.x.
Yeh, Shu-Chi, Michael Patterson, Joseph Hayward, and Qiyin Fang. 2014. "Time-Resolved Fluorescence in Photodynamic Therapy." *Photonics* 1 (4): 530–64. doi:10.3390/photonics1040530.
Yoo, Je-Ok, and Kwon-Soo Ha. 2012. *New Insights into the Mechanisms for Photodynamic Therapy-Induced Cancer Cell Death. International Review of Cell and Molecular Biology*. 1sted. Vol. 295. Elsevier Inc. doi:10.1016/B978-0-12-394306-4.00010-1.
Yue, Zhan-Guo, Wei Wei, Pi-ping Lv, Hua Yue, Lian-yan Wang, Zhi-guo Su, and Guang-hui Ma. 2011. "Surface Charge Affects Cellular Uptake and Intracellular Trafficking of Chitosan-Based Nanoparticles." *Biomacromolecules* 12: 2440–46.
Zhang, Zheng, Tannaz Ramezanli, Pei-Chin Tsai, and Bozena B. Michniak-Kohn. 2014. "Drug Delivery Systems Based on Tyrosine-Derived Nanospheres (TyroSpheres™)." In *Nanotechnology and Drug Delivery, Volume One: Nanoplatforms in Drug Delivery*, 210–232. CRC Press. doi:10.1201/b17271-7.
Zhang, Zheng, Pei Chin Tsai, Tannaz Ramezanli, and Bozena B. Michniak-Kohn. 2013a. "Polymeric Nanoparticles-Based Topical Delivery Systems for the Treatment of Dermatological Diseases." *Wiley Interdisciplinary Reviews: Nanomedicine and Nanobiotechnology* 5 (3): 205–18. doi:10.1002/wnan.1211.
———. 2013b. "Polymeric Nanoparticles-Based Topical Delivery Systems for the Treatment of Dermatological Diseases." *Wiley Interdisciplinary Reviews: Nanomedicine and Nanobiotechnology* 5 (3): 205–18. doi:10.1002/wnan.1211.
Zong, D, K Zielinska-Chomej, T Juntti, B Mörk, R Lewensohn, P Hååg, and K Viktorsson. 2014. "Harnessing the Lysosome-Dependent Antitumor Activity of Phenothiazines in Human Small Cell Lung Cancer." *Cell Death & Disease* 5: e1111. doi:10.1038/cddis.2014.56.

CURRICULUM VITAE

7. CURRICULUM VITAE

PERSONAL DATA

Name: Tayana Mazin Tsubone
Date of birth: November 16, 1989 – Andradina/SP - Brazil

EDUCATION

PhD in Science **2012 – 2017**
University of Sao Paulo (USP), São Paulo – Brazil

Bachelor of Science in Chemistry **2008 - 2011**
State University of Maringa (UEM), Paraná – Brazil

COMPLEMENTARY EDUCATION

- Scientific Instrumentation: Flow Cytometry. **September/2015.**
  Universidade Federal do ABC (UFABC), São Paulo – Brazil

- 2nd Summer School in Colloids and Surfaces. **January/2014.**
  Universidade de São Paulo (USP), São Paulo – Brazil

ACADEMIC PROFESSIONAL EXPERIENCE

- February/2012 – current: **PhD student** under supervision of Prof. Dr. Maurício S. Baptista. Scholarship grant received from FAPESP (Process number Nº 2012/10049-4 and Nº 2013/16532-1).

- May/2014 – August/2014: **PhD visiting student** on the International Summer Exchange Program at *New Jersey Center for Biomaterials – Rutgers University* (USA) to develop part of this PhD thesis.

- August/2012 – December/2013: **Teacher assistant** in Chemistry course at the Institute of Chemistry, University of Sao Paulo.

- February/2009 – December/2011: **Undergraduate researcher assistant** under supervision of Prof. Dr. Wilker Caetano. Scholarship grant received from CNPq by PIBIC program (*Programa Institucional de Bolsas de Iniciação Científica*).

PAPERS

1. **Tayana Mazin Tsubone,** Waleska Kerllen Martins, Christiane Pavani, Helena Couto Junqueira, Rosangela Itri, Maurício S. Baptista. Enhanced Efficiency of Cell Death by Lysosome-Specific Photodamage. *Scientific Reports*, **submitted.**

2. Camila Fabiano de Freitas, Diogo Silva Pellosi, Bianca Martins Estevão, Italo Rodrigo Calori, **Tayana Mazin Tsubone**, Mário José Politi, Wilker Caetano, Noboru Hioka. Nanostructured Polymeric Micelles Carrying Xanthene Dyes for Photodynamic Evaluation. *Photochemistry and Photobiology*, 92, p. 790-799**, 2016.**
   DOI: 10.1111/php.12645

3. Isabel Bacellar, **Tayana Mazin Tsubone,** Christiane Pavani, Maurício Baptista. Photodynamic Efficiency: From Molecular Photochemistry to Cell Death**.** *International Journal of Molecular Sciences*, v. 16, p. 20523-20559, **2015.**
   DOI: 10.3390/ijms160920523
   - This paper was cover of "*International Journal of Molecular Science*" at **September/2015**.

4. **Tayana Mazin Tsubone;** Gustavo Braga, Bruno H. Vilsinski, Adriana P. Gerola; Noboru Hioka, André L. Tessaro, Wilker Caetano.
   Aggregation of Aluminum Phthalocyanine Hydroxide in Water/Ethanol Mixtures. *Journal of the Brazilian Chemical Society*, v. 25, p.890-897, **2014**.
   DOI: 10.5935/0103-5053.20140058

5. Diogo Silva Pellosi, Bianca Martins Estevão, Camila Fabiano de Freitas, **Tayana Mazin Tsubone,** Wilker Caetano, Noboru Hioka.
   Photophysical Properties of Erythrosin Ester Derivatives in Ionic and Non-Ionic Micelles. *Dyes and Pigments*, v. 99, p. 2013-705-712, **2013.**
   DOI: 10.1016/j.dyepig.2013.06.026

6. Adriana Passarella Gerola, Amanda Santana, Polyana Batoqui França, **Tayana Mazin Tsubone,** Hueder Paulo Moisés de Oliveira, Wilker Caetano, Elza Kimura, Noboru Hioka. Effects of metal and the phytyl chain on chlorophyll derivatives: physicochemical evaluation for Photodynamic Inactivation of Microorganisms.
   Photochemistry and Photobiology, v. 87, p. 884-894, **2011.**
   DOI: 10.1111/j.1751-1097.2011.00935.x

7. Adriana P. Gerola, **Tayana Mazin Tsubone**, Amanda Santana, Hueder Paulo Moisés de Oliveira, Noboru Hioka, Wilker Caetano.
   Properties of Chlorophyll and Derivatives in Homogeneous and Microheterogeneous Systems.
   Journal of Physical Chemistry. B, v. 115, p. 7364-7373, **2011**.
   DOI: 10.1021/jp201278b

BOOK CHAPTER

1. **Tayana Mazin Tsubone,** Christiane Pavani, Isabel Bacellar, Maurício Baptista.
   In the search of specific PDT photosensitizers: subcellular localization and cell death pathways.
   Book chapter published on the *CRC Press* as part of book "Imaging in Photodynamic Therapy". Editors: Michael R. Hamblin, Yingying Huang.
   DOI: 10.1201/9781315278179-10

ORAL PRESENTATIONS AT INTERNATIONAL CONFERENCES

1. Organelle-specific cell death by photosensitized oxidation.
   Oral presentation in *Tsukuba Global Science Week*. Tsukuba - Japan. **September/2016.**
   - This presentation received the ***Outstanding Speaker Award***.

2. Enhanced Photodynamic Efficacy by Encapsulation of Photosensitizers in Tyrosine-Derived Nanospheres.
   Oral presentation in *10th World Biomaterials Congress*. Montreal - Canada. **May/2016.**

3. Modulating the mechanism of photoinduced cell death by using photosensitizers with different charges.
   Oral presentation in *International Photodynamic Association*. Rio de Janeiro - Brazil. **May/2015.**

4. Photoinduced autophagic cell death: an efficient mechanism to kill tumor cells.
   Oral presentation in *XII Encontro Latino Americano de Fotoquímica e Fotobiologia*. Maresias - Brazil. **April/2015.**

5. Mechanism of Photochemical Internalization.
   Oral presentation at the event organized by Department of Pharmacy at Universidade Nacional. Córdoba – Argentina. **September/2014**.

6. Light and Tyrospheres to improve Cancer Therapy.
   Oral presentation in a conference at *New Jersey Center for Biomaterials - Rutgers University*. Piscataway – United States. **August/2014.**

AWARDS AND HIGHLIGHTS

- *Outstanding Speaker Award in Tsukuba Global Science Week*. **September/2016.**

PARTICIPATION IN CONFERENCES AND EVENTS

1. 10th World Biomaterials Congress. **2016.** (Congress).

2. Tsukuba Global Science Week. **2016.** (Conference).

3. International Photodynamic Association. **2015.** (Congress).

4. XII Encontro Latino Americano de Fotoquímica e Fotobiologia. **2015.** (Congress).

5. 16th International Congress on Photobiology. **2014.** (Congress).

6. Canada-Brazil Molecular Sciences Workshop. **2014.** (Workshop).

7. Mini-Symposium on Singlet Oxygen. **2014.** (Symposium).

8. 34ª Reunião Anual da Sociedade Brasileira de Química. **2011.** (Congress).

9. 1º Workshop da Rede NANOBIO - Filmes Finos. **2010.** (Workshop).

10. 33ª Reunião Anual Sociedade Brasileira de Química. **2010.** (Congress).

11. XIX Encontro Anual de Iniciação Científica. **2010.** (Event).

12. XXVI Semana da Química. **2010.** (Event).

APPENDIX I

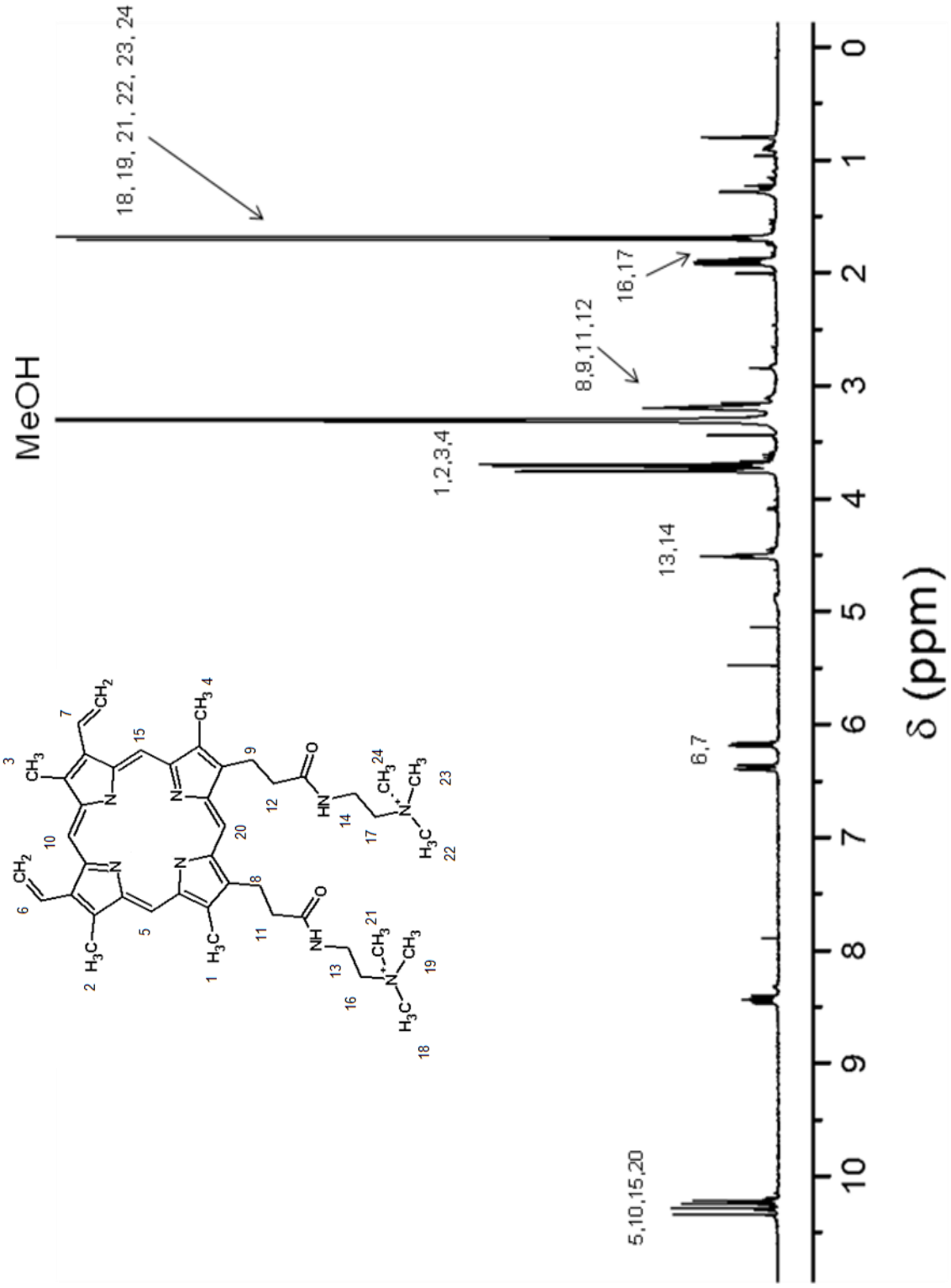
MeOH
18, 19, 21, 22, 23, 24
16,17
8,9,11,12
1,2,3,4
13,14
6,7
5,10,15,20
δ (ppm)
0
1
2
3
4
5
6
7
8
9
10